REVIEW ARTICLE

Recent search for new superhard materials: Go nano!

Stan Veprek[a)]
Department of Chemistry, Technical University Munich, Lichtenbergstr. 4, D-85747 Garching, Germany

(Received 21 January 2013; accepted 30 July 2013; published 27 August 2013)

High elastic moduli do not guarantee high hardness because upon finite shear electronic instabilities often occur that result in transformation to softer phases. Therefore, the author concentrates on the extrinsically superhard nanostructured materials, which are the most promising. Decreasing crystallite size results in strengthening and hardening because the grain boundaries impede the plasticity (e.g., Hall–Petch strengthening in case of dislocation activity). However, this hardening is limited to a crystallite size down to 10–15 nm below which softening due to grain boundary shear dominates. This softening can be reduced by forming low energy grain boundaries or a strong interfacial layer. In such a way, much higher hardness enhancement can be achieved. The emphasis will be on the understanding of the mechanisms of the hardness enhancement. A special section deals with examples of the present industrial applications of such coatings on tools for machining in order to illustrate that these materials are already in large-scale use. In the last section, the author summarizes the open questions and limitations for the preparation of the super- and ultrahard nanocomposite coatings and possible ways on how to overcome them. © *2013 American Vacuum Society*. [http://dx.doi.org/10.1116/1.4818590]

I. INTRODUCTION

Hardness is a resistance of a body to the deformation upon an applied load.[1] Thus, the nature of the load (scratch, indentation, and impact) and of the kind of the deformation (elastic/plastic) distinguishes between the scratch hardness described by the Mohs scale, indentation, and dynamic impact hardness. Scratch hardness is suitable for mineralogists, but it is less suitable for material scientist and engineers because it is strongly nonlinear (e.g., Ref. 2, p. 450). The dynamic impact hardness[1,3,4] is important, e.g., in interrupted cutting, such as milling, for the lacquer on the front part of a vehicle exposed to impact of particles and the like. The exact definition of the impact hardness can be found in Ref. 1 and more recent method of its testing in Refs. 2 and 3. The plastic indentation hardness is an average pressure under the indenter upon fully developed plastic deformation, i.e., the applied load divided by the area of contact between the indenter and the tested material after unloading should be load-invariant.[1] For more information about the definition and measurement of hardness, see Appendix A.

Because the spatial distribution of the stress under the indenter and concomitant plastic deformation are very complex, it is of fundamental interest to find the relationship between the hardness H and tensile yield strength Y, $H = C \cdot Y$, where C is the constraint factor. The tensile yield strength Y is defined as the stress under which, after unloading, the remnant plastic strain amounts to 0.2%.[2,5,6] We discuss the constraint factor of different materials briefly in Appendix B.

Intrinsically super- [$H \geq 40$ GPa; cubic boron nitride (c-BN) 46–48 GPa] and ultrahard ($H \geq 70$ GPa; diamond 70–100 GPa) materials attain high hardness through their large intrinsic strength, which is achieved by strong covalent bonds and a high coordination number in all three dimensions, whereas extrinsically super- and ultrahard materials reach such hardness as a consequence of their nanostructure which impedes plastic deformation. One notices that under the conditions of fully developed plasticity, there are many defects, such as dislocations, slips, twinning, stacking faults, and the like. Therefore, the practically achievable strength is orders of magnitude lower than the theoretical (ideal) strength of a perfect crystal. Consequently, the plastic hardness describes the behavior of a heavily defect material.

Although the plastic indentation hardness will be the focus of the present paper, one has to keep in mind that for many applications also other properties, such as high fracture toughness, low coefficient of friction, high oxidization and corrosion resistance, chemical inertness to the material being machined, and others are equally or even more important.

Diamond is the intrinsically hardest material because of its strong nonpolar covalent C-C bonds and the high coordination number of 4. It is a metastable polymorph to graphite (the enthalpy of the transformation $\Delta H \approx +1.9$ kJ/mol), but the graphite-to-diamond as well as the reverse transformation requires a very high activation energy of about $\geq$700 kJ/mol, comparable with the evaporation enthalpy of graphite, to promote the carbon atoms from the sp^2 state of electronic structure to the sp^3 hybridization (and vice versa).[7,8] Diamond also has very high elastic moduli, in particular, the shear modulus $G \approx 553$–576 GPa (Refs. 5, 7, and 9), which is relevant for plastic deformation.[2,5] The frequently quoted

a)Electronic mail: stan.veprek@lrz.tum.de

experimental correlation of shear modulus with hardness, which however shows large scatter,[10] reflects the fact that the stress needed for the multiplication and propagation of dislocations ("crystal plasticity"[11]) is proportional to G, and similar dependence on G is expected also for other mechanisms of plastic deformation, such as slip, twinning, and the like.

Large values of elastic moduli, however, do not guarantee high hardness because upon plastic flow, when the shear strain reaches high values on the atomic level, electronic instabilities, and transformation to softer phases may occur and limit the achievable strength and hardness, as we shall discuss in the following section. Diamond also transforms into graphite upon shear within the $(111)[11\bar{2}]$ slip system[12] (see also Fig. 2 in Ref. 13), but because of its simple electronic structure and strong nonpolar covalent bonds, this transformation requires a very high shear stress of about 80–90 GPa (Refs. 9 and 12–14), as observed also experimentally upon indentation.[15] The intrinsic hardness of natural diamond at room temperature is between about 70 and 100 GPa (Ref. 7), but it can be enhanced above 100 GPa due to solid solution hardening when, e.g., several hundred parts per million (ppm) of the carbon atoms are substituted by nitrogen to impede dislocation motion, as frequently found in industrial diamonds.

Although diamond will most probably remain the intrinsically hardest material, many attempts have been done recently to synthesize or theoretically predict new superhard materials, which could approach the hardness of diamond. These attempts will be briefly illustrated in the next section to show that electronic instabilities upon finite shear limit many materials with high values of elastic moduli to be superhard. This will lead us to the conclusion that the most promising way toward the preparation of new super- and ultrahard materials is the design of nanostructured ones.

Li *et al*. were the first researchers who reported about the large hardness enhancement up to 70 GPa when silicon has been added to TiN, as shown in Fig. 1.[16] The films have been deposited on steel by means of plasma chemical vapor deposition (PCVD) from a mixture of $TiCl_4$, $SiCl_4$ with excess of hydrogen and nitrogen (gas flow H_2:N_2:($TiCl_4$ + $SiCl_4$) = 2:1:0.4) at a temperature of 560 °C. The hardness has been measured on films of thickness "larger than 5 μm"

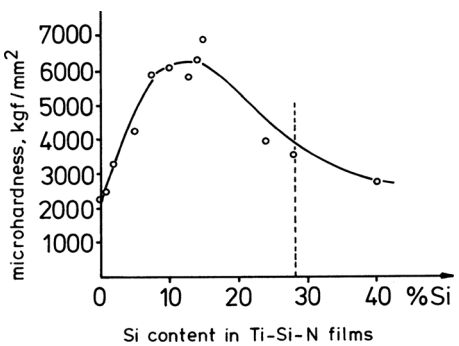

FIG. 1. Microhardness of the Ti-Si-N films deposited by Li Shizhi *et al*. (Ref. 16) (see text). Reprinted with Permission from Li *et al*., Plasma Chem. Plasma Process. **12**, 287 (1992). Copyright 1992, Springer.

by the conventional two steps Vickers method at a relatively large load of 50 gf (about 490 mN). Therefore, the high values of the hardness of 60–70 GPa reported by Li *et al*. are reliable, and they in fact underestimate the actual hardness due to the effect of the much softer steel substrate and high load used, as explained below.

The decrease of the hardness of the coatings, found by Li *et al*. several months after their preparation, characterization, and publication of the paper,[16] has been believed at first to be caused by the relatively high content of chlorine impurities of 2–3 at. %. We shall see later that it is an intrinsic problem of the quasiternary nc-TiN/a-Si_3N_4/$TiSi_2$ nanocomposites (which in fact these researchers had) related to the long-term instability of metastable phases of $TiSi_2$ deposited at relatively low temperature. (Notice that "nc-" stands for "nanocrystalline," "a-" for x-ray amorphous, and the stoichiometry Si_3N_4 symbolizes that silicon is fourfold coordinated to nitrogen, thus showing the same binding energy in x-ray photoelectron spectroscopy (XPS) as in stoichiometric Si_3N_4.) Li *et al*. reported also a second, minor Si-containing component which they attributed to elemental Si. Later on it has been identified as $TiSi_2$,[17] i.e., Li *et al*. had in fact the quasiternary nc-TiN/a-Si_3N_4/$TiSi_2$ nanocomposites, whose hardness is, however, also not stable on the time scale of 6–8 months even if the Cl impurity content is below about 0.6 at. % (Ref. 18). (Veprek *et al*. originally suggested that about 1–2 monolayers thick Si_3N_4-like interfacial layer is amorphous,[19,20] but later on they changed it to "x-ray amorphous."[18] Because there must be some pseudomorphic correlation between TiN and Si_3N_4-like interfacial layer, we shall in the following drop the "a" as it is confusing the readers.)

Li *et al*. originally attributed the hardness enhancement to precipitation hardening of Si_3N_4 (identified by means of XPS) within the TiN crystals. However, when we have later on, in collaboration with Li, evaluated the x-ray diffraction (XRD) patterns of their and our coatings, we realized that the size of the TiN nanocrystals significantly decreased upon the addition of Si, down to 3–4 nm at Si content of about 7–10 at. %, where the maximum hardness has been achieved.[19,20] Because precipitation of Si_3N_4 within such small TiN nanocrystals cannot occur, another explanation of the large hardness enhancement had to be found.

The resistance of well consolidated polycrystalline materials to plastic deformation increases with decreasing crystallite size down to about 10–15 nm, because the grain boundaries are impeding the plastic flow.[2,5,11] Therefore, one finds a strength and hardness enhancement upon refinement of the crystallite size or formation of nanosized heterostructures. In such a way, the pioneering work of Li *et al*. has initiated the research on the development of the stoichiometric, quasibinary superhard nc-TiN/Si_3N_4 and related nc-TmN/Si_3N_4 (Tm—transition metal forming hard and stable nitrides) nanocomposites, which are stable over many years,[18] and which will be the focus of this review with respect to fundamental science as well as to industrial applications. We also include short sections about the Ti-B-N system and about the possibility of the design of oxide-based

nanocomposites because these systems are of great importance for both fundamental research and applications.

Another important class of superhard nanostructured materials represents the heterostructures prepared by deposition of a repeated sequence of few nanometers thin layers of two different materials with large difference in shear moduli. The idea of this mechanism of strenghtening has been elaborated by Koehler:[21] When the thickness of the layers is so small that no dislocation multiplication source can operate, a dislocation, which was present in the layer with a smaller shear modulus $G(1)$ will, upon applied strain, move toward the interface with the stronger layer with $G(2) > G(1)$, but the elastic image back-force induced in that layer by the strain of the dislocation core will impede the dislocation to cross that interface. This mechanism of strengthening has been verified on a number of heterostructures formed of immiscible metals for strengthening in tensile tests.[22,23] When the heterostructures have been made of hard transition metal nitrides, superhardness of ≥ 40 GPa has been achieved at a period of several nanometers by several research groups[24–30] (see reviews Refs. 31–33 for further papers). However, when the lattice period decreases below about 4–5 nm, the hardness decreases because of the roughness of the interfaces.[34]

This softening may appear to be a limitation for the application of the heterostructures as protective coatings on tools because it is impossible to deposit heterostructures with sharp interface in an industrial coating system with at least two targets consisting of different materials and using a rotating turntable on which the tools are mounted. Nevertheless there are reports that show that nanolayered coatings improve the performance of the tools for machining (e.g., Ref. 35).

Interesting are the heterostructures with only one to two monolayers (1–2 ML) thin SiN_x (Refs. 36–38) or oxide[39,40] interfacial layer between several nanometers thick transition metal nitrides slabs. It is not clear if the reported hardness enhancement is due to Koehler's mechanism or to strengthening of the 1–2 ML thin SiN_x or oxide interfacial layers as it will be shown in Sec. III C dealing with the nc-TmN/Si_3N_4 nanocomposites.

In the majority of reports, it is not quite clear which mechanism is responsible for the improvement of hardness of the nanolayered coatings or of the cutting performance of coated tools, because it may be due to the Koehler's mechanism, or to the strengthening of the thin interfacial SiN_x (or oxide?) layer, or to the improvement of fracture toughness. Matthews *et al.* have shown that a modulation of elastic moduli in multilayers hinders the propagation of cracks, thus increasing the toughness of the multilayers as compared with a monoblock single layer.[41] High toughness is important in machining, particularly in interrupted cutting, such as milling. Therefore, we shall briefly discuss the possibilities of toughening of the nanocomposites in a special short section in order to emphasize that hardness is only one of many properties of materials important for applications.

Because the focus of this review is the understanding of the mechanism of hardness enhancement in the nanocomposites, we cannot discuss all the recent papers on heterostructures ("nanomultilayers" and "nanolaminates") and, therefore, we refer only to a few of them (for further details see, e.g., Refs. 29–39 and 42–52). Moreover, as we shall see, the heterostructures can serve as a model for first-principles theoretical study of the mechanism of hardening in the nc-TmN/Si_3N_4 nanocomposites.

Many researchers have reported a significant hardness enhancement when the hard coatings have been deposited by plasma assisted techniques under energetic ion bombardment at relatively low temperatures. Valvoda *et al.* reported a hardness increase of TiN up to 60 GPa (Ref. 53) [intrinsic hardness is about 21 GPa (Ref. 54)], but upon annealing, the hardness enhancement decreased.[55,56] Figure 2 shows other examples reported by Herr and Broszeit for HfB_2,[57] and for ZrN/Cu and ZrN/Ni nanocomposites,[58] which have been deposited by reactive magnetron sputtering by Musil *et al.* [see review (Ref. 59)].

The possible applications of coatings "hardened" by ion bombardment are very limited because of the thermal instability and the very high biaxial compressive stress, which often causes their delamination. However, as we shall see in the section about industrial applications, nc-TmN/Me nanocomposites consisting of a hard transition metal nitride TmN and a ductile metal Me that does not form stable nitrides (e.g., Ni, Cu) can significantly improve the toughness of the coatings (see, e.g., Refs. 60–62), and the performance of tools for forming, stamping, and the like, when deposited at low ion bombardment and sufficiently high temperature in order to avoid the hardness enhancement due to energetic ion bombardment and concomitant high biaxial compressive stress. These coatings are also being considered as wear-protection, load adaptable coatings with high hardness-to-Young's modulus ratio, H/E, for machine parts.[63] The idea behind such applications is that when the H/E ratio is high, the coatings on the machine parts will, under localized high load, deform and adapt elastically to the asperities of the sliding surfaces before undergoing plastic deformation and wear.

In the present paper, we shall not discuss multicomponent hard coatings, such as TiAlN, AlCrN, and others, because it is beyond its scope and because there are many excellent

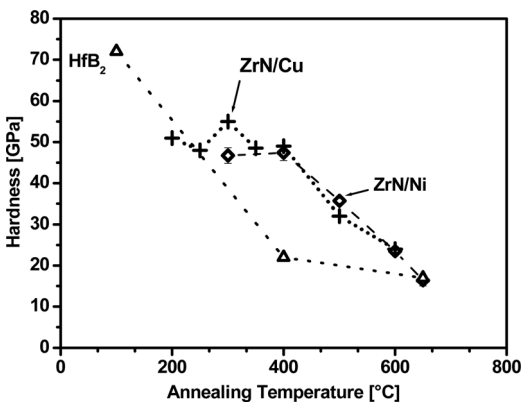

FIG. 2. Decrease of hardness upon annealing of coatings, which have been "hardened" by energetic ion bombardment during the deposition at relatively low temperatures (see text).

papers and reviews available (e.g., Refs. 64–69), particularly the recent ones from Mayrhofer, Schneider, and their coworkers. We shall only briefly touch the multicomponent "high entropy alloys" coatings in order to address an open question. Also, we cannot discuss the very important functional nanocomposite coatings with low coefficient of friction adaptable to changing environment,[70–74] and nanocomposites based on diamond-like carbon (e.g., Refs. 75–77) that find increasing applications as low friction coatings in machine parts.

Because the field of superhard nc-TmN/Si_3N_4 and related nanocomposites has been growing very fast during the last 15 years, we cannot cover all published papers, but we have to make a selection in order to emphasize what do we understand (or believe to understand) today, what we hypothesize (or believe), and what are the open questions to be answered and problems to be solved in the future.

In the next section, we shall briefly discuss the recent attempts to design new intrinsically superhard materials. This will lead us to the conclusion that the most promising way is to "go nano," i.e., to design nanostructured materials with a strong and highly stable nanostructure, and low-energy interfaces or an interfacial layer strengthened by valence charge transfer.

One notices that nanostructured materials are not thermodynamically stable with respect to their coarse-grained poly- or single-crystal counterparts, and therefore, they have to be stabilized against coarsening. For this reason, we also include a short section on their stabilization.

II. RECENT ATTEMPTS TO DESIGN NEW INTRINSICALLY SUPERHARD MATERIALS

More than 27 years ago, when the theoretical first-principles calculations were in early stage of the development and the computing power of the available computers was still limited, Cohen conducted pioneering calculations of bulk moduli of a number of materials and obtained a good agreement with the experimental data.[78] This motivated him and his coworkers to extend the calculations to new materials, such as C_3N_4, a carbon analogous of silicon nitride,[79–81] which had not been synthesized at that time. Because the calculated bulk modulus of C_3N_4 was larger than that of c-BN and close to that of diamond, Cohen *et al.* suggested that the "carbon nitride" should have hardness larger than c-BN and close to that of diamond. However, the experimentally found hardness of amorphous stoichiometric C_3N_4 thin films was below 30 GPa,[82] i.e., less than that of c-BN. (Notice that the strength and hardness of glasses is usually higher than that of their poly- and single crystalline conterparts because the mechanisms of plastic deformation by multiplication and movement of dislocation cannot operate in an amorphous network.) Recently, Zhang *et al.* provided the explanation:[14] using an advanced version of the *ab initio* density functional theory (DFT) code, they confirmed the high values of elastic moduli reported by Cohen *et al.* Moreover, they have shown that upon shear strain of 0.24 within the weakest $(111)\langle 11\bar{2}\rangle$ slip system, the nonbinding electron pairs on nitrogen in cubic C_3N_4 interact with the atomic orbitals of carbon which results in an electronic instability and transformation to a thermodynamically more stable graphitic-like structure which contains double bonds[83] that are typical of carbon in its sp^2 state, such as graphite. This is shown in Fig. 3 as an abrupt decrease of the shear stress of C_3N_4 at a strain of 0.24 and the change of the difference of the total energy with respect to the initial state to a negative value, which indicates the transformation to another, more stable structure. Diamond and c-BN sustain much larger shear strain before the elastic shear stress relaxes to zero due to plastic lattice slip which releases the elastic strain energy, and the total energy returns to its original value.

This is an example par excellence which shows that the electronic stability at large shear strain at atomic level is more important than a high value of elastic moduli, because the latter describe only the reversible resistance of the material against small strain close to equilibrium called "elastic stiffness."

Unfortunately, the early pioneering work of Cohen *et al.*, the recent explanation by Zhang *et al.*, and the fact that the experimentally found hardness of stoichiometric C_3N_4 is below 30 GPa have not been sufficiently appreciated by the scientific community, and the search for new superhard materials based on high values of elastic moduli (or "low compressibility," i.e., high bulk modulus) continues, mostly by first-principles calculations either in calculating the elastic moduli of "new" and even exotic materials, or by calculating the "hardness."[84–87] Such calculations are relatively easy nowadays as many well developed and tested first-principles codes are available either at a modest price or even as open source free of charge for the academia, and they are much easier to conduct than the time consuming experimental work in the laboratory, which also requires more expensive equipment.

The theoretical calculation of hardness, as found in the Refs. 84–87, is essentially equivalent to the approach of Cohen *et al.* based on elastic moduli because the authors of these papers calculate the valence charge density of the material in equilibrium (i.e., at zero strain), which determines

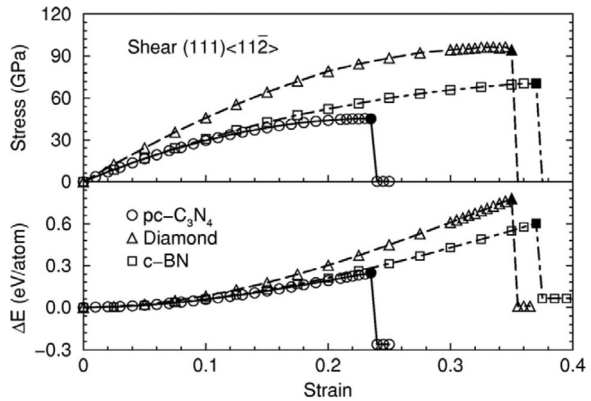

FIG. 3. Calculated stress–strain relationship (top) and changes of total energy (bottom) as function of shear strain in the $(111)\langle 11\bar{2}\rangle$ slip system for cubic C_3N_4 (see text). Reprinted with permission from Zhang *et al.*, Phys. Rev. B **73**, 144115 (2006). Copyright 2006, the American Physical Society.

the bulk modulus.[78–80] By fitting of the proportionality constants, the researchers correlate these values with the hardness of several known materials (diamond, c-BN, Si, etc.). Thus, this "hardness" describes only the resistance of the ideal crystal free of defects in equilibrium to reversible, small deformations, i.e., the elastic stiffness, but not the "plastic" hardness. We shall illustrate this problem by two examples.

Osmium has probably the highest bulk modulus B_0 of 395–462 GPa among transition metals,[88] which is in the range of diamond [$B_0 \approx 443$ GPa (Ref. 7)], but low hardness of about 4 GPa (Ref. 89) because of nondirectional metallic Os-Os bonds. Also, other 5d transition metals, such as Re, W…, have very high bulk moduli but low hardness.[90,91] Therefore, it has been suggested to synthesize borides of 5d transition metals where the presumably strong covalent bonds of boron with the metal should allow reaching superhardness. However, the hardness of OsB_2 is only $\leq$20 GPa (Ref. 92) because it displays soft behavior within the (001)[010] slip system due to metallic-like shear of the (001) Os-Os layers. The ideal shear strength within this slip system of 9.1 GPa is only slightly higher than that of pure iron of 7.2 GPa.[93]

Rhenium diboride, which consists of boron layers intercalated between hexagonal densely packed layers of Re atoms, has also a very high shear modulus G of 257 GPa, but the correctly measured load-invariant hardness of less than 30 GPa,[94] although a value of 48 GPa, which has been measured at the lowest load of 0.49 N,[95] is being frequently incorrectly quoted as the hardness of ReB_2.[92] The reason are complex electronic instabilities upon shear due to crystal field splitting of the 5d orbitals and their interaction with the surrounding boron network, which results in a much lower plastic shear resistance (the slope of the stress–strain dependence at the given strain) as compared to the equilibrium structure (slope of the stress–strain curve close to $\varepsilon \rightarrow 0$), as shown in Fig. 4.[94] The relatively weak Re-B bonds break at strain larger than 0.29 and recover again at strain 0.5 (see Fig. 2 in Ref. 94). M_1 and M_2 are metastable phases because the stress passes through zero and the total energy goes through a local minimum, being however larger than that in equilibrium at zero strain. The boron layers' network intercalated between the Re atomic layers holds the system together up to a strain of 1.6. At strain of about 1.7, where the original structure should recover because it corresponds to a slip by one structural unit (see Fig. 6 in Ref. 94), the system becomes inherently unstable as seen from the decrease of the shear stress with increasing strain in Fig. 4, and the whole system disintegrates because the B-B bonds break (see Fig. 7 in Ref. 94).

These complex electronic and structural transformations upon shear, which develop beneath the indenter during the hardness measurement, are most probably responsible for the sluggish approach of the enhanced measured hardness to the correct load-invariant one at large load of >6 N (see Fig. 2A in Ref. 95). As we shall see later, materials which do not undergo electronic instabilities and have well-defined carriers of the plastic flow, such as the grain boundaries in the nanocomposites discussed below, reach load-invariant hardness already at a small load of 30–50 mN.

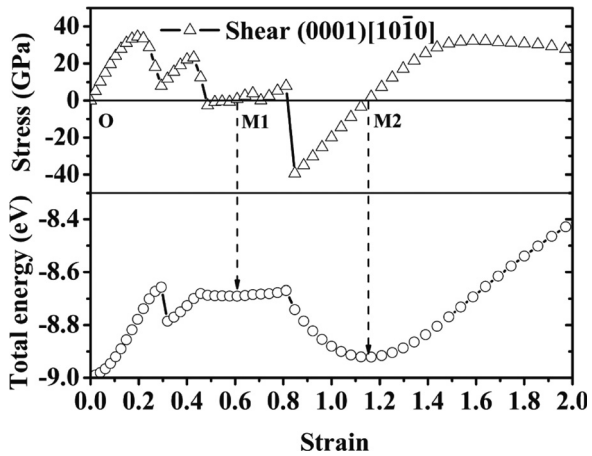

FIG. 4. Dependence of the stress and total energy on the shear strain within the (0001) plane in the [10$\bar{1}$0] direction. The strain point O corresponds to the equilibrium stable hcp-derived structure, and the points M1 and M2 correspond to two metastable trigonal structures formed during the shear-induced phase transformation. Reprinted with permission from Zhang *et al.*, Phys. Rev. Lett. **108**, 255502 (2012). Copyright 2012, the American Physical Society.

Similar instabilities upon shear have been reported also for some other materials, but systematic studies are rare because, as mentioned, the search for new intrinsically superhard materials focuses mainly on those with high elastic moduli because of still prevailing believe that high values of elastic moduli guarantee high plastic hardness. (Another reason might be that the first-principles calculations of the plastic deformation upon shear are much more complex than the calculations of equilibrium properties.) Moreover, there are materials, such as boron suboxide B_6O, which, although having smaller moduli than 5d Tm diborides, have higher hardness of 45 GPa because of their strong three-dimensional boron bond network [see review (Ref. 90) and references therein].

Of interest is c-BC_5 because of its high load-invariant hardness of 71 GPa (Refs. 96 and 97) in spite of much lower ideal shear strength than that of c-BN whose hardness is about 46–48 GPa.[98] The properties of this "heavily boron-doped diamond" material have been reported by Jiang *et al.* who found that there is a relatively weak ordering tendency and small differences in the mechanical properties of ordered and disordered structures both being strong.[99] Therefore, it is unlikely that c-BC_5 is intrinsically harder than c-BN. The explanation for its high hardness is the crystallite size of 10–15 nm of the material prepared by high-temperature and high-pressure synthesis reported in Ref. 97. This is in the range of the so called "strongest size," where the Hall-Petch strengthening due to decreasing crystallite size is balanced by grain boundary shear (also called "sliding"), which becomes dominant upon a further decrease of the grain size,[11,100,101] as it will be discussed in the next section. Let us emphasize that a similar explanation has been proposed also for c-BC_2N,[103] which also has hardness higher than c-BN[102] although its ideal shear strength, calculated by first-principles method, is also lower than that of c-BN.[103]

These results suggest that the most promising way toward the design of new superhard materials is to synthesize nanosized and nanostructured materials as we shall discuss in the next section, which will begin with the discussion of the stability of nanosized materials against coarsening.

III. EXTRINSICALLY SUPERHARD NANOSTRUCTURED MATERIALS AND NANOCOMPOSITES

A. Thermal stability of nanostructured materials

Fine-grain polycrystalline materials are thermodynamically unstable with respect to their coarse-grained poly- or single-crystal counterparts and, therefore, they undergo coarsening ("Ostwald ripening") when annealed to about $\geq$40% of the melting point T_m(K), where diffusion becomes sufficiently fast.[6] In order to be of any practical use in applications where the systems reach a higher temperature, nanosized materials have to be "protected" against this coarsening. Therefore, the question arises as how to avoid coarsening in nanosized and nanostructured materials.

The Gibbs free energy $\Delta G_f^0(r)$ of a nanocrystal of radius r per unit volume is given by Eq. (1), where ΔG_f^0 is the standard Gibbs free energy of coarse grained bulk material and γ_{Surf} is the surface energy. If the material under consideration is stable in bulk, the standard Gibbs free energy is negative, $\Delta G_f^0(\infty) < 0$ (or zero for elements in their standard state), but the surface energy ("surface tension") is always positive $\gamma_{Surf} > 0$ because of missing chemical bonds at the surface, i.e., it is destabilizing the nanocrystal. This is reflected in many phenomena, such as decrease of melting point, hysteresis of the transition pressure of structural phase transition, localization of electronic states, plasmons, and phonons, increasing catalytic activity etc., with decreasing crystallite size[104–106]

$$\Delta G_f^0(r) \cong \Delta G_f^0 + \frac{3 \cdot \gamma_{Surf}}{r}. \quad (1)$$

In the case of nanostructured materials where the nanocrystals are connected via grain boundaries, a similar relationship as Eq. (1) applies, but the surface energy is replaced by the energy of grain boundaries $\gamma_{G.B.} > 0$, which represents the thermodynamic driving force for coarsening ("grain growth"[107] and "recrystalization"[6]). Thus, if one wants to utilize, at elevated temperature, the unique properties of nanostructured materials derived from the small crystallite size, the coarsening due to recrystallization has to be avoided. This can be achieved either by controlling the kinetics or the thermodynamics of the system as discussed, e.g., in Chapter 3 of Ref. 107 and in the recent review.[108] The kinetic approach aims to reduce the recrystallization by hindering the grain boundary diffusion whereas the thermodynamic approach is based on a decrease of the energy of grain boundaries $\gamma_{G.B.}$, which decreases the thermodynamic driving force for coarsening. Because we focus here on hard and superhard nanostructured materials, which should be applied as wear protection coatings under harsh environmental conditions and at high temperatures, we focus on the thermodynamic approach. However, it should be kept in mind that there is probably neither a pure thermodynamic nor kinetic stabilization in the superhard nc-TmN/Si_3N_4 nanocomposites because the thermodynymic stabilization of the Si_3N_4 interfacial layer and the very high immiscibility of the stoichiometric and pure TiN and Si_3N_4, which will be described later, simultaneously hinder the diffusion of Ti-atoms through the Si_3N_4 interfacial layer thus kinetically impeding the coarsening of the TiN nanocrystals.

The lowering of the grain-boundary energy is achieved in a multicomponent system by the segregation of one component (solute atoms) into the grain-boundary of the nanostructured solvent.[107–114] A typical example is the segregation of impurities, such as oxygen[64,115–118] or carbon[64,119] into the grain boundaries, which refines the nanostructure and stabilizes the grains against growth. However, in many cases, such grain boundary segregation of impurities will result in an embrittlement of such a nanocomposite, as it is the case with bismuth in copper, oxygen in Al-films, and in the Ti-Si-N nanocomposites to be discussed later. A special case of thermodynamic stabilization of nanocomposites is the formation of a nanostructure in a spinodally decomposed quasi-binary system, such as TiN-Si_3N_4, which stabilizes the nc-Tm/Si_3N_4 nanocomposites against coarsening up to temperatures of 1100 to 1200 °C for nc-TiN/Si_3N_4 (Ref. 18) and nc-$(Ti_{1-x}Al_x)N/Si_3N_4$,[120] respectively. Such a high stabilization is remarkable because the coarsening temperature corresponds to 64–68% of homologous temperature, which is the ratio of the absolute temperature (in Kelvin) of the system to the decomposition temperature of Si_3N_4 of 2151 K at 1 atm. of N_2,[121] and it is significantly higher than the thermal stability of the metastable solid solution $(Ti_{1-x}Al_x)N$, which decomposes above 800–900 °C by spinodal mechanism.[56]

However, one should not generalize this stabilization by Si_3N_4 interfacial layer because it depends on the given Tm-Si-N system. The results available so far seem to suggest that the high thermal stability and oxidation resistance will be found only in systems that decompose by spinodal mechanism forming coherent or semicoherent grain boundaries. Therefore, large attention should be paid to this problem in the future studies. Another interesting mechanism of the stabilization of nanosized materials is their formation by twinning because the energy of the coherent twin boundaries is order of magnitude lower than that of grain boundaries in polycrystalline materials.[122,123]

B. Hardness enhancement by crystal size refinement toward "the strongest size"

The strength and hardness of materials increases with decreasing crystallite size d according to the Hall-Petch mechanism proportionally to $d^{-0.5}$ due to decreasing dislocation activity ("crystal plasticity"[11]) because the grain boundaries are impeding the multiplication and propagation of dislocations.[2,11,124,125] A similar dependence is also found for other shear mechanisms of plasticity such as twinning, slip, and others[126–128] when the boundaries impede the deformation carriers through developing elastic back-stresses

that appear when such transformations are arrested at grain boundaries. There are many examples for such increase of the strength including metals, which are however relatively soft.[107,129,133] The hardness of c-BN increased from about 42 GPa for coarse-grain samples with average crystallite size of 2000 nm to a maximum of about 60 GPa when the crystallite size decreased to 40 nm, and in the case of ultrahard nanocomposites consisting of c-BN and wurtzite BN (w-BN), the maximum load-invariant hardness reached 85 GPa at crystallite size of 14 nm.[130] Solozhenko *et al.* reported hardness increase of single-phase c-BN to load-invariant value of 85 GPa when the crystallite size decreased to about 20 nm.[131] (A crystallite size below 20 nm has not been experimentally accessible in that work.[132]) However, when the crystallite size decreases below about 10–15 nm, the hardness decreases due to increasing grain-boundary shear as shown for many metals,[107,129,133] as well as for c-BN and c- and w-BN in Ref. 130. Therefore, Yip and Argon called this regime "the strongest size."[11,100,101]

Notice that "the strongest size" of about 10–15 nm applies only for well-consolidated materials with low porosity, such as thin films deposited by CVD or PVD. For nanocrystalline materials prepared by gas phase condensation followed by consolidation,[107] the maximum hardness may appear at a higher crystallite size.[107,129] This is also seen when comparing the results of Dubrovinskaia *et al.* for the c-BN and c- and w-BN nanocomposites[130] with those of Solozhenko *et al.* who prepared single-phase c-BN.[131] In order to avoid the formation of w-BN, Solozhenko *et al.* have used, for their high-pressure and high-temperature synthesis, pure turbostratic hexagonal BN prepared by CVD. Obviously, such nanocrystalline c-BN has been better consolidated and did not show any grain boundary shear down to grain size of 20 nm, which is lower than the 40 nm where the maximum hardness has been found for c-BN in Ref. 130, but still above the "strongest size" of 10–15 nm.[11,100,101] Unfortunately, more detailed studies are not available because the high-temperature and high-pressure synthesis used for the preparation of these materials is difficult and time consuming.

Argon and Yip provided an analytical model, which describes the transition between hardening and softening upon decreasing crystallite size for copper[11,101] whereas Carsley *et al.*[134] presented a phenomenological model, which allows one to fit the experimental data according to Eq. (2)

$$H(d) = f_C \cdot (H_0 + \beta \cdot d^{-0.5}) + (1 - f_C) \cdot H_{G.B}. \quad (2)$$

Here, f_C and $(1 - f_C)$ is the volume fraction of the crystalline material and of the grain boundaries, respectively, H_0 is the intrinsic hardness of coarse grained material and $H_{G.B.}$ is the "hardness" of the grain boundaries.

Figure 5 shows schematically the fraction of the atoms within the grain boundaries [Fig. 5(a)] and the dependence of the hardness on crystallite size [Fig. 5(b)]. Although the exact dependence of the fraction of atoms within the grain boundaries depends on the thickness of the grain boundaries

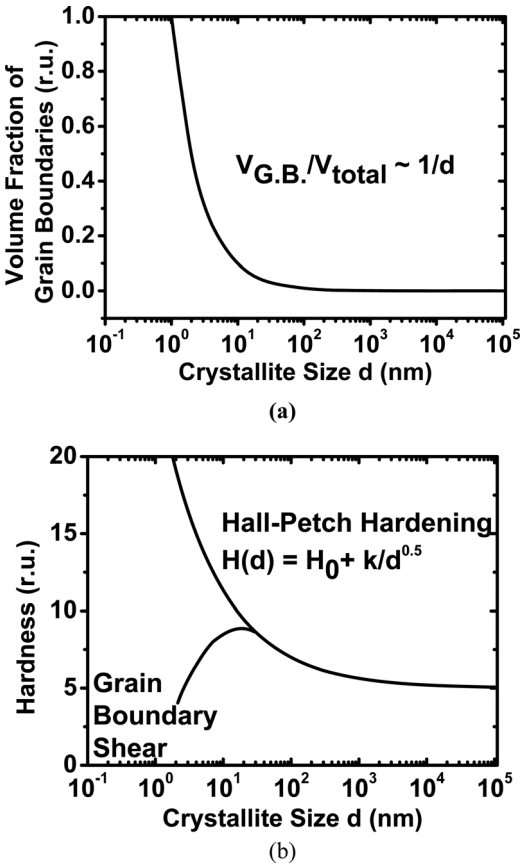

FIG. 5. (a) Dependence of the fraction of the softer materials within the grain boundaries (notice that the actual volume fraction will depend on the thickness of the grain boundaries); (b) schematic dependence of the hardness on crystallite size. Reprinted with permission from Veprek and Veprek-Heijman, Thin Solid Films **522**, 274 (2012). Copyright 2012, Elsevier B.V.

and on the shape of the nanocrystals, the strong increase, which is seen below about 10 nm, is general.[104–106] This explains in a natural manner why the "strongest size" in well-consolidated nanostructured materials is around 10–15 nm.

The mechanism of hardening by decreasing the crystallite size down to 10–15 nm is of general nature, and it is expected to operate in any well-consolidated material regardless how the crystallite size has been controled, provided of course the grain-boundaries will not embrittle due to segregated solute material. In the case of thin films deposited by plasma-assisted techniques, the crystallite size can be decreased, e.g., by energetic ion bombardment, as illustrated in Fig. 6 for nanocrystalline silicon deposited by chemical transport in hydrogen plasma.[135] As mentioned above, in the case of hard transition metal nitrides, borides, and carbides coatings deposited at low temperature, this kind of refinement combined with the formation of point defects, interstitials, biaxial compressive stress, and other effects of the ion bombardment, whose the synergistic effects are not fully understood, may result in a large hardness enhancement to $\geq$40 GPa, which is, however, not stable upon annealing, as mentioned above and shown in Fig. 2. If such coatings are deposited at sufficiently high temperature where the ion bombardment damage anneals out, the refinement of the

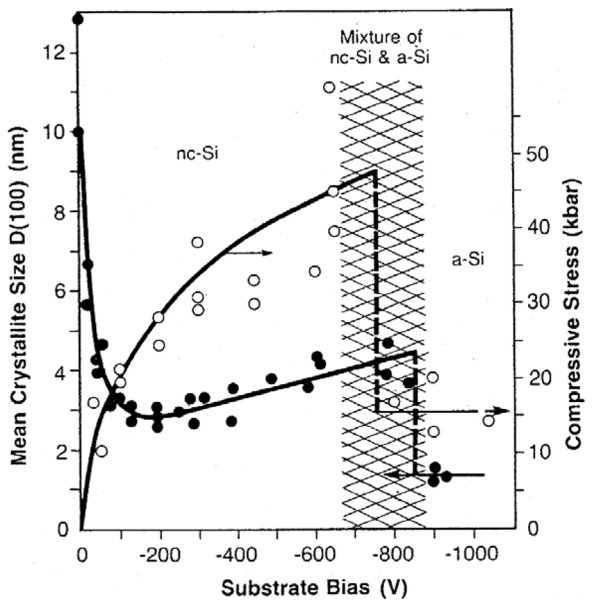

FIG. 6. Dependence of crystallite size and biaxial compressive stress of nanocrystalline silicon on substrate bias, and the crystalline-to-amorphous transition induced by radiation damage. Reprinted with permission from Veprek *et al.*, Phys. Rev. **36**, 3344 (1987). Copyright 1987, the American Physical Society.

nanostructure can still be achieved when coarsening is absent.

Another way to reduce the crystallite size is the deposition of multicomponent, metastable solid solutions which undergo decomposition that may result in hardness enhancement by a factor of about 1.5–2, as found for c-BN, c- and w-BN nanocomposites mentioned above as well as for many other materials.[107,129] Unfortunately, in the majority of the papers dealing with the nanocomposite thin films, this effect has not been studied in sufficient detail, but the present author believes to have recognized in several papers, where a maximum of the hardness enhancement has been reported in a multicomponent system, that it apparently correlated with a refinement of the crystallite size to 10–15 nm (see, e.g., the AlN/Si_3N_4 nanocomposites reported by Patscheider *et al.*[136–139]).

Another interesting example are the so called "**high entropy alloys**" coatings, which have been pioneered by Yeh *et al.* who deposited multicomponent nitride coatings consisting of many elements, such as (AlCoCrCuFeN)N, (AlCrNiSiTi)N,[140] (TiAlCrSiV)N,[141] (AlCrMoSiTi),[142] (AlCrNbSiTiV)N,[143,144] (AlBCrSiTi)N,[145] and many others, as well as oxides (AlCrTaTiZr)O_x.[146] This field became very popular as demonstrated by many papers of other groups (TiAlCrSiY)N,[147] (AlCrTaTiZr)N,[148] (AlCrTaTiZr)NC_y,[149] (TiVCrHf)N,[150] and others, where the high mixing entropy is supposed to stabilize the solid solution and the maximum hardness of 30–36 GPa is achieved with crystallite size around 10–15 nm. However, in the majority of these papers, the oxygen impurities are not reported and if they are, they are quite high up to 3–4 at. % (Refs. 151 and 152) or even 6 at. %.[153] As shown by Barna *et al.*, oxygen and other impurities can lead to the refinement of the crystallite size and morphology[64,117] of the growing films, but such impurities are also likely to cause grain boundary embrittlement. Therefore, it is difficult to decide in each particular case what is the exact mechanism of hardness enhancement: solution hardening, nanostructure refinement, and formation of nanocomposites?

The open question regarding the "high entropy alloys" is the value of the mixing enthalpy, which has not been reported but, which, according to the opinion of present author, may be quite high and destabilize the solid solution resulting in decomposition by nucleation and growth and concomitant refinement of the crystallite size. The decomposition is particularly likely to occur in systems which contain silicon and boron because the stoichiometric transition metals nitrides and Si_3N_4 as well as BN are strongly immiscible.[154]

For a simple binary (or quasibinary when A and B are compounds) $A_{1-x}B_x$ system, the Gibbs free energy of the solid solution is given by Eq. (3).[155] The first and second terms are the contributions of pure terminal phases A and B, the third term is the mixing entropy, and the last term is the mixing enthalpy with L_{AB} being the interaction parameter. Because $1-x<1$ and $x<1$, the mixing entropy is negative, i.e., it is stabilizing the solid solution, and this stabilization increases with increasing temperature

$$\Delta G_{A_{1-x}B_x} = (1-x)\Delta G_A + x\Delta G_B + RT[(1-x)\ln(1-x) + x\ln x] + a(1-x)xL_{AB}. \quad (3)$$

The idea behind the "high entropy alloys" coatings is the expectation that the more components in the solution the more negative the mixing entropy, and the more stable will be the solid solution.

However, when the interaction parameter $L_{AB}>0$, the mixing enthalpy term may destabilize the solution, particularly at a relatively low temperature of several hundred degrees centigrade, at which the coatings are usually deposited and used. (Notice that the interaction parameter is temperature dependent. If $L_{AB}>0$ at low temperature, it will decrease with increasing temperature, i.e., the stabilizing mixing entropy term will become dominant, and all phases will be miscible in the melt.) The destabilization will occur when the binding energy A-B is lower than the average value of binding energies A-A and B-B. When the positive mixing enthalpy will be sufficiently large, the solid solution will be unstable and, depending on the particular system, the destabilizing contribution of the mixing enthalpy may—with increasing number of components—increase faster than the stabilizing effect of the mixing entropy, particularly at relatively low deposition temperature.

This question has not been discussed in the literature on "high entropy alloys," and it will be difficult to answer it because the values of interaction parameters would have to be obtained by first-principles calculations, which are almost impossible to conduct for a random multicomponent systems containing five to six metal atoms, like those quoted above.

The advantage of the method of hardness enhancement due to refinement of the nanostructure toward the "strongest size" is its almost general validity, but its disadvantage is that the hardness enhancement is limited due to the grain boundary shear to about a factor of 1.5–2. Thus, the question arises if one could overcome this problem by forming a "strong interface."

One interesting possibility is to refine the crystallite size by the formation of twin boundaries at nanoscale, as found in face-centered cubic structure for the (111) mirror planes at which the normal stacking sequence of the (111) planes is reversed. We recall that the energy of twin boundaries is order of magnitude smaller than that of conventional large angle ones.[122] In the case of nanotwinned c-BN, a large enhancement of the Vickers hardness up to 108 GPa has been reported at applied load of $\geq$2 N and average twin thickness of about 3.8 nm, i.e., significantly below the "strongest size" of 10–15 nm.[123] Simultaneously, also the fracture toughness increased to 12.7 MPa·$m^{1/2}$, which is about four-times larger than that of c-BN single crystal, and the onset of oxidation temperature increased to about 1294 °C as compared with 1100 °C for single crystal c-BN. The authors of Ref. 123 attributed the large increase of the hardness to a combined effect of the smaller crystallite size and quantum confinement.

Also, stacking faults formed during severe plastic deformation upon repeated rolling resulted in a significant increase of the strength of Mg-alloy. The tensile yield strength and ultimate strength increased linearly with the reciproce value of the average distance between the stacking faults up to 575 and 600 MPa, respectively, for average distance of about 15 nm. This is a record value for this material.[156] In the case of nanotwinned Cu, the maximum strength has been found at twin thickness of about 15 nm followed by its decrease with a further decrease of the twin thickness.[122] Thus, the mechanism of strengthening with low-energy interfaces, such as twins and stacking faults, although of fundamental interest, is not sufficiently universal for a broader range of applications. Therefore, in the next section, we shall discuss a more general mechanism of strengthening, which occurs in nc-TmN/Si_3N_4 nanocomposites by the formation of an Si_3N_4-like interfacial layer that is strengthened by valence charge transfer from the transition metal nitride.

C. Hardness enhancement in nc-TiN/Si_3N_4 and related nanocomposites by self-organization upon spinodal decomposition and strengthening of the interfacial Si_3N_4

1. Formation of the nanostructure

During the deposition of the multicomponent coatings, such as Ti-Si-N or Ti-Al-Si-N, by plasma CVD, reactive sputtering, or vacuum arc evaporation from an alloyed target or from two LARC® cylindrical cathodes placed close to each other (see Sec. IV), the fluxes of different atoms toward the surface of growing film are random, i.e., a solid solution is formed in the initial stage. If the demixing driving force is sufficiently high and the diffusion fast [i.e., the deposition temperature is sufficiently high of about 550 °C (Refs. 20, 157, and 158)], the solid solution will decompose, and the formation of strong nanocomposite nanostructure will be completed during the growth of the film. For high deposition rates of $\geq$1 nm/s achieved in plasma CVD and high-rate magnetron sputtering of Tm-Si-N system, the decomposition is kinetically controlled by bulk diffusion because, in a typical Tm-SiN- system, the deposition of the mixed phase is faster than the Si-diffusion.[157,158]

There are two possible mechanism of the decomposition of such thermodynamically unstable ($\Delta G_{A_{1-x}B_x} > 0$) solution: (1) by the nucleation and growth when the second derivative of the Gibbs free energy with composition is positive, $d^2\Delta G_{A_{1-x}B_x}/dx^2 > 0$, and (2) by the spinodal mechanism when $d^2\Delta G_{A_{1-x}B_x}/dx^2 < 0$.[155,159,160] (For the meaning of the term "spinodal" see, Refs. 161 and 162.) (Note that the negative second derivative is the criterion only for chemical spinodal, because for coherently spinodal to occur one has to account also for the elastic strain energy between the decomposed phases.[159,160] We do not elaborate this problem here in more detail because for the model Ti-Si-N system the demixing energy is very high, orders of magnitude higher than the elastic strain energy of the interfaces.[157] But the problem of elastic strain energy may be crucial for systems, such as AlTiN, AlCrN, and others, which show order of magnitude smaller demixing energy.) In a system with very high demixing energy and $d^2\Delta G_{A_{1-x}B_x}/dx^2 < 0$ within the whole range of composition $0 < x < 1$, such as the Ti-Si-N, the spinodal decomposition results in a fairly regular nanostructure with sharp grain boundaries and fairly uniform crystallite size (see, e.g., Fig. 12-12 in Ref. 160 and Fig. 6.14b in Ref. 163), whereas a nanostructure formed upon the nucleation and growth consists of nanocrystals with relatively broad size distribution and not necessarily sharp grain-boundaries (see, e.g., Fig. 6.14a in Ref. 163). Therefore, systems which are spinodal with a large demixing energy are probably more promising for the design of new, superhard nanocomposites than those decomposing by nucleation and growth. In order to prove this hypothesis, experiments with clean systems, i.e., low impurities in the range of few 100 ppm or less, are highly needed. Unfortunately, the majority of the published coatings contains up to several at. % of oxygen, carbon and other impurities.[189]

Because the Ti-Si-N system has been mostly studied as a "prototype" one, we shall discuss briefly the formation of its nanostructure. Figure 7 shows the Gibbs free energy of the formation of Ti-Si-N solid solution at a typical deposition temperature of 837 K for different pressures of nitrogen with TiN and Si_3N_4 chosen as reference states, which means that the first and second term in Eq. (3) vanish.[157] One can see that even at the relatively low nitrogen pressure used during the deposition by reactive magnetron sputtering (e.g., Refs. 164–167 and many other papers), the Gibbs free energy is positive and its second derivative is negative, i.e., the system is chemically spinodal. At the composition of about 20% of Si_3N_4 corresponding to that of the nc-TiN/Si_3N_4 nanocomposites with the maximum hardness, the demixing energy is

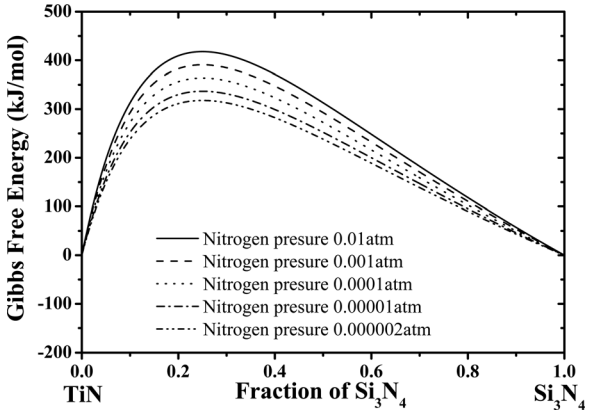

FIG. 7. Gibbs free energy of the formation of mixed TiN + Si_3N_4 system at temperature of 873 K (corresponding to the upper limit of the deposition temperature used) for five different pressures of nitrogen used in the experimental work with stoichiometric TiN and Si_3N_4 chosen as reference states. Reprinted with permission from Zhang and Veprek, Mater. Sci. Eng. A **424**, 128 (2006). Copyright 2006, Elsevier B.V.

about 300 kJ/mole even at the lowest nitrogen pressure used during reactive sputtering, which is about two orders of magnitude higher than the elastic energy of an incoherent interface.[157] Therefore, there is hardly any doubt that the decomposition is spinodal in this system provided the impurity content is small of only few 100 ppm (0.01 at. %) as it has been in our early work (see below). In Ref. 157, the interaction parameter L_{AB} has been estimated from the experimental data reported for $Ti_5Si_3N_4$. Later on, these results have been confirmed by combined first-principles DFT calculations of the interaction parameter combined with thermodynamic modeling in Ref. 168.

Figure 8 shows a medium resolution transmission electron micrograph (TEM) of (a) the nc-TiN/a-Si_3N_4 nanocomposite deposited by plasma CVD (Refs. 19, 20, and 169) and (b) of the nc-$(Al_{1-x}Ti_x)$N/a-Si_3N_4 nanocomposite coating deposited by vacuum arc evaporation in an industrial coating unit of company SHM.[170] The nanostructure of nc-TiN/Si_3N_4 is indeed typical of a spinodally decomposed system and fully isotropic with no difference seen between cross-sectional and plain images in the nanocomposites deposited by plasma CVD and having low oxygen impurity content of only a few 100 ppm.[169] The high resolution (HR TEM) images showed that the TiN nanocrystals are of regular, equiaxial shape, approximately of uniform size, and randomly oriented as it has been also found by XRD (see Fig. 3 in Ref. 169). Also the size of the TiN nanocrystal of 3–4 nm determined by XRD and by HR TEM agreed very well (see Ref. 169 for further details). It is important to emphasize that nc-TiN/Si_3N_4 nanocomposites deposited by reactive magnetron sputtering[164] have still some columnar, albeit dense morphology because of a higher content of oxygen impurity of about 2000 ppm (0.2 at. %).[171] Therefore, as we shall discuss below, they are not as fully isotropic as the nanocomposites deposited by plasma CVD. This difference should be kept in mind.

In both XRD and electron diffraction (ED), one can see only the Bragg reflections of the fcc-TiN. The maximum

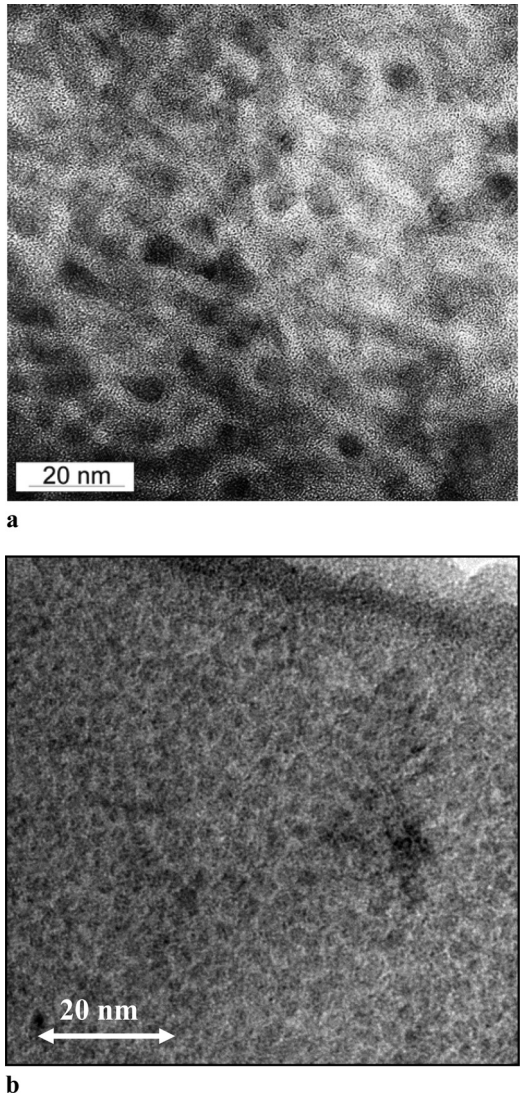

FIG. 8. TEM image of the (a) nc-TiN/a-Si_3N_4 nanocomposite coating deposited by plasma CVD (Ref. 169) and (b) nc-$(Al_{1-x}Ti_x)$N/a-Si_3N_4 nanocomposite coating deposited by vacuum arc evaporation (Ref. 170).

hardness is achieved when the thickness of the Si_3N_4-like interfacial layer is about one monolayer (1 ML) (Refs. 18 and 172) (see below). Such a layer of course does not show any Bragg reflections in XRD or ED, but its Si_3N_4-like composition is identified by the binding energy of the Si 2p signal in XPS. Tang *et al.* used atom probe tomography to analyze the TiSiN coatings[173,174] but could not find this layer because of too high oxygen impurity of 1.2–1.4 at. % in their samples as explained in Ref. 175.

More recently, Barna *et al.*[171] studied the nc-TiN/a-Si_3N_4 nanocomposites deposited by reactive magnetron sputtering[164] with a much lower oxygen impurity content of about 0.2 at. % as compared with that in samples of Tang *et al.*, and could identify the Si_3N_4-like interfacial layer by means of TEM combined with electron energy loss spectroscopy (EELS). For the convenience of the reader, we reproduce their results in Fig. 9, where Fig. 9(a) is the zero loss EELS image with two TiN nanocrystals denoted A and B, and Figs. 9(b) and 9(c) are the EELS images in Ti- and Si-loss,

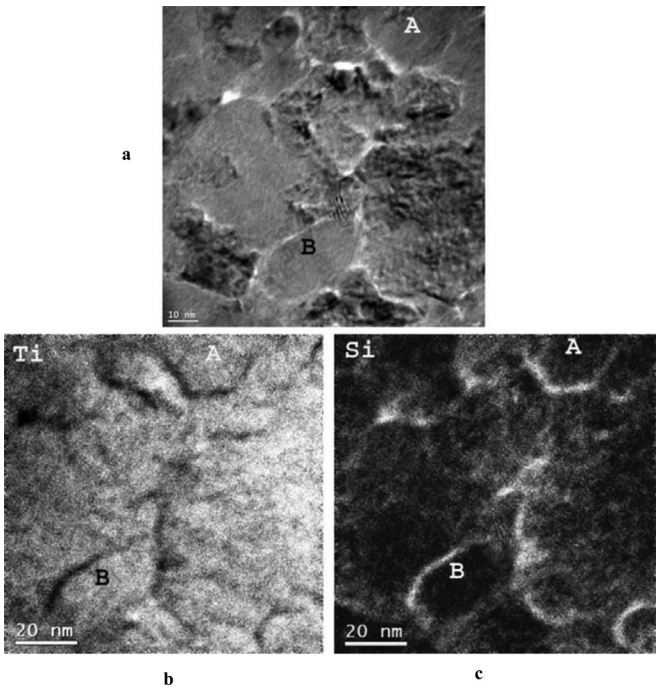

FIG. 9. Typical example of the plain view zero loss EELS image (a), and corresponding distribution of Ti (b) and Si (c). For clarity, two TiN nanocystals are marked as "A" and "B." Reprinted with permission from Barna *et al*. (submitted).

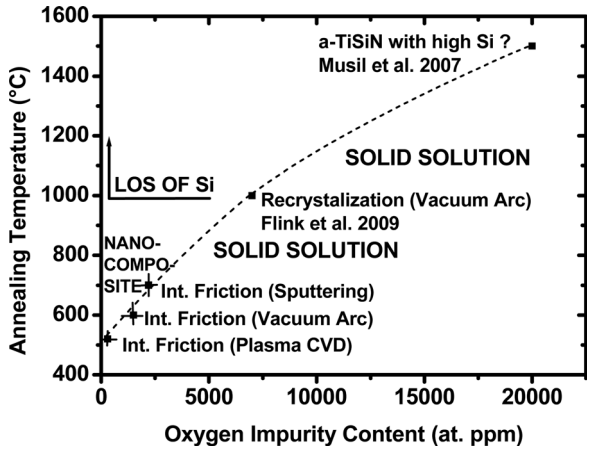

FIG. 10. Lower left corner: Dependence of the temperature needed for the full segregation of TiN and SiN_x phases, as determined by the measurement of internal friction, on oxygen impurity content in nc-TiN/a-Si_3N_4 coatings deposited by plasma CVD and reactive magnetron sputtering, and nc-TiAlN/a-Si_3N_4 coatings deposited by vacuum arc. Upper right corner: Recrystallization temperature of TiSiN solid solution reported by Flink *et al*. for coatings with Si content of about 9 at. % and oxygen impurities 0.76–0.81 at. % (Ref. 183) and the stability limit due to oxidation of amorphous TiSiN coatings with high Si-content reported in Ref. 184. Reprinted with permission from Veprek and Veprek-Heijman, Thin Solid Films **522**, 274 (2012). Copyright 2012, Elsevier B.V.

respectively. The Si_3N_4 interfacial layers are clearly visible. Their apparent higher thickness of about 1 nm is due to two factors: (1) already Prochazka *et al*. noted that this layer was thicker in these coatings than in those deposited by plasma CVD, most probably due to the higher oxygen impurity content in the coatings deposited by magnetron sputtering that requires a much higher temperature to complete the formation of the strong nanostructure as shown in Fig. 10, and (2) the sample studied in Fig. 9 was about 40–60 nm thick, i.e., one sees several TiN nanocrystals on top of each other, which makes the determination of the exact thickness of the Si_3N_4 difficult. Thus, there seems to be some indications that the interfacial SiN_x layer at the maximum hardness is somewhat thicker in the nanocomposites (as well as in the TiN-SiN_x heterostructures) when the oxygen impurities content is more than a few 100 ppm as found in nanocomposites deposited by plasma CVD.

Many researchers reported TEM studies of the Tm-Si-N coatings which have been deposited by plasma PVD and had much larger oxygen content than those studied by Barna *et al*. In the majority of such studies, one has found TmN nanocrystals of much larger crystallite size than those in nanocomposites deposited by plasma CVD when observed in plain view, and columnar morphology with longer columns in cross-sectional view. We refer to two recent papers as examples.[176,177] Obviously, the dense columnar morphology is typical of nanocomposites with high oxygen content but not for nanocomposites with low impurity content of only few 100 ppm, like those prepared by our group using plasma CVD. This important question needs more detailed investigation in the future, but such studies can be done only with pure nanocomposites having impurity content of only few 100 ppm or less. Studies on impure systems are confusing and of little use.

Nanocomposites of nc-$(Ti_{1-x}Al_x)N/Si_3N_4$ and nc-$(Cr_{1-x}Al_x)N/Si_3N_4$ are used in the industry as wear protection coatings on tools for machining (see Sec. IV), and the question arises how they form during the decomposition of the Ti-Al-Si-N and Cr-Al-Si-N solid solution, which is formed during the deposition from the gas phase (see above). The answer is found in the much smaller demixing energy of the Ti-Al-N (Refs. 178 and 179) and Cr-Al-N (Ref. 180) solid solutions as compared with the Ti-Si-N one. Therefore the driving force for the segregation of Si_3N_4 to the grain boundaries is much larger than that for the decomposition of the Ti-Al-N and Cr-Al-N solid solution and segregation of AlN into the grain boundaries. As mentioned, the Ti-Al-N (Ref. 56) and Cr-Al-N (Ref. 181) solid solutions decompose at a temperature of 800–900 °C, which is much lower than 1200 °C where coarsening and softening of nc-$(Ti_{1-x}Al_x)N/Si_3N_4$ nanocomposites occurs due to the diffusion of cobalt from the substrate.[120]

Oxygen impurities strongly hinder the formation of the nanostructure as seen in Fig. 10.[175] The temperature needed for the full segregation of the transition metal nitride and Si_3N_4 in nc-TiN/Si_3N_4 and nc-$(Ti_{1-x}Al_x)N/Si_3N_4$ nanocomposites deposited by plasma CVD, reactive magnetron sputtering, and vacuum arc evaporation (lower left corner) has been determined by means of internal friction measurements,[182] which is much more sensitive than measuring of the hardness and crystallite size after the stepwise annealing. The increase of that temperature with increasing oxygen impurity content extrapolates very well to the temperature of about 1000 °C, where Flink *et al*. reported the recrystalization

of the Ti-Si-N solid solution with 0.7–0.8 at. % of oxygen impurities,[183] and to the temperature of about 1480 °C, where Musil *et al*. reported the upper limit of the stability of amorphous Ti-Si-N solid solution with high Si-content.[184,185] As already mentioned, stoichiometric and pure TiN and Si_3N_4 are immiscible,[154,186] and therefore, TiN nanocrystals precipitated also from the Ti-Si-N solution with high Si content of 23 at. % in coatings, which had only few 100 ppm of oxygen impurities.[18,187] Although the impurities have not been reported in Ref. 184, it has been confirmed that they were in the range of 2–3 at. % (Ref. 188) in agreement with the extrapolation of the curve in Fig. 10.

The results of Musil *et al*. may be of some practical interest because they show that small oxygen impurity concentration can stabilize Si_3N_4 deposited by PVD at a relatively low temperature. Silicon nitride is an important material for final passivation of electronic devices, as dielectric in floating gate MOS transistors and other fields. When deposited by plasma CVD from silane and nitrogen or ammonia at relatively low temperatures compatible with the microelectronic technology, it always contains a too high concentration of hydrogen, which degrades its properties. Therefore, it would be interesting to investigate the electrical properties of Si_3N_4 deposited by PVD with few at. % of oxygen.

From Fig. 10, it is clear that oxygen impurities of $\geq$0.5–0.8 at. % (5000–8000 ppm) hinder the formation of superhard nanocomposites with strong nanostructure, because at a temperature of 1000–1100 °C, silicon is lost due to evaporation of SiO, and even the pure nanocomposites with only few 100 ppm impurities recrystalize and soften above 1100 °C (see Ref. 175 for further details and references).

It is therefore clear that publications reporting on the preparation and properties of TiN/SiN_x (and other nc-TmN/SiN_x) "nanocomposites" with oxygen impurities of 1–2 at. % or more should be subjected to a critical evaluation.[189] Tm-Si-N coatings with $\geq$0.5 at. % of oxygen should not be quoted "nanocomposites" but, as shown by Flink *et al*.[183] and by the results in Fig. 10, they are Ti-Si-N-O_δ solid solutions, in which some hardness enhancement can be found due to the solid solution- and to the nanostructure-refinement-hardening, which is however lost when, upon annealing, the solid solution recrystalizes and silicon leaves the system as volatile SiO.[183] The fact that Ti-Si-N coatings with $\geq$0.5 at. % of oxygen, deposited at $\leq$600 °C (in many cases even a lower temperature has been used) are not nanocomposites but solid solutions stabilized by the impurities is further supported by the important results of Tang *et al*.[173,174] who did not find any Si_3N_4 interfacial layer (see above). Flink *et al*. also mention smaller grain size as one of the reasons of the hardness increase in their coatings.[183]

It is further obvious that the "**solubility limits of Si in TmN**" reported in many papers[189] is due either to oxygen impurities or to nitrogen substoichiometry, because as mentioned, stoichiometric and pure transition metal nitrides and Si_3N_4 (as well as BN) are immiscible.[154,186] Last but not least, these result show that the measurements of the scattering of the electric charge carriers in Tm-Si-N coatings deposited at $\leq$ 440 °C and having up to 2 at. % of oxygen as well as carbon impurities[190,191] does not reveal the nanostructure of nc-TmN/SiN_x nanocomposites with SiN_x interfacial layers because such layers are absent in these coatings with too high oxygen impurities, as shown by Tang *et al*.[173,174] Most likely, the impurities are responsible for the observed charge carrier scattering. This is another open question that requires careful critical clarification on pure samples. From the results discussed so far, it is clear that oxygen impurity content of more than few 100 ppm, low nitrogen pressure and low temperature during the deposition are limiting the possibility of preparation of superhard nanocomposites.[158,175]

Another limit is the **mechanism of the decomposition of the solid solution**. As discussed above, all the results which have been obtained so far strongly suggest that the superhardness of >50 GPa can be achieved only in a system, which forms regular nanostructure with sharp interfaces, and that the 1 ML interfacial layer should be strengthened by valence charge transfer because when this layer becomes 2 ML thick the hardness enhancement is lost in pure system (see Ref. 172 and discussion in Sec. III C 3). Thus, only Tm-Si-N systems, which decompose by the spinodal mechanism, are expected to reach high superhardness, whereas those which decompose by nucleation and growth may probably reach only the hardness enhancement expected from the "strongest size." Zhang and Sheng studied several system using the combined DFT calculation and thermodynamic modeling, and obtained the following results:

(1) The Zr-Al-N system should decompose by nucleation and growth.[192] Thus, a formation of a regular strong nanostructure with sharp and strong AlN interfacial layer is unlikely.
(2) Similar conclusion also applies to the Zr-Si-N (Ref. 193) and Al-Si-N (Ref. 194) systems, which should decompose by nucleation and growth.
(3) The $Ti_{1-x}B_xN$ system consisting of stoichiometric TiN and BN should be chemically spinodal, but the frequently reported nitrogen deficient TiB_xN_{1-x} ("TiN + TiB_2") system should decompose by nucleation and growth.[195] However, the large difference of the sizes of boron and titanium atoms make a coherent or semicoherent interfacial BN layer impossible to form (see Fig. 12a in Ref. 196) and, therefore, there are always some Ti-B bonds in the interface between stoichiometric TiN and BN interfacial layer.[196] Nevertheless the fact that a maximum hardness has been found also when the interfacial BN has been about one monolayer thick (see Fig. 7 in Ref. 196) suggests that the observed maximum hardness enhancement is due probably to the strongest size with possibly some contribution by the valence charge transfer to the interfacial BN as in the TiN-SiN_x system, because the electronegativity of boron is somewhat larger than that of silicon.[83] We shall return to this interesting system in Sec. III D.
(4) Promising is the Zr-Al-O system because it is chemically spinodal[197] and should have an "infinitive oxidation resistance," which is very important in many industrial applications. However, because the hard corundum α-Al_2O_3 modification forms only at high temperatures of

≥1000 °C, the mixed α-$(Al_{1-x}Cr_x)_2O_3$–ZrO_2 and in particularly Cr_2O_3–ZrO_2 systems may be more suitable to form hard and superhard nanocomposites. The latter system is also expected to be spinodal, but detailed DFT and thermodynamic calculations are not available. We shall discuss the oxide-based nanocomposite systems in Sec. III E.

Of course further calculations are needed to see if one can find another system which would also form the superhard nanocomposites and offer some other advantages as compared with Ti-Si-N, Ti-Al-Si-N, and Cr-Al-Si-N and other ones studied so far.

Not in all cases a superhardness is needed. For example, although—as mentioned—the Al-Si-N system is not spinodal[194] and the AlN-Si_3N_4 nanocomposites reach only a hardness of about 30 GPa,[136] they are of great interest as hard transparent coatings because in the daily environment there is almost nothing which could scratch them. These coatings have been studied in much detail by Patscheider and coworkers.[136–139] Interestingly, the maximum hardness is achieved when the crystallite size is close to about 10 nm (c.f. Figs. 3 and 4 in Ref. 136), but because of relatively high content of oxygen and carbon impurities in these coatings, it is difficult to speculate about the exact mechanism of the hardness enhancement. Probably it is due to the "strongest size."

These examples illustrate that much further work is needed on pure coatings with low impurity content in order to elucidate new systems with enhanced hardness and optimized other properties. The combined DFT calculations and thermodynamic modeling are cost- and time-efficient as compared with the experimental trial and error approach.

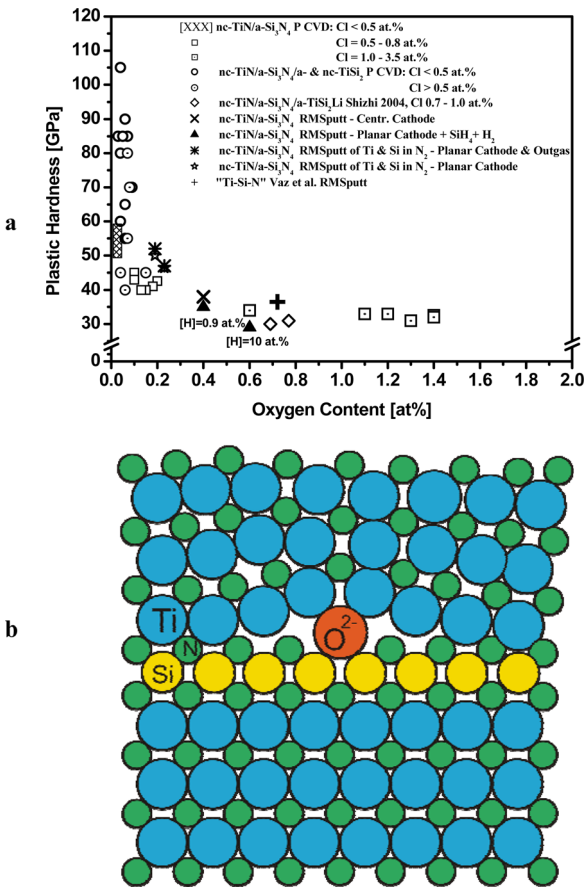

FIG. 11. (Color online) (a) Dependence of hardness of nc-TiN/a-Si_3N_4/$TiSi_2$ and nc-TiN/a-Si_3N_4 nanocomposites on oxygen impurity content and (b) the oxygen substituting nitrogen in the SiN_x interfacial layer. Reprinted with permission from Veprek *et al.*, J. Vac. Sci. Technol. B **23**, L17 (2005). Copyright 2005, American Vacuum Society.

2. What is the achievable hardness, elastic limit, and fracture toughness of the nc-TiN/Si_3N_4 and related nanocomposites?

The maximum achievable hardness in the nc-TiN/Si_3N_4 nanocomposites is strongly sensitive to the impurity content because, as shown in Fig. 11,[198] already 0.2 at. % (2000 ppm) of oxygen strongly decrease the achievable hardness, and at oxygen content of ≥0.4–0.5 at. %, the load-invariant plastic hardness is limited to about ≤35 GPa. At that concentration, there are on average more than 20 oxygen-related defects per each TiN nanocrystal [Fig. 11(a)], which weaken the SiN_x interface [Fig. 11(b)] as confirmed also by first-principles DFT calculations of Hao *et al.*[199] Such a high sensitivity to impurities applies probably to all nc-TmN/Si_3N_4 nanocomposites with strengthened interfacial Si_3N_4 layer, which forms semicoherent interface with the TmN, because the Si-O bond is the strongest one in these systems (see Ref. 175 and references therein). In the case of the nc-TiN/BN nanocomposites, there is no noticeable degradation of the hardness with oxygen impurities of up to 1.5 at. %,[200] possibly due to the incoherent nature of the TiN/BN interface.[196]

Because, as mentioned above, in the majority of the papers of other groups, the impurities are relatively high and the achievable, correctly measured load-invariant hardness is below 40 GPa, our high values of hardness of 80 to ≥100 GPa reported for quasiternary nc-TiN/Si_3N_4/$TiSi_2$, and of 50–70 GPa for long-term stable quasibinary nc-TiN/Si_3N_4 nanocomposites (see review Ref. 18 and references therein) have been often criticized, most recently by Fischer-Cripps *et al.*[201] Because, in the present review, we focus on the understanding of the superhard nanocomposites, we do not discuss here the trivial mistake of Fischer-Cripps *et al.* who confused two different calibration and evaluation methods. Instead, we refer to our recent paper[175] and the verification of the high hardness from the size of the remnant plastic indentation measured by means of scanning electron microscope (SEM), which is shown later.

Figure 12 shows one example of the hardness, measured by an early version of Fischerscope H 100,[202,203] of ultrahard quasiternary nc-TiN/Si_3N_4/$TiSi_2$ nanocomposite coating as function of the maximum applied load[18,204] in comparison with the hardness of industrial diamond and a 1 μm thick ultra-nanocrystalline diamond film deposited in a dense plasma of a microwave discharge.[205] One can see that for maximum applied load of 30–70 mN the hardness of the 3.5 μm thin nanocomposite coating of about 105 ± 15 GPa compares well with that of the industrial diamond. At a load of 100 mN, the indentation depth was already 17% of the

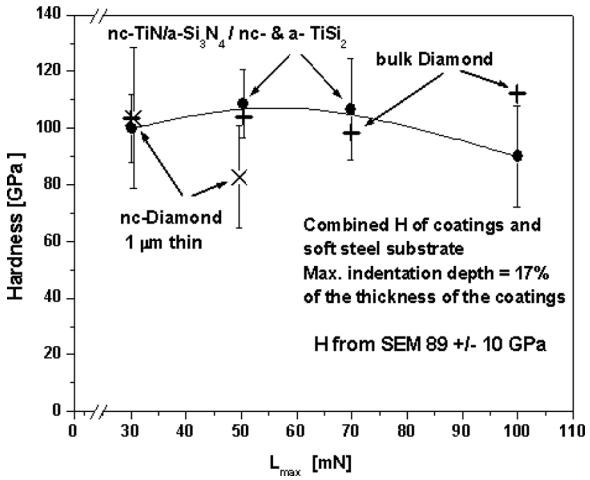

FIG. 12. Example of the hardness of 3.5 μm thick ultrahard nc-TiN/Si_3N_4/$TiSi_2$ nanocomposite coating vs the maximum applied load in comparison with industrial bulk diamond and a 1 μm thick ultra-nanocrystalline diamond film. Reprinted with permission from Veprek, J. Vac. Sci. Technol. A **17**, 2401 (1999). Copyright 1999, American Vacuum Society.

thickness of the coating. Therefore, plastic deformation in the soft steel substrate ($H \approx 2$ GPa) occurred, and the "compound" hardness of the coating and substrate decreased to about 91 ± 15 GPa. (Notice that each experimental point is an average value of more than 15 indentation measurements.) This value has been verified by measurement of the size of remnant indentation obtained from calibrated SEM which yielded about 89 ± 10 GPa in a good agreement with the data from Fischerscope H 100. One notices that the hardness of the about 1 μm thick ultra-nanocrystalline diamond film[205] deposited on Si-substrate, which is much harder ($H \approx 10.5$ GPa) than the steel substrate used for the nanocomposite coatings (2 GPa), strongly decreases already at a load of 50 mN due to the plastic deformation of the Si substrate.

Figure 13 shows the hardness of a 7.3 μm thick quasiternary ultrahard nc-TiN/a-Si_3N_4/$TiSi_2$ nanocomposite coating

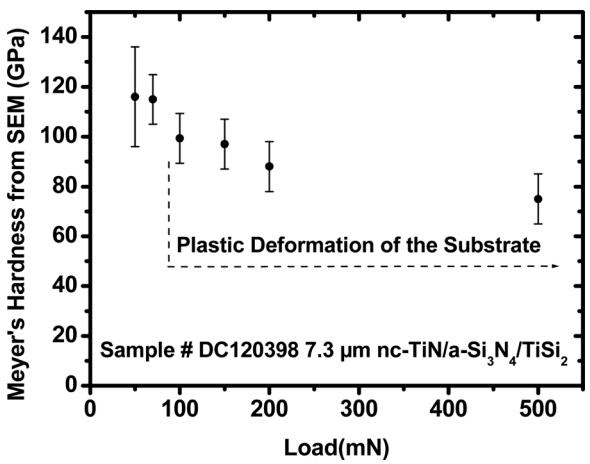

FIG. 13. Hardness evaluated from many SEM micrographs vs maximum applied load. Notice that at a load of 100 mN, the plastic deformation of the substrate already occurs, i.e., one measures a compound hardness of the coating and much softer substrate (sample # DC120398 on Si-substrate, 7.3 μm thick). Reprinted with permission from Veprek and Veprek-Heijman, Thin Solid Films **522**, 274 (2012). Copyright 2012, Elsevier B.V.

deposited on a Si substrate with a ~ 3 μm thick underlayer of TiN (sample # DC120398) evaluated from SEM micrographs (three micrographs at each load) versus maximum applied load. The indentations have been done with indentometer Fischerscope H 100,[202,203] and the applied load has been carefully calibrated and checked by the manufacturer. Also the magnification of the SEM has been verified using a lithographic photomask from semiconductor industry (Ref. 206, p. 61).

Notice that at a load of 100 mN, the plastic deformation of the substrate already occurs (for comparison see the decrease of the hardness of the ultra-nanocrystalline diamond in Fig. 12), i.e., one measures a compound hardness of the coating and of the much softer silicon substrate and of the underlaying TiN layer. It is clear from Fig. 13 that the average value of the load-invariant Meyer's hardness at an applied load of 50 and 70 mN is above 110 GPa, i.e., the Vickers hardness is above 100 GPa, particularly when one accounts for the rounding of the diamond tip to a radius of 0.5–0.7 μm due to plastic deformation as reported in Refs. 207 and 208. (For the meaning of Meyer's and Vickers hardness, see Refs. 1 and 209 and Appendix A.) At a load of 100 and 150 mN, where the plastic deformation of the substrate is already significant, the hardness is still about 100 GPa or only slightly less, respectively. Even at a load of 200 mN, where a substantial plastic deformation of the substrate occurs, the compound hardness of the coatings and the substrate is close to 90 GPa.

At this point, it is important to consider the hardness of $\leq$70 GPa reported by Shizhi *et al.*[16] and shown in Fig. 1. These researchers have measured the Vickers hardness in the conventional two-steps procedure by indenting the diamond pyramid into ≥ 5 μm thick coatings on steel with a relatively high load of 50 gf ($\approx$ 490 mN). In Fig. 13, the compound hardness of the coatings and softer substrate at a load of 500 mN is about 75 GPa. It is therefore clear that Shizhi *et al.* underestimated the hardness of their coatings. Considering the larger thickness of our coatings and the TiN underlayer, the present article estimates that the hardness of the "Ti-Si-N" coatings of Shizhi *et al.* was surely above 90 GPa.

The compound hardness is a combination of the plastic deformation of the soft substrate and plastic plus elastic deformation of the superhard coatings, which adhere very well to that substrate. When the coating has been etched by means of ion milling so that only a narrow strip of the coating was left, the coating flexed back (see Fig. 4.42 in Ref. 107, p. 194). This shows that these coatings have a very high elastic limit of more than 10% (to verify the reproducibility of this high elastic limit, see also another coating reported in Fig. 9(b) of Ref. 210). For comparison, the elastic limit of typical ceramics is $\leq$0.1%,[6] that of polycrystalline metals is about 0.2%, and that of metallic glasses is around 2%.[211] Also the metallic glass matrix composites, which have higher fracture toughness and ductility than metallic glasses, have an elastic limit of about 2%.[212] The high elastic limit of the nanocomposites is due to the high connectivity between the TiN nanocrystals and the Si_3N_4 interfacial layer, which is strengthened by valence charge transfer as shown by DFT calculations and discussed below.

This high elastic limit contradicts the statements often found in the literature, that the superhard nc-TmN/Si_3N_4 nanocomposites are brittle. What makes them brittle is a relatively high concentration of oxygen impurities of 0.5–2 at. %, or more found in the majority of the papers,[189] because there are many oxygen-related defects as illustrated in Fig. 11(b). Nanocomposites with low impurity content of few 100 ppm, which are almost free of nanocracks associated with oxygen, have a very high threshold for the crack initiation. We shall come to this point later.

The role of $TiSi_2$ in the quasiternary nc-TiN/Si_3N_4/$TiSi_2$ ultrahard nanocomposites is twofold: (1) a beneficial one because it getters the minor oxygen impurities of few 100 ppm, thus avoiding them to get incorporated into the SiN_x interfacial layers and weaken them,[199] and (2) a detrimental one because it makes the nanocomposites unstable in long terms. This instability is related to the fact that $TiSi_2$ deposited below 850 °C forms metastable, low-density phases, which, under the large stress within the grain-boundaries, undergo degradation resulting in the loss of the hardness after 5–8 months.[18,175]

After having understood this reason of the long-term instability of the quasiternary nanocomposites,[18] we concentrated on the quasibinary nc-TiN/Si_3N_4 and related nc-TmN/Si_3N_4 nanocomposites, which are stable over years (reported up to almost 3 years in Ref. 18, but measured afterward up to 5 years). These systems are stable because of the absence of the metastable $TiSi_2$ phases, but because the gettering of the minor oxygen impurities by $TiSi_2$ is absent, they are much more sensitive to the impurities. Nevertheless, it has been possible to prepare nc-TiN/Si_3N_4 nanocomposites with hardness of 65–70 GPa as illustrated in Fig. 14 for one of the nanocomposites with the lowest oxygen content.[175]

These results strongly support the expectation that it should be possible to achieve long-term stable hardness of 80–100 GPa and may be even more if the impurities in this system could be reduced significantly below 100 ppm. Such coatings would also display a high elastic limit, i.e., they would not be susceptible to easy brittle fracture in applications, such as wear protection coatings on tools for machining. This is surely a challenge for both the academia interested in basic science and industry interested in applications. The very high hardness of nanotwinned c-BN reported recently in Ref. 123 lends further motivation to the attempt to try to achieve this goal.

3. How to understand such the high hardness enhancement?

The ideal shear and tensile strength of perfect crystals of about 10% of shear G and Young's E_Y modulus, respectively,[2,5] is orders of magnitude larger than the practically achievable strength of engineering materials because of the presence of defects in the latter. Defects, such as dislocations, twinning, grain boundaries, microcracks, and others easily shear and grow upon a stress much smaller than the ideal strength. Upon plastic deformation, such defects also develop in an originally perfect single crystal and limit its real strength and hardness. The strengthening in plastically deforming real materials occurs by introducing some obstacles which impede the plastic deformation by whatever mechanism it occurs, most common being a hindering of dislocation multiplication and motion in crystal plasticity.[11]

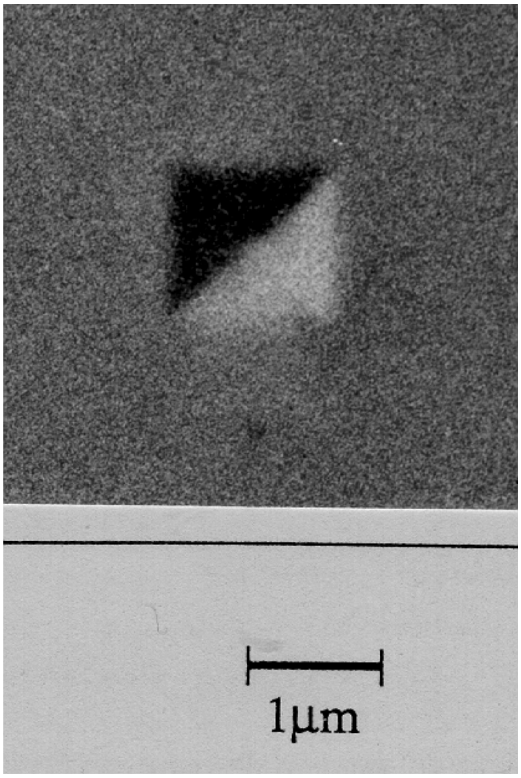

FIG. 14. Scanning electron micrograph of an indentation into about 8 μm thick, long-term stable quasibinary nc-TiN/a-Si_3N_4 nanocomposite coating with a Vickers diamond indenter at a load of 110 mN. The magnification of the scanning electron microscope has been calibrated using a photomask for optical lithography in semiconductor industry. One notices that the plastically deformed indentation area of 1 μm^2 ($= 10^{-12}$ m^2) produced under a load of 100 mN corresponds to a Meyer's hardness of 0.1 $N/10^{-12}$ $m^2 = 10^{11}$ $N/m^2 = 100$ GPa. Reprinted with permission from Veprek and Veprek-Heijman, Thin Solid Films **522**, 274 (2012). Copyright 2012, Elsevier B.V.

The large enhancement of the hardness in the nanocomposites can be understood in terms of the absence of defects, such as dislocations, twins, and the like in the 3–4 nm size nanocrystals and strengthened grain boundaries, as discussed in Ref. 213. The strengthening of the SiN_x interfacial layer is due to valence charge transfer from TiN nanocrystals to that layer because of larger electronegativity of Si as compared with Ti, as it will be shown now.

Hao *et al.* have conducted extensive computational DFT studies of the heterostructures consisting of few nanometers thick TiN slabs with Si_3N_4-like interfacial layers of different thickness and crystallographic (hkl) nature and found that the decohesion strength of the 1 ML of α- and β-Si_3N_4 layer is the highest one, significantly larger than that of an ideal Si_3N_4 single crystal.[214,215] Zhang *et al.* have shown for a variety of heterostructures with the pseudomorphic SiN-like interfaces that the strengthening is due to the valence charge transfer from TiN as illustrated by the valence charge density differences (VCDDs) in Fig. 15 for the (111) interface.[216]

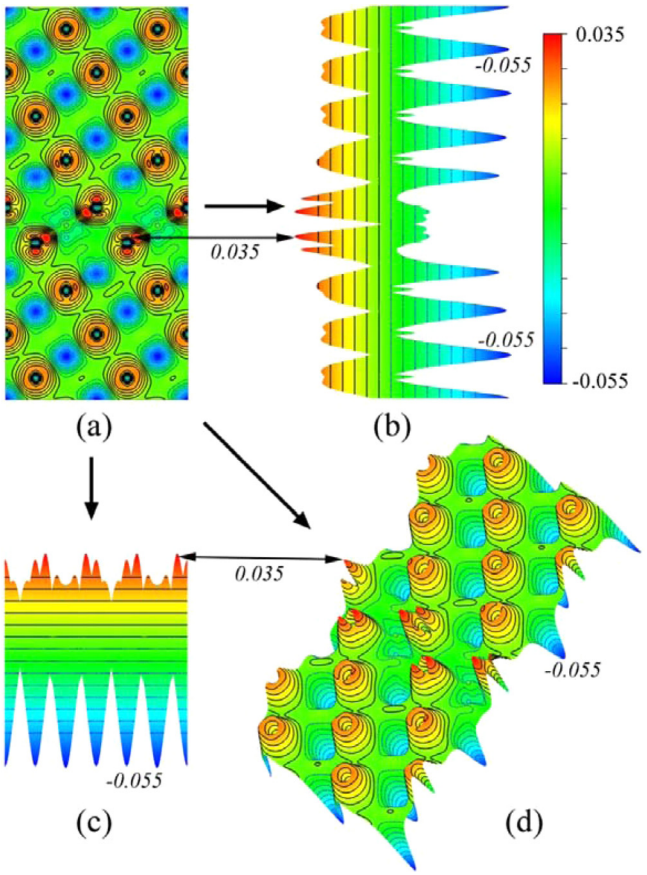

FIG. 15. (Color online) (a) VCDD of the TiN(111)/1 ML SiN/TiN(111) heterostructure, (b) and (c) the side view as indicated and (d) prospective view. The color scale runs from −0.055 (bottom blue) to 0.035 electrons/Bohr^3 (top red). The small italic numbers indicate the values of VCDD. Reprinted with permission from Zhang *et al.*, Phys. Rev. B **79**, 245426 (2009). Copyright 2009, the American Physical Society.

One can see that the valence charge density is higher, i.e., the bonds to the neighbors are stronger, on nitrogen in the SiN layer than on nitrogen in the TiN slab, and it is also higher on Si than on Ti. Similar strengthening has been found also for other (hkl) interfaces.[216]

However, the strengthening of the SiN_x interfacial layer is accompanied by a weakening of the Ti-N bonds near by the SiN_x interface, which are the "weak link" in the system where, upon an applied shear and tensile stress, the shear plastic deformation and decohesion occur in agreement with high-pressure XRD study.[217] This is illustrated in Fig. 16 for decohesion of the (111)-TiN/1 ML SiN/TiN heterostructure. We refer to the recent papers[216,218] for the decohesion and shear of other interfaces and for further details. These results confirm that the grain boundary regions are the carrier of the plastic flow in the nanocomposites, as discussed in Ref. 213, whereas the TiN nanocrystals deform only elastically, as observed experimentally.[217]

Because of the weakening of the Ti-N bonds near the SiN_x interfacial layer, the decohesion and shear strength of heterostructures consisting of few nanometers thick slabs of TiN with 1 ML of SiN_x interfacial layer is lower than that of an ideal TiN single crystal.[219] Nevertheless, because the TiN

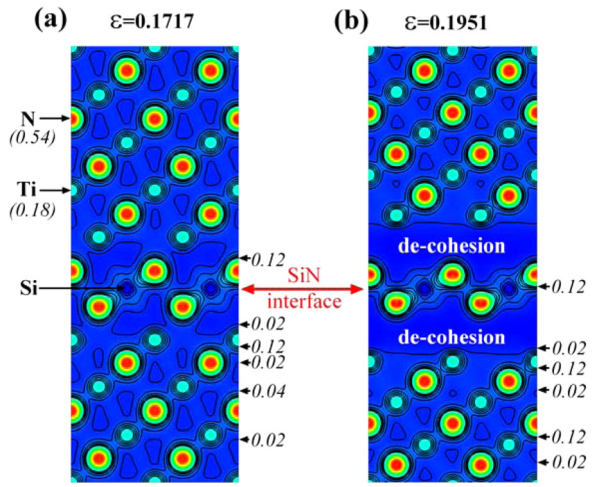

FIG. 16. (Color online) Changes of the valence charge density of the (111)-TiN/SiN/TiN heterostructure under an applied tensile strain normal to the (111) interface just before the decohesion instability (a) and just after it (b) at the strains as indicated. The valence charge density scales range from 0 (dark blue) to 0.54 electrons/Bohr^3 (bright red). Reprinted with permission from Zhang *et al.*, Phys. Rev. Lett. **102**, 015503 (2009). Copyright 2009, the American Physical Society.

is stronger than Si_3N_4, and the grain boundaries in the nanocomposites with the strengthened SiN_x layer are stronger than those in polycrystalline TiN alone, the overall effect is a strengthening and hardness enhancement of the nanocomposites.[213] Based on these results and on the shear resistance of the interfaces calculated by *ab initio* DFT, a simple calculation has shown that in well prepared and pure nc-TiN/Si_3N_4 nanocomposites with randomly oriented TiN nanocrystals hardness significantly above 100 GPa should be possible to achieve.[213]

It has been found experimentally[172] that the hardness enhancement in the nanocomposites is lost when the thickness of the Si_3N_4 reached about 2 ML, as shown for several nc-TmN/Si_3N_4 nanocomposites in Fig. 17. In order to explain this loss of the hardness enhancement, Zhang *et al.* have compared the decohesion and shear strengths of the

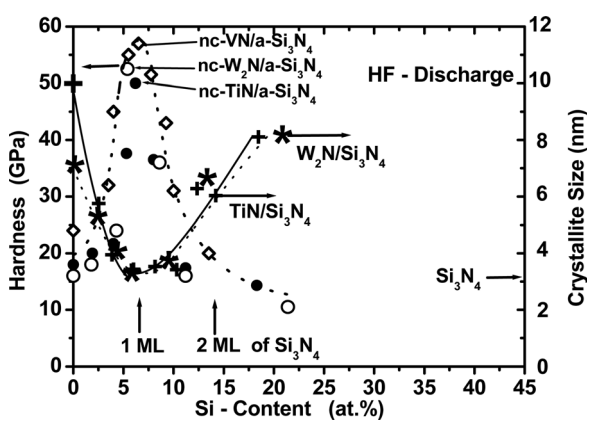

FIG. 17. Dependence of hardness and size of the TiN nanocrystals in stoichiometric, quasibinary nc-TmN/a-Si_3N_4 nanocomposites deposited by PCVD on silicon content. Reprinted with permission from Veprek and Veprek-Heijman, Surf. Coat. Technol. **201**, 6064 (2007). Copyright 2007, Elsevier B.V.

TiN/SiN/TiN heterostructures with 1 and 2 ML interfacial pseudomorphic SiN and found that the heterostructures with 2 ML are about a factor of 2 weaker than those with 1 ML. This is due to the much larger weakening of the neighbor Ti-N bonds as a result of the larger valence charge transfer from the TiN nanocrystals to the 2 ML SiN interfacial layer.[220] These experimental results and theoretical explanation clearly show that if the maximum hardness is achieved for 1 ML SiN_x interfacial layer, such an interface has to be sharp.

A critical reader may object that the static DFT calculations of the fcc-TiN-SiN-TiN heterostructures are not sufficiently reliable because of inherent thermodynamic[157,168] and dynamic phonon instability of the bulk fcc-SiN.[221,222] Therefore, Ivashchenko *et al.*[223] recently conducted first-principles quantum molecular dynamics (QMD) studies, which allow one to perform the calculations at elevated temperatures. Ivashchenko *et al.* also extended the calculations to the Si_3N_4-like interfacial layers. The results of Zhang *et al.* have been essentially confirmed,[223] the calculated ideal strength of the heterostructures at 0 K and after annealing at 1400 K and cooling to 300 K being similar.[219]

A very surprising result was the finding of Ivashchenko *et al.*[223] that the fcc-(111) TiN/1 ML SiN/TiN heterostructure remains unchanged after annealing to 1400 K and cooling down to 300 K (see Fig. 18), because according to the conventional macroscopic thermodynamics it should decompose as $4SiN \rightarrow Si_3N_4 + Si$ with Gibbs free reaction energy of -136 kJ/mole·atom.[157,168] Such a high value of negative Gibbs free energy of the reaction represents a large thermodynamic driving force for the decomposition reaction to occur. It is not clear yet if, in spite of such a high driving force at macroscopic scale, the high stability of the 1 ML (111) interfacial SiN layer is due to different thermodynamics at the nanoscale, or to kinetic reasons. The impeded kinetics in 1 ML seems to be more likely because structural transformations require a certain critical activation volume and simultaneous rearrangement of several atoms to occur. Therefore, such transformations are impeded in nanosized materials.[224–226] A simultaneous rearrangement and breaking of several bonds is obviously needed also for the decomposition reaction $4SiN \rightarrow Si_3N_4 + Si$ to commence.

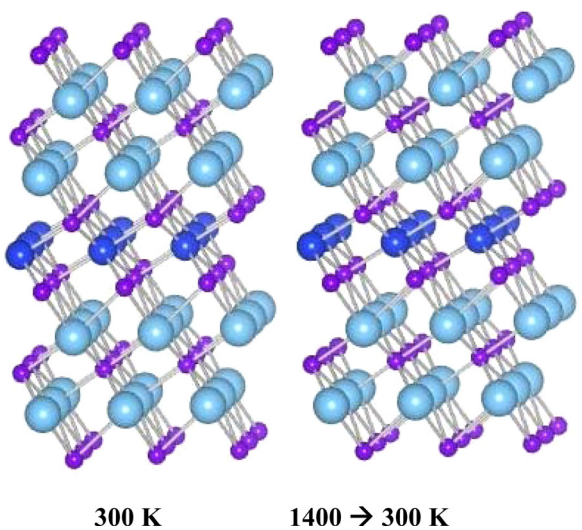

FIG. 18. (Color online) Structure of the fcc-(111) TiN-SiN-TiN heterostructure calculated by first-principles QMD at 300 K and after annealing to 1400 K and cooling down to 300 K. Reprinted with permission from Ivashchenko *et al.*, Phys. Rev. B **85**, 195403 (2012). Copyright 2012, the American Physical Society.

The recent dynamic study of the phonon stability of a variety of (001) TiN/1 ML XY/TiN heterostructures[227] suggest that, in agreement with the first-principles quantum molecular dynamics studies,[223] the TiN/1 ML SiN/TiN heterostructure should display condensed ("soft") modes, i.e., the 1 ML SiN interfacial layer should be unstable in its symmetric fcc configuration. However, this instability results only in a disordered 1 ML SiN but not in any decomposition and rearrangement of several atoms, which is needed for the nucleation of a new phase during the above mentioned decomposition. Furthermore, it is shown in that paper that a variety of interfacial materials (XY = BN, SiC, etc.), which have been used in the deposition of TiN/XY/TiN heterostructures by several groups, are unlikely to form superhard nanocomposites with very high hardness enhancement by the same mechanism as found in the TiN/1 ML SiN_x/TiN system, because of their inherent dynamical instability. We refer to Ref. 227 for further details.

These first-principles calculations provided important insight into the stability and strength of the heterostructures, and into the mechanism of their plastic deformation and decohesion, but one should not overestimate their outcome because in the nanocomposites with 3–4 nm size nanocrystals, many different (hkl) interfaces have to coexist. The important conclusion of these calculations is that also interfaces with SiN layers that are unstable according to the macroscopic thermodynamics may be stabilized as 1 ML interfacial layer and therefore should not be ruled out. Furthermore, one should also consider the effect of the boundaries between the 1 and 2 nm^2 small interfaces between the 3 and 4 nm size TiN nanocrystals with different (hkl) and of the triple points, which occur in the nanocomposites but are absent in the heterostructures. Such calculations are beyond the capability of the present first-principle codes and computing capacity of modern computers. Therefore, classical, large ensemble molecular dynamics calculations with exact interatomic potentials derived from first-principles, which are being presently developed,[228,229] are highly demanding for the future studies of the formation and properties of the nanocomposites.

4. Properties of the superhard nc-TmN/Si_3N_4 nanocomposites: Is there really a need for toughening them?

Because the basic properties of superhard nanocomposites with low oxygen impurity content of few 100 ppm, such as high thermal stability, oxidation resistance, and others, have been summarized in earlier reviews,[18,204] we only briefly mention them here referring to the reviews and original papers quoted therein for further details. Let us devote more

attention to the **effect of oxygen impurities on the fracture toughness of the nanocomposites**. As mentioned, Fig. 11 shows the dependence of the hardness and size of the Tm nanocrystals on silicon content in stoichiometric, quasibinary nc-TmN/Si_3N_4 nanocomposites with three different transition metal nitrides deposited by plasma CVD and having low oxygen impurity content of few 100 ppm.[198] These coatings were deposited in high-frequency glow discharge plasma, where the ions reaching the surface of the growing film had low energy.[19,20,230,231] If such coatings were deposited at the cathode of direct current glow discharge under energetic ion bombardment, the crystallite size decreased with increasing Si content in a similar manner to about 3 nm, but upon a further increase of Si, it remained nearly constant (see Fig. 2 in Ref. 232) because the energetic ion bombardment decreases the crystallite size as shown in Fig. 6. This has to be taken into account when trying to reproduce these results. As mentioned, the maximum hardness enhancement by about a factor of 3 corresponds to Si_3N_4 content with about 1 ML thick interfacial layer, but the hardness enhancement is lost when the thickness of the interfacial Si_3N_4 layer reaches 2 ML. One notices that the crystallite size at the maximum hardness of only 3 nm is much smaller than the "strongest size" of 10–15 nm discussed above. This is a consequence of the reduction of the grain boundary shear due to the strengthening of the interfacial Si_3N_4-like layer. However, in the presence of higher oxygen impurity content of $\geq$2000 ppm, the thickness of the Si_3N_4 layer—at which the maximum hardness is achieved—is obviously much larger, as seen in Fig. 9 and often reported in papers of other groups.[189]

This also remains an open question, which requires further studies, and it can be answered only when nc-TiN/Si_3N_4 nanocomposites with low oxygen impurities of few 100 ppm or less will be prepared by other groups. Obviously, a high hardness of >50 GPa or even 80–100 GPa cannot be achieved in Ti-Si-N coatings with oxygen impurity of 0.5–2 at. % or more (see Fig. 11) found in the majority of published papers.[189]

In Ref. 233, we have reported that a 6.1 μm thick coating of the quasiternary nc-TiN/a-Si_3N_4/$TiSi_2$ nanocomposites deposited on soft steel can, when indented with 1000 mN load, sustain a very large elastic deformation of more than 10%. In Fig. 19, we show an example of indentation with the high load of 1000 mN into a 7.3 μm thick quasiternary nc-TiN/a-Si_3N_4/$TiSi_2$ coating deposited on a silicon substrate whose hardness is shown in Fig. 13. Although the maximum indentation depth was almost 2 μm, no cracks are seen in the coatings. The size of the remnant indentation corresponds to the combined hardness of the substrate and the coatings in which large part of the deformation seen in the SEM micrographs is elastic because of the high elastic limit and excellent adherence of the coatings to the substrate.

The high elastic limit of the nanocomposites should not be confused with high fracture toughness, which is the resistance of a material against the propagation of the pre-existing (prefabricated) crack and characterized by stress intensity factor or energy release rate.[5,234] The stress intensity factor $K_I = \sigma(\pi a)^{0.5}$ describes the stress σ needed to propagate a prefabricated crack of size $2a$. (A simple criterion which allows to asses if a material is brittle or ductile is the ratio of bulk B to shear G modulus. High B/G ratio is associated with ductility whereas low ratio with brittleness.[235]) There is no reason why the fracture toughness of the nanocomposites should be enhanced, and there are unfortunately no measurements of fracture toughness available on high-quality superhard nanocomposites with low oxygen content.

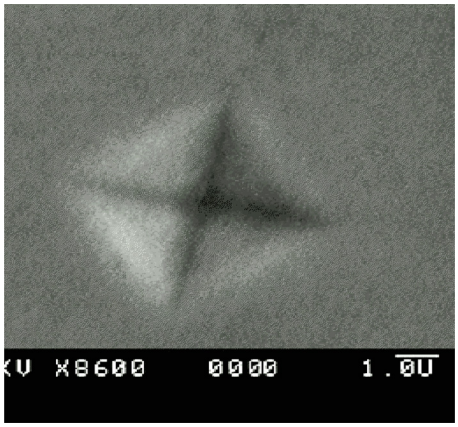

FIG. 19. (Color online) An example of indentation into a 7.3 μm thick quasiternary nc-TiN/a-Si_3N_4/$TiSi_2$ coatings deposited on silicon substrate with a load of 1000 mN (Vickers indenter, sample DC120398).

The high elastic limit of the superhard nanocomposites is due to the fact that any pre-existing crack, such as a fault from insufficient segregation of TiN and Si_3N_4, scales with the size of the nanocrystals. According to Griffith, the critical stress σ_C needed to propagate a crack of size $2a$ increases with decreasing size as $\sigma_C = \sqrt{2E_Y\gamma_S/\pi a}$.[2,5,234] When the size of the TiN nanocrystals at the maximum hardness reaches 3 nm, the size of the different (hkl) interfaces, where the nanocracks may be present, decreases below 1 nm, i.e., it is becoming comparable to interatomic bond length a_0 and, consequently, the strength approaches the ideal one given by $\sigma_{ideal} = \sqrt{2E_Y\lambda_S/\pi a_0}$.[5,234] Thus, the high elastic limit of the nanocomposites with low oxygen impurity content is due to a high threshold for initiation of <1 nm small nanocracks. When the cracks are initiated upon a very high stress, they may propagate, grow, and percolate as in an ordinary TiN. However, when other defects, such as those caused by oxygen impurities [Fig. 11(b)], are present in large number, they will, upon applied stress, easily grow, join each other, and percolate to large cracks, which will than simply propagate. This explains why the nanocomposites with oxygen content of $\geq$0.3–0.4 at. % are brittle and need some kind of toughening.

The common method of increasing the toughness of the nanocomposites (and other hard coatings) is composition modulation of the coatings during their deposition from two cathodes, e.g., by deposition of multilayers. The example shown in Fig. 20 illustrates such a composition variation of the nc-$(Ti_{1-x}Al_x)N/Si_3N_4$ industrial coatings deposited by vacuum arc evaporation from two cylindrical rotating

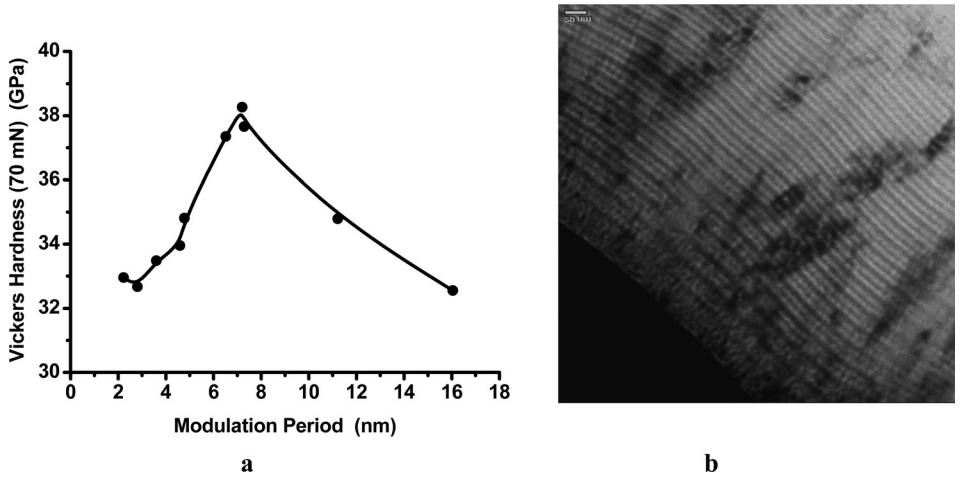

FIG. 20. (a) Maximizing the hardness of the nc-$(Ti_{1-x}Al_x)N$/a-Si_3N_4 nanocomposite coatings by optimising the period of the compositional modulation in the deposition equipment results in (b) nanolayered superhard nanocomposite coatings with a high hardness and high resistance against brittle fracture (Ref. 237).

cathodes made of Ti and Al + Si.[170,236–238] When the tool being coated is, during the rotation of the turntable on which it is mounted, closer to the Ti cathode the layer will be Ti-rich and when it will be closer to the Al + Si cathode the layer will be Al + Si-rich, as seen on the TEM micrograph in Fig. 20(b) by alternating darker and brighter nanolayers. By appropriately adjusting the deposition rate and the rotation speed, one can optimize the period of the compositional modulation and increase the hardness and toughness as shown in Fig. 20(a).[170,239]

There are many papers dealing with multilayers for toughening of the nanocomposites whose discussion is beyond the scope of this paper. Worth-mentioning is the recent work of Wo *et al*. who prepared TiN/TiSiN multilayers consisting of 10 and 50 nm thick TiSiN layers between thicker TiN.[48] These researchers provided in-depth studies of the mechanism of toughening. Although the hardness of the multilayers was somewhat smaller than that of monolithic TiSiN, the toughness significantly increased because of the transition of deformation mechanism from brittle (transgranular) cracking in monolitic TiSiN (probably associated with oxygen impurities which are not reported in that paper) to inelastic shear sliding governed by the microstructural characteristics of the coatings. The work of Wo *et al*. has been supported by detailed TEM analysis and finite element modeling (FEM). Of interest is also the recent work of Wang *et al*. on the CrAlSiN/CrAlN multilayers where increase of toughness by a factor of 5 has been combined with a modest increase of hardness.[62]

As mentioned in Ref. 48, the work of Wo *et al*. has been motivated by the difficulty to prepare coatings with low oxygen impurity content. It would be of great interest to have a comparison of these results with nanocomposites that have oxygen impurity content of 100 ppm or less. Would there be really any advantage of such toughening in pure nanocomposite coatings?

Zhang *et al*. have also shown that the scratch adhesion strength and higher resistance against crack propagation of CrAlSiN coatings can be improved by gradient composition starting from CrAlN and increasing the Si content during the deposition of the coatings.[240] It should be noted that hard and superhard nanocomposite coatings with composition gradient are used in industrial applications since several years (see, e.g., 237 and 238 and references therein). For example, gradient TiAlCN with diamond-like carbon coatings as solid lubricant are offered by company PLATIT AG for the milling, tapping, punching, and stamping to avoid built up edges, for forming applications to optimize release and for machining of high alloyed materials, such as nickel alloys, Inconel, superalloys, and the like.[236]

Another method of toughening of the nanocomposite coating is the introduction of a ductile metal, which does not form stable nitrides, such as Ni studied in some detail by Zhang *et al*.[60,61,241] The toughness of TiSiN and CrAlSiN coatings with a relatively high oxygen content of 1.2–1.5 at. % (Ref. 240) could be significantly improved from about 1.15 $MPa \cdot m^{0.5}$ to 2.60 $MPa \cdot m^{0.5}$ by the addition of about 40 at. % of Ni while the hardness still remainded at about 14 GPa relatively low.[61] In the case of nc-CrAlN/Si_3N_4 nanocomposites, addition of relatively small amount of Ni decreased the grain size from 7 to 2 nm at Ni content of about 4.2 at. % and increased the scratch toughness by 200% at expense of 18% decrease of the hardness. But upon a further increase of Ni content to about 40 at. %, the grain size increased and hardness and toughness decreased again.[242] We are again left with the open question how would such nanocomposites behave if their impurity content were low, in the few 100 ppm or even lower range.

Unlike the TmN/Ni coatings reported by Musil *et al*., which have high hardness but also high biaxial compressive stress due to energetic ion bombardment at relatively low temperature (see discussion above), the coatings deposited by Zhang *et al*. have relative modest hardness but high toughness and low biaxial compressive stress. However, the question remains if this toughening would be needed when the impurity content could be decreased to few 100 ppm or less. It is possible that the high elastic limit, as demonstrated for the pure ultrahard nanocomposites above, would make

such toughening unnecessary. This is another open question which calls for the preparation of pure nanocomposites with low oxygen impurity content. We shall show one example of successful applications of $Ti_{1-x}Cr_xN$/Ni nanocomposites for forming by the company SHM[243] in Sec. IV on industrial applications.

D. $TiB_{2+\delta}$ and Ti-B-N superhard nanocomposites

Titanium diboride, TiB_2, has a high intrinsic hardness of about 30 GPa.[54] Therefore, many papers deal with the preparation and properties of this interesting material. The drawback of TiB_2 and other borides with respect to applications in machining is the low melting point of boron oxide of about 450 °C.[121] Therefore, borides do not posses the high oxidation resistance that is often required.

Of great scientific interest are **TiB_2/B nanocomposites** which reach hardness up to 60 GPa.[244] Several authors reported very high hardness in "overstoichiometric" $TiB_{2+\delta}$ with $\delta \approx 0.2$–0.4.[245–248] Neidhardt *et al.* conducted detailed studies of the compositional evolution of the Ti-B films deposited by sputtering from a compound target.[249] The microstructure of superhard $TiB_{2.4}$ nanocomposites prepared by magnetron sputtering has been studied by Mayrhofer *et al.*[244] The films had dense columnar morphology consisting of about 20 nm wide columns with 0001 preferential orientation, encapsulated by boron-rich interfacial layers. These columns were formed of a bundle of about 5 nm diameter TiB_2 subcolumns, which have been separated by an ultrathin B-rich material. This hierarchic nanostructure provided the nanocomposites with the very high hardness of 60 GPa, which was stable upon annealing in vacuum up to 700 °C. It would be interesting to conduct first-principles studies of this system in order to see if the boron interfacial layers are also strengthened like the Si_3N_4 ones in the nc-TiN/Si_3N_4 nanocomposites discussed above.

Numerous studies have been devoted to the **Ti-B-N system** in which coatings with hardness of 35 to 55 GPa have been reported (see, e.g., Refs. 250–253). When deposited at a relatively low temperature of 300 °C, the hardness of about 37 GPa increased to 43 GPa upon annealing at 800 °C but decreased again upon annealing to $\geq$900 °C.[254] Hammer *et al.* deposited Ti-B-N coatings at room temperature with hardness of about 27–29 GPa. Upon annealing to 800 °C, the hardness increased to 40 GPa as result of nanocomposite formation and remained constant for 200 min.[250]

Similar results have been reported also for the Cr-B-N system. When the deposition has been done at a sufficiently high pressure of nitrogen, nanocomposites consisting of the stoichiometric nitrides CrN and BN have been formed with hardness of 29 GPa.[255,256]

Of particular interest was the attempt to replace the Si_3N_4 in the nc-TmN/Si_3N_4 nanocomposites by an alternate covalent nitride, such as BN and to form stoichiometric **nc-TiN/BN nanocomposites** with BN as interfacial 1 ML layer. As discussed above, one has to distinguish between the nitrogen deficient TiB_xN_{1-x} and nitrogen rich stoichiometric TiN/BN system, because the former should decompose by nucleation and growth, whereas the latter is chemically spinodal.[195] However, in view of the large difference in the size of Ti and B atoms, the system is unlikely to be coherently spinodal because the TiN-BN interface is incoherent, as seen also from the fact that some Ti-B bonds have always been detected in the interfacial BN layer.[196] Recently, Ivashchenko *et al.* have shown that the 1 ML BN in the (001) TiN/BN/TiN heterostructures is unstable in its symmetric fcc-configuration already at 0 K.[227] Nevertheless, hardness of about 50 GPa has been achieved in this system when the BN interfacial layer was about 1 ML, and the hardness enhancement has been lost when the thickness was 2 ML (see Fig. 7 in Ref. 196). More recent analysis of the results published in Ref. 196 revealed that the crystallite size in the nc-TiN/1 ML BN nanocomposites with the maximum hardness was around the "strongest size" of about 10 nm, and the crystallite size increased for both thinner and thicker BN layers. Therefore, the hardness enhancement by about a factor of 2 is more likely due to the refinement of the morphology toward the "strongest size." The strengthening of the interfacial BN layer by valence charge transfer from TiN in a similar way as in the nc-TiN/Si_3N_4 nanocomposites may also contribute to the experimentally found hardness enhancement, because the electronegativity of boron is larger than that of Ti and also somewhat larger than that of Si.[83]

First-principles study of heterostructures consisting of TiN slabs with 1 ML BN interfacial layer have shown that the shear and decohesion occur between the Ti-N bonds attached to the BN interface[257,258] in a similar manner as found for the TiN/SiN system by Zhang *et al.*[216,218,220] However, this system is unlikely to replace the nc-TiN/Si_3N_4 because it has lower oxidation resistance comparable with that of TiN (see Fig. 10 in Ref. 196), and it losses boron upon annealing.[259]

E. Oxide-based nanocomposites

Oxide-based hard and superhard nanocomposites would be of great interest for applications as wear protective coatings on tools for hard and dry machining where high oxidation resistance is important. Although, as already mentioned, hard $(Al_{1-x}Cr_x)_2O_3$ coatings with corundum structure have been successfully deposited by PVD in intense plasmas at temperature $\leq$600 °C,[260] attempts have been made to prepare oxide-based nanocomposite in the hope to obtain higher hardness.

Klostermann *et al.* reported the deposition of nc-Al_2O_3/ZrO_2 nanocomposites by reactive cosputtering from Al and Zr targets at temperature of 500–700 °C.[261] The Al_2O_3 has been formed in the γ-phase, which is somewhat softer than corundum (21 ± 1.5 GPa). A hardness enhancement to about 30 GPa has been found at a Zr concentration of about 8 at. %. At an alumina content of less than 18 at. %, the coatings consisted of tetragonal zirconia with hardness of about 17 GPa. However, the hardness of pure γ-Al_2O_3 of about 28 GPa reported in that paper seems to be too high, and the enhancement upon formation of the nanocomposites is

therefore relatively small. Therefore, more detail study of this system are demanding. Zukerman deposited such nanocomposites by means of filtered vacuum arc and obtained maximum hardness of about 22–26 GPa at deposition temperature of 500 °C.[262]

Jilek studied the deposition of Cr-Zr-O coatings by vacuum arc evaporation at about 500–520 °C. At a Zr content of about 5.5 at. %, he obtained a pronounced hardness enhancement to 41–42 GPa, whereas at lower and higher Zr content the hardness decreased to about 20 GPa or less.[263]

Interesting is also the recent paper on the nc-Al_2O_3/a-Al_2O_3 nanocomposites deposited by pulsed laser depposition at either room temperature or at 600 °C.[264] Coatings deposited at room temperature had relatively low hardness of 10 GPa and moderate stiffness ($E_Y = 195$ GPa) resulting in an H/E_Y ratio of 0.049. When grown at 600 °C, the hardness of the nanocomposites of 25 GPa increased above that of Sapphire (21 GPa) and the stiffness increased as well ($E_Y = 277$ GPa) resulting in a high H/E_Y ratio of 0.091, which suggests an outstanding resistance to wear. The crystallite size of the nc-Al_2O_3 was about 2–5 nm.

These examples show that there seems to be a possibility to prepare oxide-based nanocomposites with an enhanced hardness. It is however not clear which mechanism of hardening is responsible for the observed hardness enhancement. The strengthening of the interfacial ZrO_2 layer by a similar mechanism as in the nc-TiN/Si_3N_4 nanocomposites is unlikely because Zr has a lower electronegativity than Cr and Al. Nevertheless we speculate that the decomposition of the $CrZrO_x$ solid solution by spinodal mechanism should be advantageous because it would result in a regular nanostructure with sharp interface. As mentioned above, the Al-Zr-O_x system is spinodal.[197] The stoichiometric $Cr_2O_3 + ZrO_2$ system is below about 1800 °C immiscible[265] and possibly spinodal. Unfortunately, the data in Ref. 265 are limited to high temperatures of ≥ 1100 °C. Therefore, the combined DFT calculations and thermodynamic modeling would be highly demanding to better understand this system. Nevertheless, even if the decomposition would occur by nucleation and growth the concomitant hardness enhancement by a factor of 1.5–2, which may be achieved by an appropriate control of the grain size of the nanocrystalline phase toward the "strongest size," may provide very useful coatings for industrial applications.

IV. INDUSTRIAL APPLICATIONS OF HARD AND SUPERHARD NANOCOMPOSITES

The applications of hard nitride-, boride-, and carbide-based coatings have been discussed in many papers and books (e.g., Refs. 266–269). The breakthrough was the development of PVD process for the deposition of TiN at relatively low temperatures compatible with tools made of high speed steel (HSS) in 1980s, followed by the development of TiAlN in 1986 and more recently CrAlN. Presently, there are more than about 70 different types of dedicated hard coatings applied on tools for a variety of machining, forming, stamping, injection molding, casting, and other applications. A significant progress has been achieved recently by the development of PVD techniques that allows to deposit hard $(Cr_{1-x}Al_x)_2O_3$ oxides with corundum structure at 500 °C, which is much lower than temperature of about 1000 °C needed in thermal CVD.[260,270,271]

Here we focus on the industrial applications of the hard and superhard nc-TmN/Si_3N_4 nanocomposite coatings on tools for machining (turning, drilling, milling, forming, stamping, injection molding, and the like) of steels, superalloys, and other metals[237–239,272–276] of Al alloys in combination with graphite fibers reinforced carbon composites or plastics[277] and for injection molding.[278] Because most of the information is proprietary, it is difficult to obtain representative examples from the companies. Therefore, our selection is a combination of what should be shown, and what we could obtain and were allowed to present in this review.

As emphasized at the beginning of this paper, high hardness is only one of many important properties, such as high fracture toughness, high thermal stability and oxidation resistance, low coefficient of friction, compatibility of the coatings with the material being machined, low thermal conductivity and others which have to be optimized for a given application. For example, diamond cannot be used for machining of materials which form carbides, such as ferrous steels and the like. During continuous turning of steel at high cutting speed of 200 m/min, the temperature of the flank of indexable insert reaches almost 900 °C (see Fig. 1 in Ref. 279). Obviously, high thermal stability, oxidation resistance, and low thermal conductivity, which reduces the heat flow into the cutting edge, are important in that case. Fortunately, the nc-TiN/Si_3N_4 has significantly higher oxidation resistance than TiN (Refs. 19 and 20) and nc-$(Ti_{1-x}Al_x)N$/Si_3N_4 as well as nc-$(Cr_{1-x}Al_x)N$/Si_3N_4 nanocomposites with a sufficiently high silicon content of 8–10 at. % begin to oxidize only above 1000 °C.[18,280–284] The low thermal conductivity of the nanocomposites is due to strong phonon scattering within the few nanometer size TmN nanocrystals surrounded by a material (SiN_x) with a different phonon spectrum.

Tanaka *et al.* have originally developed "Ti-Al-Si-N" solid solution coatings and demonstrated their superior cutting performance as compared with the TiAlN,[280,281] but later on they have shown that the nanocomposites display an even better cutting performance than the solid solution[282] (see also review 237 and references therein).

Because of the above discussed detrimental effect of oxygen impurities on the segregation of TmN and Si_3N_4 phases, which hinders the formation of strong nanostructure and degrades the mechanical properties, many authors and companies complain about the brittle nature of the nanocomposite coatings. However, there are examples of coatings deposited in industrial coating systems with oxygen impurity of $\leq$1000 ppm (0.1 at. %). Figure 21 shows an example of the composition and impurity concentration, measured by means of elastic recoils detection [ERD (Refs. 285 and 286)], of TiN coating deposited in an industrial coating unit ORM by company SHM (Ref. 243) with impurity content of about 700 ppm (0.07 at. %). In collaboration with that company, we have analyzed many nc-$(Ti_{1-x}Al_x)N$/a-Si_3N_4 and

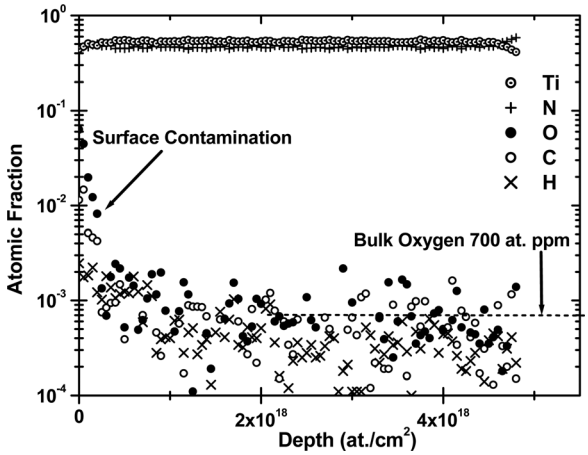

FIG. 21. Example of a TiN coating deposited in industrial coating unit ORM by SHM s.r.o. with low oxygen impurity content of 700 ppm (Ref. 243).

other nanocomposite coating and found fairly reproducibly the impurity to be $\leq$1200 ppm. (In the industrial community one uses for these coatings a simplified term "TiAlSiN." We shall use it in the following as well. Accordingly, AlTiN means $(Ti_{1-x}Al_x)N$ coatings with higher content of Al than Ti, and similar terminology will be used for CrAlN etc.)

Also, the company Balzers achieved a low oxygen impurity content of about 0.16 at. % in the conventional AlCrN "Alcrona" coatings (the coatings have been analyzed by the present author using ERD). These coatings are known for their very good cutting performance, which is probably related to their high toughness, but there seems to be no systematic study if this is a result of the relatively low impurity content. It is also experience of the present author, who analyzed a number of coatings from other companies, that the oxygen (and other) impurity content in the coatings is usually much higher, often in the range of 1–2 at. %.[189] Therefore, in view of the results shown in Figs. 10 and 11, it is clear that the problem of impurities, mainly oxygen, is much more serious for the nanocomposite coatings deposited in industrial coating equipments. The best presently available industrial nanocomposite coatings with oxygen impurities of $\leq$0.1 at. % are still not optimum. As we shall see, in spite of that problem, they show very good cutting performance in many applications. Nevertheless, a further improvement of the purity is demanding.

With reference to Fig. 10, we see that these coatings need relatively high deposition or annealing temperature in order to complete the decomposition of the solid solution and segregation of the TiAlN and Si_3N_4 with the formation of strong nanostructure. Indeed it has been reported that the hardness of as-deposited industrial nanocomposite coatings increases upon annealing.[120] Therefore, these coatings are applied mostly on tools made of cemented carbides, whereas on tools made of HSS one still prefers AlTiN/TiAlN or CrAlN/AlCrN multilayers. The nanomultilayers consisting of $\geq$50 about 50–100 nm thick CrAlN layers with varying Cr:Al ratio have been developed and are used under the name "Nanosphere®" on hobs made of HSS for the cutting of teeth in the wheels for gears by company LMT.[287,288] Such tools are very expensive and therefore the prolonged life time and the posibility to strip the used coatings, regrind, and recoat the tools are very important.

The advantage of the CrAlN nanolayered multilayers as compared with TiAlN is the lower thermal conductivity which reduces the heat flow into the tool made of HSS because the temperature of the cutting edge should not exceed 530 °C. The life time of hobs coated with the CrAlN nanomultilayers ("Nanospheres") increased by about 40% as compared with monoblock CrAlN layer.[288] Hobs made of cemented carbides are much more expensive, but because they survive much higher temperature, the nc-$(Cr_{1-x}Al_x)N$/Si_3N_4 nanocomposites have been used and the life time increased by more than a factor of 5 as compared with standard coatings (see Fig. 14 in Ref. 237).

The nanocomposites alone may not be always the optimum solution. Therefore, they are often used in combination with conventional coatings as illustrated in Fig. 22, from Refs. 237 and 238. The simple AlTiN + TiSiN coatings (TiSiN = nc-TiN/Si_3N_4 nanocomposites) from company Mitsubishi are in dry ball nose milling performing significantly better (curve 2) than the conventional AlTiN ones (curve 1). The first generation of the nc-$(Ti_{1-x}Al_x)N/Si_3N_4$ nanocomposites coatings has been performing much better than the TiSiN ones until, after about 1200 m machined length, a sudden unpredictable wear occurred (curve 3). This is typical failure behavior of a tool or a machine part due to fatigue. However, the particular failure was not due to the fatigue of the coatings, but to the fatigue of the cemented carbide substrate. The solution has been found by inserting a "buffer layer" between the substrate and the nanocomposite top layer, and to increase the Si-content in the nanocomposite layer, which resulted in a predictable wear and significantly increased life time (curve 4). Similar results have

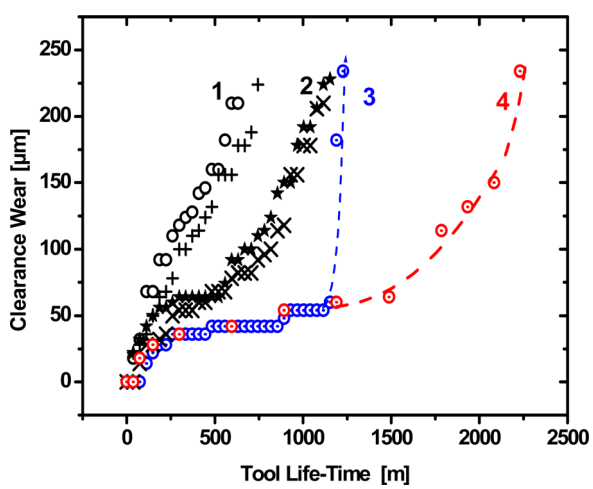

FIG. 22. (Color online) Hard ball nose milling of 57 HRC hard steel using end mills made of cemented carbide coated with different coatings, diameter 10 mm with minimum jet lubrication. Curve **1:** state-of-the-art $(Al_{1-x}Ti_x)N$, **2:** AlTiN + TiSiN coatings, **3:** first generation of nc-$(Ti_{1-x}Al_x)N$/a-Si_3N_4 nanocomposite coatings, **4:** second generation of nanocomposite coatings with a softer under-layer and gradient top-nanocomposite layer with higher Si-content. 18 500 rpm, f = 0.18 mm, a_P = 0.25 mm, a_e = 0.6 mm (From Ref. 238).

been reported recently also for the nc-$(Cr_{1-x}Al_x)N/Si_3N_4$ nanocomposite coatings by Ding *et al.*[284]

Meanwhile these "TripleCoatings®" shown in Fig. 23 became a standard in many companies.[236,243,289,290] The gradient Ti → TiN thick adhesion layer about 300 nm provides a very good adhesion of the TripleCoatings of more than 150 N in the standard scratch test. After the adhesion layer, about 2 μm thick TiAlN interlayer is deposited, which absorbs localized stresses during machining and distributes them over larger volume, thus protecting the cemented carbide substrate. On the top is than deposited the superhard, about 1 μm thick nanocomposite layer. When coatings with (CrAl)N interlayer and nc-$(Cr_{1-x}Al_x)N/Si_3N_4$ top layer are deposited, gradient Cr → CrN adhesion layer is used. These coatings are cenveniently deposited by the LARC© technology which uses vacuum arc evaporation from rotating cylindrical cathodes placed close to each other.[236,243,291] By simply changing the arc current on the different cathodes, one can control the composition and change it during the deposition.[289,290] When using planar cathodes, one has to optimize the deposition in another appropriate manner, e.g., using many smaller targets made of different materials.

The advantages of the nanocomposite coatings as compared with the conventional ternary ones, such as TiAlN, CrAlN, and others, is mainly the higher hardness, oxidation resistance, and low thermal conductivity. For example, the hardness of the CrAlSiN nanocomposite coatings with medium and high silicon content remains stable or even increases after 2 h annealing at 1000 °C.[283] This can be used either to increase the life time of an expensive tool or to increase the machining speed and consequently the productivity when the tools are not too expensive. An example par excellence of increasing the life time is shown in Fig. 24. Because the saw made of cemented carbide is expensive, the increase of the life time by a factor of 25 is very important.

When the tools are not too expensive, one prefers to increase the machining speed yet having similar life time,

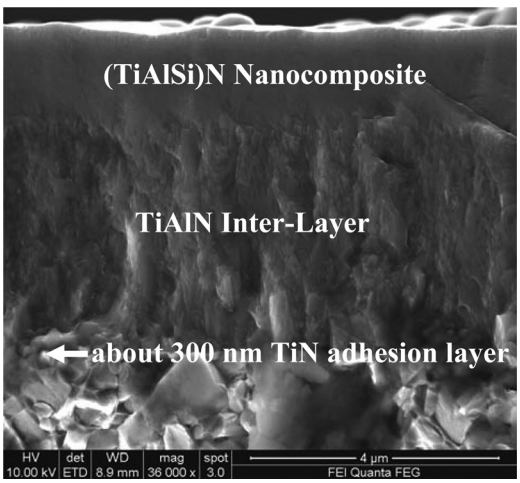

FIG. 23. Example of "Triplecoatings®" (Ref. 236): The gradient Ti → TiN about 300 nm thick adhesion layer provides a very good adhesion followed by about 2 μm thick TiAlN border layer, which absorbs localized stresses during machining and distributes them over larger volume, thus protecting the substrate. On the top is a superhard thick nanocomposite layer of about 1 μm.

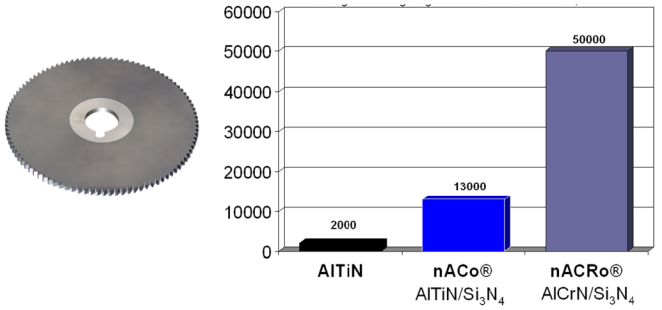

FIG. 24. (Color online) Effect of different coatings on the life time of expensive saw made of cemented carbide (diameter 125 mm, thickness 3.6 mm). Precision cutting of sintered workpiece material Co1 with tolerance 0.2 mm. Conditions: n = 300 rev./min, v_f = 800 mm/min, a_p = 35 mm, coolant: 7% emulsion. Source: Prétat, Selzach, CH. Reprinted with permission from www.platit.ch Compendium 2012, p. 88. Copyright 2012, BCI Group.

and in such a way to increase also the productivity, as illustrated in Fig. 25. In an identical drilling of cast iron, the drills coated with the nanocomposites were operated at 50% higher surface speed and feed rate still having the same or slightly longer life time. This increase in machining speed corresponds to a significant increase of the productivity by 56%.

Not always superhardness is needed. For forming of soft but tough steel high fracture toughness, low internal stress and excellent adherence of the very thick coating to the substrate tool is more important. In the given example, the goal was to form about 15 tons of the standardized rectangular profiles with a prescribed small tolerance, made of unalloyed steel DIN 1.0028. For the given number of more than 1000 pieces, about 5–6 conventional forming tools made of hardened steel were usually needed. Instead, one old, worn tool has been coated with about 100 μm thick $Ti_{1-x}Cr_xN/Ni$ nanocomposites with a modest hardness of about 17–20 GPa deposited at high rates of $\geq$10 μm/h.[292] The crystallite size of the nitrides and nickel was about 3–5 nm, and the deposition conditions were optimized as to reach an almost zero stress and a high adherence of the thick coatings. It is not possible to report the increase of the lifetime of the coated tool because, after finishing the whole batch of 15 tons (1065 tubes each 8 m long), no wear of the coating could be measured. Besides saving the 5–6 conventional uncoated tools, which would have been needed for this fabrication, the total production time has been reduced to half because of saving time for the service, for the exchange of worn tools, and because the coatings allowed to increase the forming speed from 8.6 to 13.7 m/min. This resulted in an increase of the productivity by about 100%.

The structure of the TmN/Ni or TmN/Cu nanocomposites differ significantly from that of the nc-TmN/Si_3N_4 ones because the soft and ductile metal is not "wetting" the hard transition metal nitride, but it forms also nanocrystals as mentioned for the $Ti_{1-x}Cr_xN/Ni$ nanocomposites above, and reported also for the ZrN/Cu (Ref. 293) and nc-CrAlN/Si_3N_4/Ni (Ref. 242) nanocomposites.

Molten metals, in particularly aluminum alloys, are very aggressive media. Therefore, dies for casting and injection

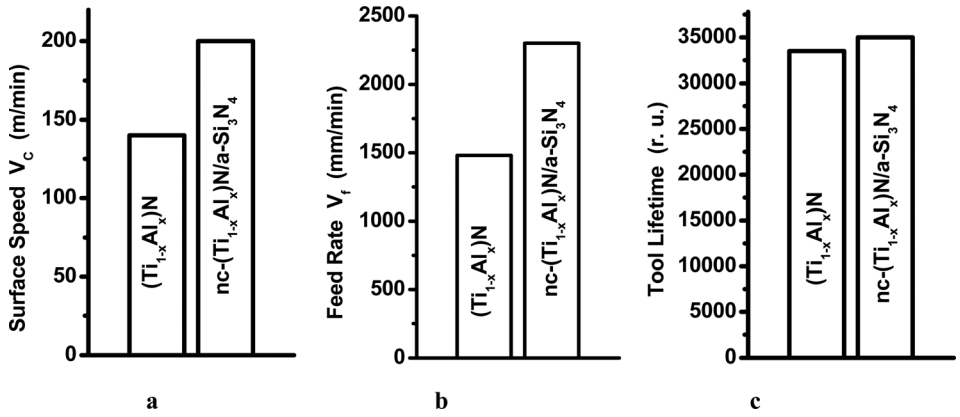

FIG. 25. Comparison of the state-of-the art TiAlN coatings with nc-$(Ti_{1-x}Al_x)N$/a-Si_3N_4 nanocomposite coatings on drills made of cemented carbide of diameters between 7.1 and 12 mm. Cast iron GGG40, internal cooling 50 bar 5% emulsion. Note that the drills coated with the nanocomposites were operating at 50% higher cutting speed (a) and feed rate (b) still having the same life time (c) resulting in an increase of the productivity by 56%. (Source Sauer Danfoss Steerings DK).

molding have to be protected by surface layers. In the case of injection molding of Al alloys, the conventional treatment of tools made of steel is plasma nitriding which results in a gradient nitrided layer of several 10 μm thick. Figure 26 shows tools for injection molding of aluminum alloys for automotive industry after the fabrication of 15 000 parts. Whereas the conventionally treated tool shows already serious wear, the one coated with 2–3 μm thick nc-$(Cr_{1-x}Al_x)N$/Si_3N_4 nanocomposite coatings displays no visible wear.[292]

We have mentioned above that, because of oxygen impurities, there are some problems to apply the nanocomposite coatings on tool made of high speed steel HSS. Yet, there are examples where these coatings improve the machining performance of tools made of HSS. Figure 27 shows the dependence of the lifetime of end mills made of HSSCo8 and coated with different coatings: "nACo" and "nARCo" are nc-$(Al_{1-x}Ti_x)N$/Si_3N_4 and nc-$(Cr_{1-x}Al_x)N$/Si_3N_4 nanocomposite coatings, respectively, and AlTiN and TiAlCN are the conventional coatings.[236] Whereas the life time of mills coated with the conventional coatings decreases with increasing cutting speed, it increases for mills coated with the nanocomposites, probably because of the higher hardness and much lower thermal conductivity of the nanocomposites, as compared with the conventional coatings (see Ref. 236, p. 84, and Refs. 294 and 295), which reduced the heat flow to the cutting edge. As mentioned, the low thermal conductivity is due to the intense phonon scattering in the nanostructure where the few nm small $(Al_{1-x}Ti_x)N$ and $(Cr_{1-x}Al_x)N$ nanocrystals are surrounded by Si_3N_4-like interfacial layer with a different phonon spectrum. Of course there is a maximum life time at a certain cutting speed above which the life time decreases again, because each tool in a given operation has an optimum cutting speed where it shows the maximum life time.[296]

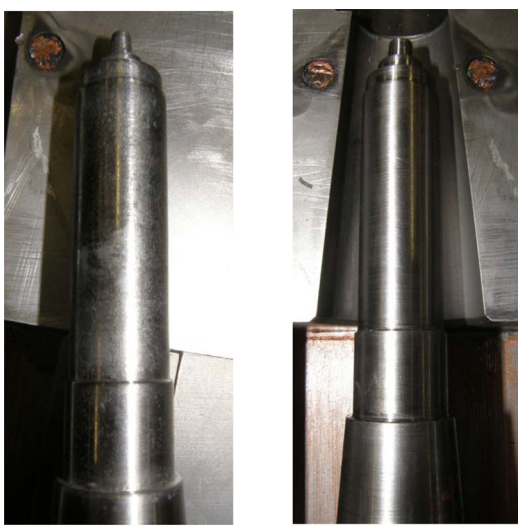

FIG. 26. (Color online) Tools for injection molding of Al-alloys for automotive industry after the fabrication of 15 000 parts. The length is about 200 mm and diameter 15–25 mm. (a) Conventionally treated by plasma nitriding, which forms several 10 μm thick layer, (b) coated with 2–3 μm thick layer of nc-$(Cr_{1-x}Al_x)N$/a-Si_3N_4 nanocomposite (Ref. 292).

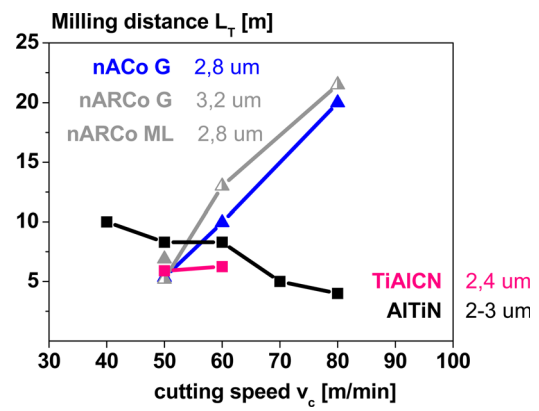

FIG. 27. (Color online) Dependence of the lifetime of mills made of HSSCo8 and coated with different coatings: "nACo" and "nARCo" are nc-$(Al_{1-x}Ti_x)N$/a-Si_3N_4 and nc-$(Cr_{1-x}Ti_x)N$/a-Si_3N_4 nanocomposite coatings. Material being machined Cmo4 heat treated steel, HB 310, Mill FRAISA 10 mm, $z=4$, $a_e=5$ mm. $a_p=5$ mm, $F_z=0.05$ mm, emulsion ARAL 230, 8 l/min. The criterion of the lifetime if wear $VBC_{max}=0.6$ mm. Reprinted with Permission from www.platit.ch Compendium 2012, p. 82. Copyright 2012, BCI Group.

V. CONCLUSIONS AND OUTLOOK

The recent search for new intrinsically superhard materials focused mainly on those with high elastic moduli. However, because electronic instabilities and concomitant transformation to phases with lower plastic resistance limit the possibility to achieve high intrinsical hardness, this approach brought only limited success. Therefore, this work is of some interest for basic science but of limited impact for industrial applications. More promising is the design of nanostructured materials, such as single- or polycrystalline heterostructures, nanosized single-phase materials, and nanocomposites. In general, strength and hardness enhancement can be achieved by decreasing the crystallite size because of decreasing dislocation activity down to a grain size of 10–15 nm called "the strongest size." Upon a further decrease of the grain size, softening occurs due to increasing grain boundary shear, which limits the achievable hardness enhancement typically to a factor of 1.5–2.

This softening can be reduced by forming nc-TmN/Si_3N_4 nanocomposites with strengthened Si_3N_4-like interfacial layer due to valence charge transfer from the TmN to the Si_3N_4, as result of a larger electronegativity of Si as compared to the transition metal Tm (Ti, V, ($Ti_{1-x}Al_x$), ($Cr_{1-x}Al_x$), and others). Such nanocomposites are formed by self-organization upon spinodal decomposition of the Tm-Si-N solid solution. So far, no other covalent nitride has been found to perform better than Si_3N_4.

Although superhardness of 50 GPa could be achieved in the nc-TiN/BN nanocomposites, their relatively low oxidation resistance is similar to that of TiN due to the low melting point of boron oxide of 450 °C. Whereas the strengthening due to "the strongest size" is fairly general and operates in many systems, the formation of superhard nc-TmN/Si_3N_4 nanocomposites has some limitations, which have been discussed in this paper and in Ref. 175.

Large progress has been achieved in the understanding of the nc-TmN/Si_3N_4 nanocomposites by means of careful preparation and characterization as well as by theoretical first-principles calculations and thermodynamic modeling. Theoretical studies have shown that in a pure nc-TiN/Si_3N_4 nanocomposite system hardness in excess of 100 GPa can be achieved. In practice, it is limited by a variety of flaws of which oxygen impurities are the most "dangerous" ones. Therefore, the hardness of $\geq$100 GPa could be so far achieved only in the quasiternary nc-TiN/Si_3N_4/$TiSi_2$ nanocomposites with low oxygen impurity of only few 100 ppm, because the $TiSi_2$ phase acts as a getter of oxygen thus removing it from the Si_3N_4 interfacial layer. However, this beneficial effect of $TiSi_2$ is contrasted by its long-term mechanical instability that results in decrease of the hardness of the nanocomposite coatings after several months.

The quasibinary nc-TiN/Si_3N_4, nc-($Ti_{1-x}Al_x$)N/Si_3N_4, and other nc-TmN/Si_3N_4 nanocomposites are long-term stable but, because of the absence of the gettering effect of $TiSi_2$, they are more sensitive to the oxygen impurities. Nevertheless, hardness of 65–70 GPa has been demonstrated when the oxygen impurities were in the low 100 ppm regime (Fig. 14). From the point of view of fundamental research, it is challenging to decrease the impurities significantly below 100 ppm because the available experimental results and theoretical modeling suggest that it should be possible to reach long-term stable hardness of 100 GPa or more. The relatively low load-invariant hardness enhancement reported by many groups for Tm-Si-N coatings is, most probably, due to the relatively high content of oxygen impurities of 0.5 to several at. %.[189] On the other hand, some reports of very high hardness in the Tm-Si-N systems containing oxygen impurities should be taken with care because these values have often been obtained at very low load and, therefore, are not guaranteed to be load-invariant.

The high hardness reported by Veprek *et al.* has been measured correctly. The contradictory claim of Fischer-Cripps *et al.*[201] is their trivial mistake due to fitting of the incorrect indentation curves as shown by Veprek *et al.* already in 2003 (Ref. 297) and outlined in more detail recently.[175] The hardness evaluated from the size of remnant plastic deformation obtained from the SEM micrographs (e.g., Fig. 13) provides reliable values because it is not subjected to any of the errors which may occur during the automatic load-depth indentation measurements.

Tm-Si-N coatings with $\geq$0.5 at. % of oxygen should not be denoted "nanocomposites" but, as shown by Flink *et al.*, Tang *et al.*, and by the results in Fig. 10 for the Ti-Si-N system, they are likely to be polycrystalline Ti-Si-N-O_δ (or Tm-Si-N-O_δ) solid solutions, sometimes with small crystallite size in the 10 nm range due to size refinement by the impurities, and with a limited hardness enhancement due to solution- and reduced-grain-size-hardening. TEM studies of such systems show often a nanostructure similar to the nanocomposites with low oxygen content of a few 100 ppm, particularly when taken in plain view, but careful studies of the cross-sectional TEM micrographs reveal a columnar morphology with much larger crystallite size than that found in nanocomposites deposited by plasma CVD that have low impurity content of few 100 ppm.

Besides impurities, there are several other limits to the preparation of the super- and ultrahard nc-TmN/Si_3N_4 nanocomposites, which were briefly summarized in this review and discussed in more detail in Ref. 175. Important is the finding that, although the stoichiometric and pure transition metal nitrides TmN and Si_3N_4 are immiscible,[154] not all the Tm-Si-N_y systems are spinodal, but many of them decompose by the mechanism of nucleation and growth, which does not yield any regular nanocrystals of a similar size of 3–4 nm with sharp TmN/Si_3N_4 interfaces. Hardness enhancement to 30–35 GPa can be achieved in these systems by optimizing the nanostructure toward "the strongest size" with grain size of 10–15 nm, but superhardness of >40 GPa can be—as far as we understand these systems so far—achieved only in Tm-Si-N systems, which are spinodal and free of impurities. It is demanding to continue the combined DFT and thermodynamic studies of Zhang and Sheng to find other suitable systems because such studies are much faster and less expensive than the empirical approach.

The presently available industrial applications of the nanocomposite coatings on tools are very encouraging, but a further improvement of the quality of the nanocomposites, mainly to lower the oxygen content, is demanding. The results obtained so far suggest that high-quality nanocomposite coatings could be deposited also on tools made of HSS, which should not be heated above 530 °C, if the impurities would be decreased to few 100 ppm. The presently achieved lowest impurity content of 700–1000 ppm (0.07–0.1 at. %) in industrial coatings by the company SHM (Fig. 20) needs an improvement by a factor of 3–4 to achieve this goal. This is another big challenge. If this problem could be solved, the economic impact would be great.

From the scientific point of view, it is highly challenging to further decrease the oxygen impurities significantly below 100 ppm in order to verify the theoretical prediction[13] that hardness in excess of 100 GPa should be achievable in the nc-TiN/Si_3N_4 system. Because hardness of 65–70 GPa has been demonstrated in these nanocomposites[175] when the impurity content was about 100 ppm, the lowest achieved so far, the hardness in excess of 100 GPa predicted theoretically seems to be possible. This is a great challenge, particularly for younger researchers.

ACKNOWLEDGMENTS

The author would like to thank all his coworkers and colleagues who have participated in the work and in many discussions during the past years, and in particular Paul Mayrhofer, Ruifeng Zhang, Dominik Legut, Zhijun Lin, and Ali S. Argon for critical reading of the manuscript and many helpful comments. The author also thanks his wife Maritza Veprek-Heijman for much help with writing this review, checking the references, and many comments and recommendations to the manuscript.

APPENDIX A: MEANING AND MEASUREMENT OF HARDNESS

The initial, elastic deformation upon indentation with low load is described by the well-known Hertz's equations[298,299] until plastic deformation commences in a depth of about half of the contact radius between the indenter and the material. At this point of yielding, the average pressure under the indenter is about $1.1 \cdot Y$ where Y is the yield strength of the material.[1,299,300] Hertz originally defined the indentation hardness as the pressure under the indenter upon onset of yielding. However, at this stage the amount of plastic deformation is limited to a small region below the surface of the area of contact, and the overall deformation is dominated by elastic one. It has been shown by Meyer in 1908 that, with increasing applied load, the average pressure further increases and reaches a constant value only at a sufficiently large load L,[209] where the plasticity is fully developed. During this transition, the maximum of the deviatoric strain moves toward the surface of the contact as shown by nonlinear finite element modeling (see Fig. 8 in Ref. 301, and a more recent study by means of advanced FEM by Song and Komvopoulos[323]). Under the conditions of fully developed plasticity, the average pressure under the indenter is constant, i.e., the measured hardness $H = L/A_C$ is independent of the applied load.

For these reasons, the industrial norms require that the indentation hardness is measured under the conditions of fully developed plasticity, i.e., a sufficiently large load has to be applied for a sufficiently long time to allow the plastic deformation to fully develop. Conventionally, the indenter (e.g., Vickers which is a four-faced pyramid with angle between opposite faces of 136°; this angle has been chosen as to make the Vickers measurements comparable with the Brinell test; see Ref. 1, p. 98) [here we consider only indentation hardness measured with self-similar indenters, such as diamond pyramid of Vickers or Berkovich geometry, where the contact area A_C is proportional to the square of the indentation depth h, $A_C = \text{Const.}h^2$ (Ref. 1)] is pressed into the material with a load L, the load is kept constant for a given period of several ten seconds, and after unloading, the size of the contact area of the remnant plastic deformation, A_C, is measured by a microscope. The Vickers hardness is calculated from $H_{Vickers} = L/A_C$. [In the engineering measurement of Vickers hardness one takes the average of the length of the diagonals of the impression d and calculates the projected area $d^2/2$, which then yields the Vickers hardness $H_V = 0.927 \cdot L \cdot 2/d^2$ (Ref. 1, p. 98).] Load divided by the projected area A_P of the remnant deformation is called Meyer's hardness H_{Meyer} L/A_P.[209] For an ideally sharp Vickers indenter, $H_V = 0.927 \cdot H_{Meyer}$. The maximum applied load divided by the contact area upon that load contains both the elastic and plastic deformation, and is called "Martens" (or "universal") hardness. It is suitable for the characterization of materials which in service are exposed to combined elastic and plastic deformation.

As mentioned in Sec. II when discussing ReB_2, materials which undergo complex electronic instabilities upon finite shear show sluggish approach toward the load-invariant hardness, which is often reached only at a very large load of several N.[94,95,302] However, materials which are electronically stable upon finite shear because of well-defined carriers of the plastic flow, such as the grain boundaries in the nanocomposites,[13] reach the regime of load-invariant hardness already at a relatively small applied load of 30–100 mN, as seen in Figs. 12 and 28. This has to be kept in mind when measuring the hardness using the "nanoindentation."

Nowadays, automatic load-depth-sensing technique is conveniently used to measure the hardness. The first published relatively simple and empirical method of Doerner and Nix (D. & N.)[303] used a linear extrapolation of about 30% of the initial unloading curve, which has been obtained from the as measured indentation curve by numerical transformation using a polynomial obtained during the calibration of the instrument,[202,203] to determine the "indentation depth" $h_{R'}$ from which the Vickers hardness is obtained using the relationship $HU_{plast} = F_{max}/26.43 \cdot (h_{R'})^2$.[202,203] This method has been used for example by the early version of Fischerscope H 100, which has been on the market shortly after the paper of D. & N. has been published. As emphasized by Behncke, $h_{R'}$ is not any real indentation depth but

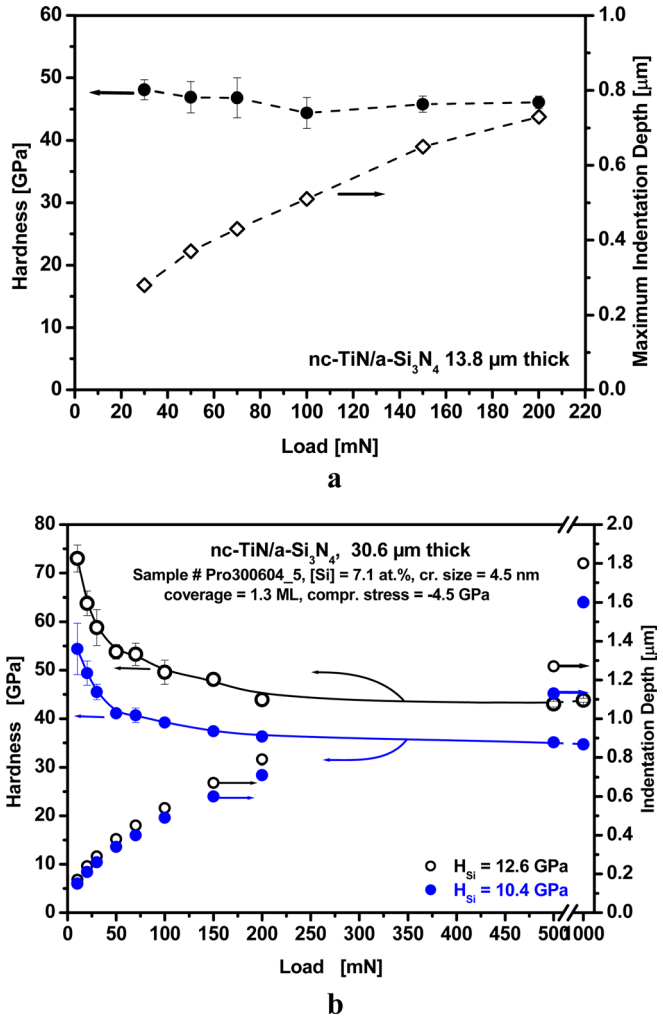

FIG. 28. (Color online) Hardness and indentation depth vs maximum applied load for 13.8 μm (a) and 30.6 μm (b) thick superhard nc-TiN/Si_3N_4 coatings deposited by plasma CVD (a) and reactive sputtering (b). In (b), we show the effect of the choice of the hardness of Si used for the calibration: using the value of 12.6 GPa, as done in many papers, increases significantly the measured hardness of the nanocomposite coatings as compared with the case when the hardness of silicon of 10.4 GPa has been used during calibration of the instrument in our work. (a) Reprinted with permission from Veprek *et al.*, Surf. Coat. Technol. **200**, 3876 (2006). Copyright 2006, Elsevier B.V. (b) From the work of Prochazka *et al.* (Ref. 164).

only a "number for a calculation" (Rechenwert" in German),[203] and the curves transformed by the software of the Fischerscope H 100 during the calibration are not any real load-depth dependences, because the "as measured" indentation curves, which are the real load-depth dependences, are transformed to another ones which yields, by the linear extrapolation, the value of $h_{R'}$, which then gives the correct hardness. (See the Appendix in Ref. 175.)

Six years after the paper of D. & N., Oliver and Pharr published an improved method for the evaluation of hardness.[304] Their method uses a power law to fit the unloading curve and correction factor ε to better estimate the corrected indentation depth. Therefore, the method of O. & P. is more flexible than that of D. & N. However, also in this case, great care has to be excercised when applying the O. & P. method because as emphasized in later papers (e.g., Refs. 305–307), numerous corrections are needed when studying a large variety of materials with different elastic–plastic behavior. For example, when using the Young's modulus of fused silica for the calibration and tip area correction, an incorrect value of the hardness of Sapphire of 28–32 GPa is obtained (see, e.g., Ref. 308 and Ref. 309, Appendix 5, p. 239) instead of the correct value of about 21 GPa reported in many papers, which has been measured by the conventional two-step Vickers method (see, e.g., Refs. 54, 310, and 311). When, however, the instrument Fischerscope has been calibrated (using the early method of D. & N.) at a constant hardness using, e.g., silicon, correct hardness of Sapphire of about 21 ± 1.5 GPa has been obtained for loads between about 20 and 1000 mN.[210] Also, the method of O. & P. will yield correct hardness of Sapphire when the calibration would be done for constant hardness instead of modulus. There are many other sources of possible errors, which may occur during the measurement of the hardness using the modern "nanoindentometers" as discussed in Refs. 305–307, which we cannot discuss here in detail. We only point out that both the simple, more empirical method of D. & N. and the more advanced method of O. & P. can yield correct values of the hardness when correctly used, but one should always check the obtained values using the classical two-step method.

Of course, one must not mix-up these techniques as done recently by Fischer-Cripps *et al.* who evaluated, using the method of O. & P., the "transformed" curves, which were obtained from Fischerscope H 100 that has been calibrated according to D. & N. method. It is not surprising that Fischer-Cripps *et al.* obtained wrong value of hardness of our nanocomposites, lower by a factor of 2.[201] We published this effect already 10 years ago,[297] but in spite of that, these workers repeat such mix-up of the two methods now. I refer to our early[297] and recent[175] papers for further details.

APPENDIX B: CONSTRAINT FACTOR

The constraint factor (this part is based on an unpublished joint study[316]), which is the ratio between the plastic hardness H and tensile yield strength Y, $H = C \cdot Y$, has been subject of many investigations. Probably, the first study of this has been by Prandtl[312] who suggested that this problem can be treated under the assumption that plastic flow occurs under constant volume, which is a good approximation for materials, which display a well-defined (not necessary an ideal as assumed by Prandtl) transition between elastic and plastic behaviors. His idea has been further extended by Hencky[313] and in much more detail by Ishlinsky[314] (because I could not find the English translation quoted by Tabor in his book[1] on pp. 43 and 66, and also several authors who quoted it recently could not provide it to us, I obtained the Russian original and studied it), who, for the conditions of fully developed plasticity, calculated the slip-line fields and obtained a value of the constraint factor of 2.84. Later studies have shown that the materials' flow depends also on the shape of the indenter and on the coefficient of friction between the indenter and material being tested, but it is between about 2.6 and 3 for the majority of metals and

ceramics (see, e.g., Ref. 2, p. 454 and Ref. 315, p. 260). However, this applies only under conditions of fully developed plasticity. As pointed out by Tabor, just at the onset of plasticity (i.e., in the predominantly elastic regime of deformation) the constraint factor is only about 1.1 (see Ref. 1, p. 46) and it increases to about 3 in the regime of "fully developed plasticity" (see Fig. 29 in Ref. 1, p. 50). Therefore, in the elastic–plastic transition regime—where the plastic hardness should never be measured—the constraint factor increases from about 1 to 3.

The flow of the material upon indentation depends also on the friction between the indenter and the material being tested (for a wedge indenter see Fig. 13. in Ref. 2, p. 454). Because the coefficient of friction of diamond indenter with metals is about 0.1–0.15 (Ref. 1, p. 42), the hardness measurements on metals, metallic nitrides, carbides, borides, and the like will operate under conditions of sliding. One notices that in any case, upon the indentation, there is a flow of the material out of the surface in regions somewhat remote from the contact area between the indenter and the material being studied. The flow of the material out of the surface occurs also for indentation into very hard materials, such as the super- and ultrahard nanocomposites, which, upon indentation, show sink-in instead of pile-up (the latter found, e.g., for Al). This is illustrated in Fig. 29.[317] The reader should notice the similarity of the materials flow in the nanocomposite and in the diamond indenter.

In order to explain his results of the indentation into silicate glasses, Marsh[318] used the expanding cavity model because as he pointed out, "… highly elastic material is less rigid and would be more amenable to radial flow" (Ref. 318, p. 424). With reference to Fig. 5 in Ref. 318, one notices that the expanding cavity model describes reasonably well the typical oxide glasses with constraint factor $C \approx 1.5$ and several polymers with C approaching 1 for polyacetate resin, but being still about 2.3 for the relatively brittle poly(methylmethacrylate) (PMMA). As discussed by Argon, about half of the apparent plastic deformation upon indentation into oxide glasses is due to compaction, which, however, can be recovered by high-temperature annealing, whereas about the other half of the deformation, which is due to plastic shear flow, remains preserved even after long-term annealing (see, Ref. 319, p. 97 and references therein). We have studied the possible changes of the size of the remnant indentations, measured by SEM, after long-term annealing of the superhard nc-TiN/Si_3N_4 nanocomposites and found only a very small recovery of few percentage, which we attributed to a relaxation of elastic strain.[320]

The expanding cavity model has been originally developed to describe the deformation of the barrels of guns and canons upon firing (Ref. 315, p. 97 ff). For the expansion of a spherical cavity in an infinitive medium, there are only radial components of material flow. As mentioned by Marsh and further developed by Johnson,[321] the constraint factor expressed as the ratio of mean pressure to yield strength is a function of the nondimensional strain shown in Fig. 6.14 in Ref. 321, p. 176. Therefore, the "elastic–plastic" regime where the expanding cavity model works well corresponds

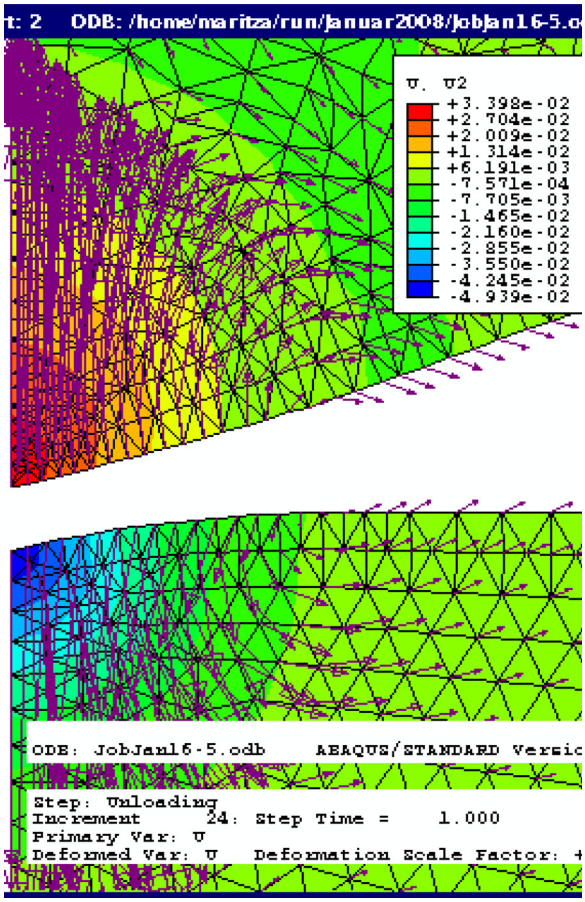

FIG. 29. (Color online) Resulting flow of material upon indentation into ultrahard nanocomposites with yield strength $Y \approx 35$ GPa and hardness of about 100 GPa (lower part) and in the diamond indenter (upper part) after unloading (Ref. 317). One notices that there is also material flow "out of the surface" in regions outside the contact area between the indenter and the material under study, as expected from the slip-line fields.

to the transition from elastic to fully plastic deformation of the material under study. However, in the case of the hardness measurement on the super- and ultrahard nanocomposites, the reported hardness was load-invariant (see Fig. 28), i.e., the materials operated in the regime of fully developed plasticity, and there was a significant flow of the material outward (see Fig. 29), which is not the case in the expanding cavity model with only a radial component of the flow.

In summary, the slip-line field model developed by Hencky, Ishlinsky, and Hill with a constraint factor 2.6–3 describe well the relationship between the plastic hardness and yield strength for material with well-defined elastic to fully plastic regime, whereas the expanding cavity model applies for materials with a significant or predominant component of radial flow, such as oxide glasses, which undergo compaction, and polymers, which deform by viscoelastic flow.[322] The nonlinear finite element modeling[301] allows one to treat this problem in a general manner as shown for number of different materials including polymers, metals, and ceramic superhard nanocomposites.[208] A more recent study by means of advanced FEM by Song and Komvopoulos[323] provides a very deep insight into the problem of the development of the elastic–plastic zones under the indenter and

about the constraint factor. We cannot discuss it here in more detail, but the reader is recommended to study this paper.

In conclusion to this Appendix, we showed that a deep understanding of the elastic–plastic properties of the material in combination with nonlinear FEM is needed to understand the constraint factor for a given material. A simple fitting of curves, based on the ratio of hardness and Young's modulus,[201] which have been derived from the expanding cavity model for infinitive medium of spherical symmetry for a combined elastic–plastic regime, as applied by Marsh to glasses and polymers, is inappropriate for the superhard nanocomposites.

[1]D. Tabor, *The Hardness of Metals* (Clarendon, Oxford, 1951).
[2]F. A. McClintock and A. S. Argon, *Mechanical Behavior of Materials* (Addison-Wesley, Reading, 1966).
[3]O. Knotek, B. Bosserhoff, A. Schrey, T. Leyendecker, O. Lemmer, and S. Esser, Surf. Coat. Technol. **54/55**, 102 (1992).
[4]K.-D. Bouzakis, I. Mirisidis, N. Michailidis, E. Lili, A. Sampris, G. Erkens, and R. Cremer, Plasma Processes Polym. **4**, 301 (2007).
[5]A. Kelly and N. H. Macmillan, *Strong Solids*, 3rd. ed. (Clarendon, Oxford, 1986).
[6]G. Gottstein, *Physical Foundations of Materials Science* (Springer-Verlag, Berlin, 2004).
[7]*The Properties of Natural and Synthetic Diamond*, edited by J. E. Field (Academic, San Diego, 1992).
[8]F. A. Cotton and G. Wilkinson, *Advanced Inorganic Chemistry*, 3rd ed. (Wiley, New York, 1972).
[9]Y. Zhang, H. Sun, and C. Chen, Phys. Rev. B **73**, 144115 (2006).
[10]D. M. Teter, Mater. Res. Soc. Bull. **23**, 22 (1998).
[11]A. S. Argon, *Strengthening Mechanisms in Crystal Plasticity* (Oxford University, Oxford, 2008).
[12]H. Chacham and L. Kleinman, Phys. Rev. Lett. **85**, 4904 (2000).
[13]S. Veprek, A. S. Argon, and R. F. Zhang, Philos. Mag. **90**, 4101 (2010).
[14]Y. Zhang, H. Sun, and C. F. Chen, Phys. Rev. B **73**, 064109 (2006).
[15]Y. Gogotsi, A. Kailer, and K. G. Nickel, Nature **401**, 663 (1999).
[16]S. Z. Li, Y. Shi, and H. R. Peng, Plasma Chem. Plasma Process. **12**, 287 (1992).
[17]S. Veprek, A. Niederhofer, K. Moto, T. Bolom, H.-D. Männling, P. Nesladek, G. Dollinger, and A. Bergmaier, Surf. Coat. Technol. **133–134**, 152 (2000).
[18]S. Veprek, M. G. J. Veprek-Heijman, P. Karvankova, and J. Prochazka, Thin Solid Films **476**, 1 (2005).
[19]S. Veprek, S. Reiprich, and S. Z. Li, Appl. Phys. Lett. **66**, 2640 (1995).
[20]S. Veprek and S. Reiprich, Thin Solid Films **268**, 64 (1995).
[21]J. S. Koehler, Phys. Rev. B **2**, 547 (1970).
[22]S. L. Lehoczky, Phys. Rev. Lett. **41**, 1814 (1978).
[23]S. L. Lehoczky, J. Appl. Phys. **49**, 5479 (1978).
[24]U. Helmersson, S. Todorova, S. A. Barnett, J.-E. Sundgren, L. C. Markert, and J. E. Greene, J. Appl. Phys. **62**, 481 (1987).
[25]M. Shinn, L. Hultman, and S. A. Barnett, J. Mater. Res. **7**, 901 (1992).
[26]P. B. Mirkarimi, L. Hultman, and S. A. Barnett, Appl. Phys. Lett. **57**, 2654 (1990).
[27]K. K. Shih and D. B. Dove, Appl. Phys. Lett. **61**, 654 (1992).
[28]W. D. Sproul, Science **273**, 889 (1996).
[29]S. H. Lee, K. H. Nam, J.-W. Lim, and J.-J. Kim, Surf. Coat. Technol. **174–175**, 758 (2003).
[30]J. Lin, J. J. Moore, B. Mishra, M. Pinkas, X. Zhang, and W. D. Sproul, Thin Solid Films **517**, 5798 (2009).
[31]S. A. Barnett, "Physics of thin films," in *Mechanic and Dielectric Properties*, edited by M. H. Francombe and J. L. Vossen (Academic, Boston, 1993), Vol. 17.
[32]S. A. Barnett and A. Madan, Phys. World **11**, 45 (1998), available at http://physicsworld.com/cws/archive/print/11/3.
[33]S. A. Barnett, A. Madan, I. Kim, and K. Martin, Mater. Res. Soc. Bull. **28**, 169 (2003).
[34]X. Chu and S. A. Barnett, J. Appl. Phys. **77**, 4403 (1995).
[35]W.-D. Münz, D. B. Lewis, P. Eh. Hovsepian, C. Schönjahn, A. Ehiasarian, and I. J. Smith, Surf. Eng. **17**, 15 (2001).
[36]H. Söderberg, M. Oden, J. M. Molina-Aldareguia, and L. Hultman, J. Appl. Phys. **97**, 114327 (2005).
[37]X. P. Hu, H. J. Zhang, J. W. Dai, G. Y. Li, and M. Y. Gu, J. Vac. Sci. Technol. A **23**, 114 (2005).
[38]W. Li, P. Liu, Y. Zhao, K. Zhang, F. Ma, and X. Liu, Thin Solid Films **534**, 367 (2013).
[39]W. Li, P. Liu, J. Wang, F. Ma, X. Liu, X. Cheng, and L. Yang, Mater. Lett. **65**, 636 (2011).
[40]W. Li, P. Liu, Y. Zhao, F. Ma, X. Liu, X. Cheng, and D. He, J. Alloys Compd. **562**, 5 (2013).
[41]A. Matthews, R. Jones, and S. Dowey, Tribol. Lett. **11**, 103 (2001).
[42]L. Hultman, G. Häkansson, U. Walström, J. E. Sundgren, I. Petrov, F. Adibi, and J. E. Greene, Thin Solid Films **205**, 153 (1991).
[43]M. Setoyama, A. Nakayama, M. Tanaka, N. Kitagawa, and T. Nomura, Surf. Coat. Technol. **86–87**, 225 (1996).
[44]T. An, M. Wen, L. L. Wang, C. Q. Hu, H. W. Tian, and W. T. Zheng, J. Alloys Compd. **486**, 515 (2009).
[45]C. Ziebert and S. Ulrich, J. Vac. Sci. Technol. A **24**, 554 (2006).
[46]G. Li, J. Lao, J. Tian, Z. Han, and M. Gu, J. Appl. Phys. **95**, 92 (2004).
[47]C. H. Lin, Y. Z. Tsai, and J. G. Duh, Thin Solid Films **518**, 7312 (2010).
[48]P. C. Wo, X. L. Zhao, P. R. Munroe, Z. F. Zhou, K. Y. Li, D. Habibi, and Z. H. Xie, Acta Mater. **61**, 193 (2013).
[49]S. H. Zhang, F. Cai, and M. G. Li, Surf. Coat. Technol. **206**, 3572 (2012).
[50]S. H. Zhang, L. Wang, Q. M. Wang, and M. G. Li, Surf. Coat. Technol. **214**, 160 (2013).
[51]S. H. Zhang, L. Wang, Q. M. Wang, and M. G. Li, Surf. Coat. Technol. **214**, 153 (2013).
[52]W. Li, P. Liu, Y. S. Zhao, F. C. Ma, X. K. Liu, X. H. Chen, and D. H. He, Surf. Coat. Technol. **214**, 168 (2013).
[53]V. Valvoda, R. Kuzel, R. Cerny, and J. Musil, Thin Solid Films **156**, 53 (1988).
[54]H. Holleck, J. Vac. Sci. Technol. A **4**, 2661 (1986).
[55]P. H. Mayrhofer, F. Kunc, J. Musil, and C. Mitterer, Thin Solid Films **415**, 151 (2002).
[56]P. H. Mayrhofer, A. Hörling, L. Karlsson, J. Sjölén, T. Larsson, C. Mitterer, and L. Hultman, Appl. Phys. Lett. **83**, 2049 (2003).
[57]W. Herr and E. Broszeit, Surf. Coat. Technol. **97**, 335 (1997).
[58]P. Karvánková, H.-D. Männling, C. Eggs, and S. Veprek, Surf. Coat. Technol. **146–147**, 280 (2001).
[59]J. Musil, Surf. Coat. Technol. **125**, 322 (2000).
[60]S. Zhang, D. Sun, Y. Fu, and H. Du, Surf. Coat. Technol. **198**, 2 (2005).
[61]S. Zhang, D. Sun, Y. Fu, Y. T. Pei, and J. Th. M. De Hosson, Surf. Coat. Technol. **200**, 1530 (2005).
[62]Y. X. Wang, S. Zhang, J.-W. Lee, W. S. Lew, D. Sun, and B. Li, Nanosci. Nanotechnol. Lett. **4**, 375 (2012).
[63]A. Matthews and A. Leyland, in *Proceedings of the SVC Techcon*, Chicago, April 19–24, 2008 (Society of Vacuum Coaters, Albuquerque, 2008), p. 40.
[64]I. Petrov, P. B. Barna, L. Hultman, and J. E. Greene, J. Vac. Sci. Technol. A **21**, S117 (2003).
[65]P. H. Mayrhofer, C. Mitterer, L. Hultman, and H. Clemens, Prog. Mater. Sci. **51**, 1032 (2006).
[66]F. Rovere, D. Music, S. Ershov, M. to Baben, H.-G. Fuss, P. H. Mayrhofer, and J. M. Schneider, J. Phys. D: Appl. Phys. **43**, 035302 (2010).
[67]R. Rachbauer, D. Holec, M. Lattemann, L. Hultman, and P. H. Mayrhofer, Int. J. Mater. Res. **102**, 735 (2011).
[68]D. Rafaja, C. Wüstefeld, M. Motylenko, Ch. Schimpf, T. Barsukova, M. R. Schwarz, and E. Kroke, Chem. Phys. Rev. **41**, 5081 (2012).
[69]G. S. Fox-Rabinovich, K. Yamamoto, B. D. Beake, I. S. Gershman, A. I. Kovalev, S. C. Veldhuis, M. H. Aguirre, C. Dosbaeva, and J. L. Endrino, Sci. Technol. Adv. Mater. **13**, 043001 (2012).
[70]A. A. Voevodin and J. S. Zabinski, Compos. Sci. Technol. **65**, 741 (2005).
[71]A. A. Voevodin, T. A. Fitz, J. J. Hu, and J. S. Zabinski, J. Vac. Sci. Technol. A **20**, 1434 (2002).
[72]C. Muratore, A. A. Voevodin, J. J. Hu, and J. S. Zabinski, Tribol. Lett. **24**, 201 (2006).
[73]C. Muratore, J. J. Hu, and A. A. Voevodin, Thin Solid Films **515**, 3638 (2007).
[74]C. Muratore, J. J. Hu, and A. A. Voevodin, Surf. Coat. Technol. **203**, 957 (2009).

[75]K. Sedlackova, P. Lobotka, and G. Radonczi, Carbon **43**, 2192 (2005).
[76]W. Gulbinski, S. Mathur, H. Shen, T. Suszko, A. Gilewicz, and B. Warcholinski, Appl. Surf. Sci. **239**, 302 (2005).
[77]D. Caschera, F. Federici, L. Pandolfi, S. Kaciulis, M. Sebastiani, E. Bemporad, and G. Padeletti, Thin Solid Films **519**, 3061 (2011).
[78]M. L. Cohen, Phys. Rev. B **32**, 7988 (1985).
[79]A. Y. Liu and M. L. Cohen, Science **245**, 841 (1989).
[80]M. L. Cohen, Solid State Commun. **92**, 45 (1994).
[81]A. Y. Liu and R. M. Wentzcovitch, Phys. Rev. B **50**, 10362 (1994).
[82]S. Veprek, J. Weidmann, and F. Glatz, J. Vac. Sci. Technol. A **13**, 2914 (1995).
[83]N. N. Greenwood and A. Earnshaw, *Chemistry of the Elements* (Pergamon, Oxford, 1984); Quoted after the German translation *Chemie der Elemente* (VCH Verlag, Weinheim, 1991).
[84]F. Gao, J. He, E. Wu, S. Liu, D. Yu, D. Li, S. Zhang, and Y. Tian, Phys. Rev. Lett. **91**, 015502 (2003).
[85]A. Simunek and J. Vackar, Phys. Rev. Lett. **96**, 085501 (2006).
[86]A. Simunek, Phys. Rev. B **80**, 060103 (2009).
[87]K. Li, X. Wang, F. Zhang, and D. Xue, Phys. Rev. Lett. **100**, 235504 (2008).
[88]H. Cynn, J. E. Klepeis, C.-S. Yoo, and D. Young, Phys. Rev. Lett. **88**, 135701 (2002).
[89]J. B. Levine, S. L. Nguyen, H. I. Rasool, J. A. Wright, S. E. Brown, and R. B. Kaner, J. Am. Chem. Soc. **130**, 16953 (2008).
[90]S. Veprek, R. F. Zhang, and A. S. Argon, J. Superhard Mater. **33**, 409 (2011).
[91]R. F. Zhang, D. Legut, Z. J. Lin, Y. S. Zhao, H. K. Mao, and S. Veprek, Phys. Rev. Lett. **108**, 255502 (2012).
[92]H. Y. Chung, J. M. Yang, S. H. Tolbert, and R. B. Kaner, J. Mater. Res. **23**, 1797 (2008).
[93]J. Yang, H. Sun, and C. F. Chen, J. Am. Chem. Soc. **130**, 7200 (2008).
[94]R. F. Zhang, D. Legut, R. Niewa, A. S. Argon, and S. Veprek, Phys. Rev. B **82**, 104104 (2010).
[95]H. Y. Chung, M. B. Weinberger, J. B. Levine, A. Kavner, J. M. Yang, S. H. Tolbert, and R. B. Kaner, Science **316**, 436 (2007).
[96]M. Calandra and F. Mauri, Phys. Rev. Lett. **101**, 016401 (2008).
[97]V. L. Solozhenko, O. Kurakevych, D. Andrault, Y. Le Godec, and M. Mezouar, Phys. Rev. Lett. **102**, 015506 (2009).
[98]R. F. Zhang, S. Veprek, and A. S. Argon, Phys. Rev. B **80**, 233401 (2009).
[99]C. Jiang, Z. Lin, and Y. Zhao, Phys. Rev. B **80**, 184101 (2009).
[100]S. Yip, Nature **391**, 532 (1998); Nature Mater. **3**, 11 (2004).
[101]A. S. Argon and S. Yip, Philos. Mag. Lett. **86**, 713 (2006).
[102]V. L. Solozhenko, D. Andrault, G. Fiquet, M. Mezouar, and D. C. Rubie, Appl. Phys. Lett. **78**, 1385 (2001).
[103]Y. Zhang, H. Sun, and C. F. Chen, Phys. Rev. Lett. **93**, 195504 (2004).
[104]E. Roduner, *Nanoscopic Materials: Size Dependent Phenomena* (RSC, Cambridge, 2006).
[105]D. Vollath, *Nanomaterials: An Introduction to Synthesis, Properties, and Applications* (Wiley-VCH Verlag, Weinheim, 2008).
[106]G. Cao, *Nanostructures & Nanomaterials* (Imperial College, London, 2004).
[107]C. C. Koch, I. A. Ovidko, S. Seal, and S. Veprek, *Structural Nanocrystalline Materials, Fundamentals, and Applications* (Cambridge University, Cambridge, 2007).
[108]C. C. Koch, R. O. Scattergood, M. Saber, and H. Kotan, J. Mater. Res. **28**, 1785 (2013).
[109]J. Weissmüller, NanoStruct. Mater. **3**, 261 (1993).
[110]R. Kirchheim, Acta Mater. **50**, 413 (2002).
[111]R. Kirchheim, Acta Mater. **55**, 5129 (2007); , **55**, 5139 (2007).
[112]J. R. Trelewicz and C. A. Schuh, Phys. Rev. B **79**, 094112 (2009).
[113]T. Chookajorn, H. A. Murdoch, and C. A. Schuh, Science **337**, 951 (2012).
[114]J. R. Weertman, Science **337**, 921 (2012).
[115]A. Barna, P. B. Barna, G. Radnoczi, F. M. Reicha, and L. Toth, Phys. Status Solidi **55**, 427 (1979).
[116]P. B. Barna, M. Adamik, G. Safran, B. Pecz, A. Bergauer, and H. Bangert, Phys. Status Solidi **146**, 317 (1994).
[117]P. B. Barna and M. Adamik, Thin Solid Films **317**, 27 (1998).
[118]M. Adamik, P. B. Barna, and I. Tomov, Thin Solid Films **317**, 64 (1998).
[119]D. Biro, A. Kovacs, F. Misjak, T. Szüts, and P. B. Barna, Surf. Coat. Technol. **180–181**, 425 (2004).
[120]S. Veprek, H.-D. Männling, M. Jilek, and P. Holubar, Mater. Sci. Eng., A **366**, 202 (2004).
[121]M. W. Chase, C. A. Davies, J. R. Downey, D. J. Frurip, R. A. McDonald, and A. N. Syverud, *JANAF Thermochemical Tables*, 3rd ed. (1985) [J. Phys. Chem. Ref. Data **14** (1985)].
[122]L. Lu, X. Chen, X. Huang, and K. Lu, Science **323**, 607 (2009).
[123]Y. Tian *et al.*, Nature **493**, 385 (2013).
[124]E. O. Hall, Proc. Phys. Soc. London, Sect. B **64**, 747 (1951).
[125]N. J. Petch, J. Iron Steel Inst., London **174**, 25 (1953).
[126]A. S. Argon, in *Comprehensive Composite Materials*, edited by A. Kelly, C. Zweben, and T.-W. Chou (Pregamon, Oxford, 2000), Vol. 1, p. 763.
[127]R. O. Ritchie, Nature Mater. **10**, 817 (2011).
[128]A. S. Argon, *The Physics of Deformation and Fracture of Polymers* (Cambridge University, Cambridge, 2013).
[129]R. W. Siegel and G. E. Fougere, Nanostruct. Mater. **6**, 205 (1995).
[130]N. Dubrovinskaia, V. L. Solozhenko, N. Miyajima, V. Dimitrev, O. O. Kurakevich, and L. Dubrovinsky, Appl. Phys. Lett. **90**, 101912 (2007).
[131]V. L. Solozhenko, O. O. Kurakevych, and Y. Le Godec, Adv. Mater. **24**, 1540 (2012).
[132]V. L. Solozhenko, private communication (2012).
[133]J. Schiotz, F. D. Di Tolla, and K. W. Jacobsen, Nature **391**, 561 (1998).
[134]J. E. Carsley, J. Ning, W. W. Milligan, S. A. Hackney, and E. C. Aifantis, Nanostruct. Mater. **5**, 441 (1995).
[135]S. Veprek, F.-A. Sarott, and Z. Iqbal, Phys. Rev. B **36**, 3344 (1987).
[136]A. Pelisson, M. Parlinska-Wojtan, H. J. Hug, and J. Patscheider, Surf. Coat. Technol. **202**, 884 (2007).
[137]C. A. Pignedoli, D. Passerone, H. J. Hug, A. Pelisson-Schecker, and J. Patscheider, Appl. Phys. Lett. **96**, 071908 (2010).
[138]A. Pelisson, H. J. Hug, and J. Patscheider, J. Appl. Phys. **108**, 023508 (2010).
[139]E. Lewin, D. Loch, A. Montagne, A. P. Ehiasarian, and J. Patscheider, "Comparison of Al-Si-N nanocomposite coatings deposited by HIPIMS and DC magnetron sputtering," Surf. Coat. Technol. (in press).
[140]T. K. Chen, M. S. Wong, T. T. Shun, and J. W. Yeh, Surf. Coat. Technol. **200**, 1361 (2005).
[141]C. H. Lin, J. G. Duh, and J. W. Yeh, Surf. Coat. Technol. **201**, 6304 (2007).
[142]H. W. Chang, P. K. Huang, A. Davison, J. W. Yeh, C. H. Tsau, and C. C. Yang, Thin Solid Films **516**, 6402 (2008).
[143]P. K. Huang and J. W. Yeh, J. Phys. D: Appl. Phys. **42**, 115401 (2009).
[144]P.-K. Huang and J. W. Yeh, Thin Solid Films **518**, 180 (2009); Scr. Mater. **62**, 105 (2010).
[145]C. W. Tsai, S. W. Lai, K. H. Cheng, M. H. Tsai, A. Davison, C. H. Tsau, and J. W. Yeh, Thin Solid Films **520**, 2613 (2012).
[146]M. I. Lin, M. H. Tsai, W. J. Shen, and J. W. Yeh, Thin Solid Films **518**, 2732 (2010).
[147]G. S. Fox-Rabinovich, S. C. Veldhuis, G. K. Dosbaeva, K. Yamamoto, A. I. Kovalev, D. L. Wainstein, I. S. Gershman, L. S. Shuster, and B. D. Beake, J. Appl. Phys. **103**, 083510 (2008).
[148]C. H. Lai, K. H. Cheng, S. J. Lin, and J. W. Yeh, Surf. Coat. Technol. **202**, 3732 (2008).
[149]S. Y. Lin, S. Y. Chang, Y. C. Huang, F. S. Shieu, and J. W. Yeh, Surf. Coat. Technol. **206**, 5096 (2012).
[150]D. C. Tsai, S. C. Liang, Z. C. Chang, T. N. Lin, M. H. Shiao, and F. S. Shieu, Surf. Coat. Technol. **207**, 293 (2012).
[151]V. Braic, A. Valdescu, M. Balaceanu, C. R. Luculescu, and M. Braic, Surf. Coat. Technol. **211**, 117 (2012).
[152]I. Endler, M. Höhn, J. Schmidt, S. Scholz, M. Herrmann, and M. Knaut, Surf. Coat. Technol. **215**, 133 (2013).
[153]M.-H. Hsieh, M.-H. Tsai, W.-J. Shen, and J.-W. Yeh, Surf. Coat. Technol. **221**, 118 (2013).
[154]P. Rogl and J. C. Schuster, *Phase Diagrams of Ternary Boron Nitride and Silicon Nitride Systems* (ASM International, The Materials Information Society, Materials Park, OH, 1992).
[155]M. Hillert, *Phase Equilibria, Phase Diagrams, and Phase Transformations: Their Thermodynamic Basis* (Cambridge University, Cambridge, 1998).
[156]W. W. Jian, G. M. Chen, W. Z. Xu, H. Yuan, M. H. Tsai, Q. D. Wang, C. C. Koch, Y. T. Zhu, and S. N. Mathaudhu, Mater. Res. Lett. **1**, 61 (2013).

[157]R. F. Zhang and S. Veprek, Mater. Sci. Eng., A **424**, 128 (2006).
[158]S. Veprek, H.-D. Männling, P. Karvankova, and J. Prochazka, Surf. Coat. Technol. **200**, 3876 (2006).
[159]D. A. Porter and K. E. Easterling, *Phase Transformations in Metals and Alloys*, 2nd ed. (Stanley Thornes, Cheltenham, 2001).
[160]H. Schmalzried, *Chemical Kinetics of Solids* (VCH Verlag, Weinheim, 1995).
[161]The term "spinodal" was introduced by Van der Waals in order to describe that part of the binodal line in his isotherm between the inflection points where the second derivative of pressure with volume is negative, corresponding to an apparently negative compressibility (Ref. 162). The negative second derivative means an inherent instability because any small concentration fluctuation will decrease the total energy of the solution and the decomposition occurs spontaneously. The positive second derivative means that such a fluctuation increases the total energy of the solution, i.e., the decomposition of the thermodynamically unstable solution requires activation energy and entropy for the formation of the nuclei.
[162]Van der Waals, "Over de Continuiteit van den Gas-en Vloeistoftoestand," Ph.D. dissertation (University of Leiden, Leiden, 1873); *English translation: On the Continuity of the Gaseous and Liquid States*, edited by J. R. Rowlinson (North-Holland, Amsterdam, 1988), p. 254.
[163]J. Zarzycki, *Glasses and the Vitreous State* (Cambridge University, Cambridge, 1991).
[164]J. Prochazka, P. Karvankova, M. G. J. Veprek-Heijman, and S. Veprek, Mater. Sci. Eng., A **384**, 102 (2004).
[165]M. Diserens, J. Patscheider, and F. Levy, Surf. Coat. Technol. **120–121**, 158 (1999).
[166]F. Vaz, L. Rebouta, S. Ramos, M. F. da Silva, and J. C. Soares, Surf. Coat. Technol. **108–109**, 236 (1998).
[167]F. Vaz, L. Rebouta, B. Almeida, P. Goudeau, J. Pacaud, J. V. Riviere, and J. Bessa e Sousa, Surf. Coat. Technol. **120–121**, 166 (1999).
[168]R. F. Zhang and S. Veprek, Thin Solid Films **516**, 2264 (2008).
[169]S. Christiansen, M. Albrecht, H. P. Strunk, and S. Veprek, J. Vac. Sci. Technol. B **16**, 19 (1998).
[170]P. Holubář, SHM Ltd., Průmyslová 3, CZ-787 01 Šumperk, Czech Republic, private communication (2003).
[171]P. B. Barna, I. Kovács, G. Radnóczi, B. Pécz, and S. Veprek, "Experimental evidence of Si_3N_4 interfacial phase encapsulating the TiN nanocrystals in TiN/Si_3N_4 nanocomposite coatings deposited by reactive magnetron sputtering" (unpublished).
[172]S. Veprek and M. G. J. Veprek-Heijman, Surf. Coat. Technol. **201**, 6064 (2007).
[173]F. Tang, B. Gault, S. P. Ringer, P. Martin, A. Bendavid, and J. M. Cairney, Scr. Mater. **63**, 192 (2010).
[174]F. Tang B. Gault, S. P. Ringer, and J. M. Cairney, Ultramicroscopy **110**, 836 (2010).
[175]S. Veprek and M. G. J. Veprek-Heijman, Thin Solid Films **522**, 274 (2012).
[176]M. Kong, W. Zhao, L. Wie, and G. Li, J. Phys. D: Appl. Phys. **40**, 2858 (2007).
[177]J. Jiang, J. He, Y. H. Cheng, and E. I. Meletis, paper presented at the IC4N Conference at Corfu, Greece, June 16–20, 2013; "Microstructural analysis of TiSiN nanocomposite thin films by HRTEM," Surf. Coat. Technol. (submitted).
[178]P. H. Mayrhofer, D. Music, and J. M. Schneider, Appl. Phys. Lett. **88**, 071922 (2006).
[179]R. F. Zhang and S. Veprek, Mater. Sci. Eng., A **448**, 111 (2007).
[180]R. F. Zhang and S. Veprek, Acta Mater. **55**, 4615 (2007).
[181]P. H. Mayrhofer, H. Willmann, and A. E. Reiter, Surf. Coat. Technol. **202**, 4935 (2008).
[182]S. Z. Li, Q. F. Fang, Q. Liu, Z. S. Li, J. Gao, P. Nesladek, J. Prochazka, M. G. J. Veprek-Heijman, and S. Veprek, Compos. Sci. Technol. **65**, 735 (2005).
[183]A. Flink, M. Beckers, J. Sjölén, T. Larsson, S. Braun, L. Karlsson, and L. Hultman, J. Mater. Res. **24**, 2483 (2009).
[184]J. Musil, P. Zeman, and P. Dohnal, Plasma Processes Polym. **4**, S574 (2007).
[185]J. Musil, Surf. Coat. Technol. **207**, 50 (2012).
[186]S. Sambasivan and W. T. Petuskey, J. Mater. Res. **9**, 2362 (1994).
[187]A. Niederhofer, P. Nesladek, H.-D. Männling, K. Moto, S. Veprek, and M. Jilek, Surf. Coat. Technol. **120–121**, 173 (1999).
[188]P. Zeman, private communication (2008).
[189]In majority of publications, the impurities are not reported, and in those where they were reported they have been in the range of 0.7 to several at. %. I don't quote all particular papers, but I hope that more attention will be devoted to this problem in the future.
[190]C. S. Sandu, F. Medjani, R. Sanjines, A. Karimi, and F. Levy, Surf. Coat. Technol. **201**, 4219 (2006).
[191]C. S. Sandu, S. Harada, R. Sanjines, and A. Cavaleiro, Surf. Coat. Technol. **204**, 1907 (2010).
[192]S. H. Sheng, R. F. Zhang, and S. Veprek, Acta Mater. **56**, 968 (2008).
[193]S. H. Sheng, R. F. Zhang, and S. Veprek, Acta Mater. **59**, 297 (2011).
[194]S. H. Sheng, R. F. Zhang, and S. Veprek, Acta Mater. **61**, 4226 (2013).
[195]R. F. Zhang, S. H. Sheng, and S. Veprek, Acta Mater. **56**, 4440 (2008).
[196]P. Karvankova, M. G. J. Veprek-Heijman, D. Azinovic, and S. Veprek, Surf. Coat. Technol. **200**, 2978 (2006).
[197]S. H. Sheng, R. F. Zhang, and S. Veprek, Acta Mater. **59**, 3498 (2011).
[198]S. Veprek, P. Karvankova, and M. G. J. Veprek-Heijman, J. Vac. Sci. Technol. B **23**, L17 (2005).
[199]S. Hao, B. Delley, and C. Stampfl, Phys. Rev. B **74**, 035424 (2006).
[200]P. Karvankova, private communication (2004).
[201]A. C. Fischer-Cripps, S. J. Bull, and N. Schwarzer, Philos. Mag. **92**, 1601 (2012).
[202]Fischerscope H 100 Manual Version 2.2 issued in May 1991 (in German).
[203]H.-H. Behncke, Härterei-Technische Mitteilungen **48**, 3 (1993) (in German).
[204]S. Veprek, J. Vac. Sci. Technol. A **17**, 2401 (1999).
[205]A. Erdemir, O. L. Eryilmaz, M. Urgen, K. Kazmanli, N. Mehta, and B. Prorok, *Handbook of Nanomaterials* edited by Y. Gogotsi (CRC, Boca Raton, FL, 2005), p. 685.
[206]P. Karvankova, "Superhard nc-TiN/a-BN/a-TiB_2 and nc-MnN/a-metal nanocrystalline composite coatings," Ph.D. dissertation (Technical University Munich, 2003).
[207]S. Veprek, S. Mukherjee, P. Karvankova, H.-D. Männling, J. L. He, K. Moto, J. Prochazka, and A. S. Argon, Thin Solid Films **436**, 220 (2003).
[208]M. G. J. Veprek-Heijman, R. G. Veprek, A. S. Argon, D. M. Parks, and S. Veprek, Surf. Coat. Technol. **203**, 3385 (2009).
[209]E. Meyer, Zt. Vereins Deutscher Ingenieure **52**, 645 (1908).
[210]S. Veprek, S. Mukherjee, P. Karvankova, H.-D. Männling, J. L. He, K. Moto, J. Prochazka, and A. S. Argon, J. Vac. Sci. Technol. A **21**, 532 (2003).
[211]A. R. Yavari, J. L. Lewandowski, and J. Eckert, Mater. Res. Soc. Bull. **32**, 635 (2007).
[212]D. C. Hofmann, J. Y. Suh, A. Wiest, G. Duan, M.-L. Lind, M. D. Demetriou, and W. L. Johnson, Nature **451**, 1085 (2008).
[213]S. Veprek, A. S. Argon, and R. F. Zhang, Philos. Mag. Lett. **87**, 955 (2007).
[214]S. Hao, B. Delley, S. Veprek, and C. Stampfl, Phys. Rev. Lett. **97**, 086102 (2006).
[215]S. Hao, B. Delley, and C. Stampfl, Phys. Rev. B **74**, 035402 (2006).
[216]R. F. Zhang, A. S. Argon, and S. Veprek, Phys. Rev. B **79**, 245426 (2009).
[217]S. G. Prilliman, S. M. Clark, A. P. Alivisatos, P. Karvankova, and S. Veprek, Mater. Sci. Eng., A **437**, 379 (2006).
[218]R. F. Zhang, A. S. Argon, and S. Veprek, Phys. Rev. Lett. **102**, 015503 (2009).
[219]V. I. Ivashchenko and S. Veprek, "QMD calculations currently in progress (2012)" (unpublished).
[220]R. F. Zhang, A. S. Argon, and S. Veprek, Phys. Rev. B **81**, 245418 (2010).
[221]B. Alling, E. I. Isaev, A. Flink, L. Hultman, and I. A. Abrikosov, Phys. Rev. B **78**, 132103 (2008).
[222]T. Marten, E. I. Isaev, B. Alling, L. Hultman, and I. A. Abrikosov, Phys. Rev. B **81**, 212102 (2010).
[223]V. I. Ivashchenko, S. Veprek, P. E. A. Turchi, and V. I. Shevchenko, Phys. Rev. B **85**, 195403 (2012).
[224]S. H. Tolbert and A. P. Alivisatos, Annu. Rev. Phys. Chem. **46**, 595 (1995).
[225]A. S. Argon and M. J. Demkowicz, Philos. Mag. **86**, 4153 (2006).
[226]M. J. Demkowicz and A. S. Argon, Phys. Rev. Lett. **93**, 025505 (2004).

[227]V. I. Ivashchenko and S. Veprek, "First-principles molecular dynamics study of the thermal stability of the BN, AlN, SiC and SiN interfacial layers in TiN-based heterostructures: Comparison with experiments," Thin Solid Films (in press).
[228]M. Mrovec, M. Moseler, C. Elsässer, and P. Gumbsch, Prog. Mater. Sci. **52**, 230 (2007).
[229]E. R. Margine, A. N. Kolmogorov, M. Reese, M. Mrovec, C. Elsässer, B. Meyer, R. Drautz, and D. G. Pettifor, Phys. Rev. B **84**, 155120 (2011).
[230]S. Veprek, M. Haussmann, and S. Reiprich, J. Vac. Sci. Technol. A **14**, 46 (1996).
[231]S. Veprek, M. Haussmann, S. Reiprich, S. H. Li, and J. Dian, Surf. Coat. Technol. **86–87**, 394 (1996).
[232]A. Niederhofer, T. Bolom, P. Nesladek, K. Moto, C. Eggs, D. S. Patil, and S. Veprek, Surf. Coat. Technol. **146–147**, 183 (2001).
[233]S. Veprek and A. S. Argon, J. Vac. Sci. Technol. B **20**, 650 (2002).
[234]R. W. Hertzberg, *Deformation and Fracture Mechanics of Engineering Materials*, 3rd ed. (John Wiley & Sons, New York, 1989).
[235]S. F. Pugh, Philos. Mag. **45**, 823 (1954).
[236]See: http://www.platit.ch for Compendium 2012.
[237]S. Veprek and M. G. J. Veprek-Heijman, Surf. Coat. Technol. **202**, 5063 (2008). Original reference: SHM Ltd. Průmyslová 3, CZ-787 01 Šumperk, Czech Republic, www.shm-cz.cz.
[238]T. Cselle, *Vacuum's Best 2005* (Wiley-VCH Verlag, Weinheim, 2005), p. 33.
[239]P. Holubar, M. Jilek, and M. Sima, Surf. Coat. Technol. **133–134**, 145 (2000).
[240]Y. X. Wang, S. Zhang, J.-W. Lee, W. S. Lew, D. Sun, and B. Li, "Toward hard yet tough CrAlSiN coatings via compositional grading," Surf. Coat. Technol. (to be published).
[241]S. Zhang, D. Sun, and X. Zheng, J. Mater. Res. **20**, 2754 (2005).
[242]Y. X. Wang, S. Zhang, Y. W. Lee, W. S. Lew, and B. Li, Appl. Surf. Sci. **265**, 418 (2013).
[243]See: htpp://www.shm-cz.cz for Company SHM s.r.o.
[244]P. H. Mayrhofer, C. Mitterer, J. G. Wen, J. E. Greene, and I. Petrov, Appl. Phys. Lett. **86**, 131909 (2005).
[245]P. Losbichler and C. Mitterer, Surf. Coat. Technol. **97**, 567 (1997).
[246]C. Mitterer, J. Solid State Chem. **133**, 279 (1997).
[247]R. Wiedemann and H. Oettel, Surf. Eng. **14**, 299 (1998).
[248]M. Berger, L. Karlsson, M. Larsson, and S. Hogmark, Thin Solid Films **401**, 179 (2001).
[249]J. Neidhardt, S. Mraz, J. M. Schneider, E. Strub, W. Bohne, B. Liedke, W. Möller, and C. Mitterer, J. Appl. Phys. **104**, 063304 (2008).
[250]P. Hammer, A. Steiner, R. Villa, M. Baker, P. N. Gibson, J. Haupt, and W. Gissler, Surf. Coat. Technol. **68/69**, 194 (1994).
[251]J. Neidhardt, Z. Czigany, B. Sartory, R. Tessadri, M. O'Sullivan, and C. Mitterer, Acta Mater. **54**, 4193 (2006).
[252]J. Neidhardt, M. O'Sullivan, A. E. Reiter, W. Rechberger, W. Grogger, and C. Mitterer, Surf. Coat. Technol. **201**, 2553 (2006).
[253]J. Neidhardt, Z. Czigany, B. Sartory, R. Tessadri, and C. Mitterer, Int. J. Refract. Met. Hard Mater. **28**, 23 (2010).
[254]P. H. Mayrhofer, C. Mitterer, J. G. Wen, I. Petrov, and J. E. Greene, J. Appl. Phys. **100**, 044301 (2006).
[255]K. Polychronopoulou, J. Neidhardt, C. Rebholz, M. A. Baker, M. O'Sullivan, A. E. Reiter, A. E. Gunnaes, K. Ginnakopoulos, and C. Mitterer, J. Mater. Res. **23**, 3048 (2008).
[256]K. Polychronopoulou *et al.*, Surf. Coat. Technol. **204**, 246 (2009).
[257]W. Gao, F. Xie, and K. Jia, Adv. Mater. Res. **335–336**, 502 (2011).
[258]B. Wang, F. Xie, and K. Jia, Appl. Mech. Mater. **110–116**, 1020 (2012).
[259]P. Karvankova, M. G. J. Veprek-Heijman, M. F. Zawrah, and S. Veprek, Thin Solid Films **467**, 133 (2004).
[260]J. Ramm, M. Ante, T. Bachmann, B. Widrig, H. Brändle, and M. Döbeli, Surf. Coat. Technol. **202**, 876 (2007).
[261]H. Klostermann, B. Böcher, F. Fietzke, T. Modes, and O. Zyvitzki, Surf. Coat. Technol. **200**, 760 (2005).
[262]I. Zukerman, V. N. Zhitomirsky, G. Beit-Ya'akov, R. L. Boxman, A. Raveh, and S. K. Kim, J. Mater. Sci. **45**, 6379 (2010).
[263]M. Jilek, private communication (2012).
[264]F. G. Ferre, E. Bertarelli, A. Chiodoni, D. Carnelli, D. Gastaldi, P. Vena, M. G. Beghi, and F. Di Fonzo, Acta Mater. **61**, 2662 (2013).
[265]D. A. Jerebtsov, G. G. Mikhailov, and S. V. Sverdina, Ceram. Int. **27**, 247 (2001).
[266]*Spanende Fertigung*, edited by K. Weinert, 5th ed. (Vulkan-Verlag, Essen, 2008).
[267]V. P. Swaminathan, R. Wei, and D. W. Gandy, J. Eng. Gas Turbines Power **132**, 082104 (2010).
[268]L. Ning, S. C. Veldhuis, and K. Yamamoto, Mach. Sci. Technol. **11**, 45 (2007).
[269]M. Sokovic, B. Barisic, and S. Sladic, J. Mater. Process. Technol. **209**, 4207 (2009).
[270]J. Ramm, M. Ante, H. Bändle, A. Neels, A. Dommann, and M. Döbeli, Adv. Eng. Mater. **9**, 604 (2007).
[271]L. de Abreu Vieira, M. Döbeli, A. Dommann, A. Kalchbrenner, A. Neels, J. Ramm, H. Rudigier, J. Thomas, and B. Widrig, Surf. Coat. Technol. **204**, 1722 (2010).
[272]T. Cselle, Werkzeug. Technik **127**, 26 (2012).
[273]T. Cselle, O. Coddet, C. Galamand, P. Holubar, M. Jilek, J. Jilek, A. Lümkemann, and M. Morstein, J. Mach. Manuf. **XLIX-E1**, 19 (2009).
[274]S. Reich, M. Schadewald, and M. Bornemann, Mat.-wiss. u. Werkstofftech. **38**, 108 (2007).
[275]M. Piska, A. Polzer, P. Cihlarova, and D. Stankova, in *Damage and Fracture Mechanics: Failure Analysis of Engineering Materials and Structures*, edited by T. Boukharouba, M. Elboujdaini, and G. Pluvinage (Springer Science, Netherlands, 2009), p. 195.
[276]S. Carvalho, N. M. G. Parreira, M. Z. Silva, A. Cavaleiro, and L. Rebouta, Wear **274–275**, 68 (2012).
[277]R. Zitoune, V. Krishnaraj, B. S. Almabouacif, F. Collombet, M. Sima, and A. Jolin, Composites, Part B **43**, 1480 (2012).
[278]E. Torres, D. Ugues, Z. Brytan, and M. Perucca, J. Phys. D: Appl. Phys. **42**, 105306 (2009).
[279]N. Norrby, M. P. Johansson, R. M'Saoubi, and M. Oden, Surf. Coat. Technol. **209**, 203 (2012).
[280]Y. Tanaka, N. Ichimiya, Y. Onischi, and Y. Yamada, Surf. Coat. Technol. **146–147**, 215 (2001).
[281]Y. Tanaka, T. M. Gür, M. Kelly, S. B. Hagstrom, T. Ikeda, K. Wakihira, and H. Satoh, J. Vac. Sci. Technol. A **10**, 1749 (1992).
[282]Y. Tanaka, K. Sato, and N. Ichimiya, paper B5-2-1 presented at the International Conference on Metallurgical Coatings and Thin Films, San Diego, April 26, 2007. See also: http://www.hitachi-tool.co.jp.
[283]P. Karvankova, A. Karimi, O. Coddet, T. Cselle, and M. Morstein, MRS Proc. **890**, 85 0890-Y08-18.1 (2006).
[284]X.-Z. Ding, X. T. Zheng, and Y. C. Liu, Thin Solid Films **519**, 1894 (2011).
[285]W. Assmann, J. A. Davies, G. Dollinger, S. Forster, H. Huber, and R. Siegele, Nucl. Instrum. Methods Phys. Res. B **118**, 242 (1996).
[286]G. Dollinger, M. Boulouedinine, A. Bergmaier, T. Faestermann, and C. M. Frey, Nucl. Instrum. Methods Phys. Res. B **118**, 291 (1996).
[287]See: http://www.lmt-tools.com.
[288]J. Kohlscheen, H.-J. Knoche, M. Hipke, and A. Lümkemann, Key Eng. Mater. **438**, 35 (2010).
[289]T. Cselle, M. Mörstein, A. Lümkemann, and J. Prochazka, *Schweizer Präzisions-Fertigungstechnik* (Carl Hansen Verlag, Munich, 2007), Werkstatt + Betrieb 11, 30 (2009).
[290]T. Cselle, M. Mörstein, and A. Lümkemann, Werkzeug Technik **115**, 1 (2010).
[291]M. Jilek, T. Cselle, P. Holubar, M. Morstein, M. G. J. Veprek-Heijman, and S. Veprek, Plasma Chem. Plasma Process. **24**, 493 (2004).
[292]P. Holubář, SHM Ltd. (www.shm-cz.cz), Průmyslová 3, CZ-787 01 Šumperk, Czech Republic, private communication (2005).
[293]M. Audronis, O. Jimenez, A. Leyland, and A. Matthews, J. Phys. D: Appl. Phys. **42**, 085308 (2009).
[294]J. Martan and P. Benes, Thermochim. Acta **539**, 51 (2012).
[295]M. K. Samani, X. Z. Ding, S. Amini, N. Khosravian, J. Y. Cheong, G. Cheng, and B. K. Tay, Thin Solid Films **537**, 108 (2013).
[296]T. Cselle and A. Barimani, Surf. Coat. Technol. **76–77**, 712 (1995).
[297]S. Veprek *et al.*, MRS Proc. **750**, 9 (2003).
[298]H. Hertz, J. reine angewandte Mathematik **92**, 156 (1882), available at http://resolver.sub.uni-goettingen.de/purl?PPN243919689.
[299]S. Timoshenko, *Theory of Elasticity* (McGraw-Hill, New York, 1934).
[300]R. M. Davies, Proc. R. Soc. Lond. A **197**, 416 (1949).
[301]R. G. Veprek, D. M. Parks, A. S. Argon, and S. Veprek, Mater. Sci. Eng., A **448**, 3385 (2007).
[302]V. Brazkin, N. Dubrovinskaia, M. Nicol, N. Novikov, R. Riedel, V. Solozhenko, and Y. Zhao, Nature Mater. **3**, 576 (2004).
[303]M. F. Doerner and W. D. Nix, J. Mater. Res. **1**, 601 (1986).
[304]W. C. Oliver and G. M. Pharr, J. Mater. Res. **7**, 1564 (1992).
[305]W. C. Oliver and G. M. Pharr, J. Mater. Res. **19**, 3 (2004).

[306]T. Chudoba and N. M. Jennett, J. Phys. D: Appl. Phys. **41**, 215407 (2008).
[307]S. A. Rodriguez, R. Martins Souza, and J. Alcala, Philos. Mag. **91**, 1409 (2011).
[308]A. C. Fischer-Cripps, P. Karvankova, and S. Veprek, Surf. Coat. Technol. **200**, 5645 (2013).
[309]A. C. Fischer-Cripps, *Nanoindentation* 2nd. ed. (Springer, New York, 2004).
[310]A. B. Sinani, N. K. Dynkin, P. V. Konevskiy, and L. A. Litvynov, Bull. Russ. Acad. Sci. Phys. **73**, 1380 (2009).
[311]W. Kollenberg, J. Mater. Sci. **23**, 3321 (1988).
[312]L. Prandtl, Zf. f. angew. Math. Mech. **1**, 15 (1921).
[313]H. Hencky, Z. Angew. Math. Mech. **3**, 241 (1923).
[314]A. Y. Ishlinsky, J. Appl. Math. Mech. **8**, 201 (1944) (in Russian); English translation by D. Tabor, Ministry of Supply, A.R.D., Theoretical Research Transl. No. 2/47, 1947.
[315]R. Hill, *The Mathematical Theory of Plasticity* (Clarendon, Oxford, 1950).
[316]S. Veprek, M. H. J. Veprek-Heijman, and A. S. Argon, "The constraint factor of superhard nanocomposites" (unpublished).
[317]M. G. J. Veprek-Heijman, "Non-linear finite element modeling" (internal report 2010).
[318]D. M. Marsh, Proc. R. Soc. London, Ser. A **279**, 420 (1964).
[319]A. S. Argon, in *Glass Science and Technology*, edited by D. R. Uhlmann and N. J. Kreidl (Academic, New York, 1980), Vol. 5, Chap. 3, pp. 97–132.
[320]P. Karvankova and S. Veprek, "Annealing study of indentation into superhard nanocomposites" (unpublished).
[321]K. L. Johnson, *Contact Mechanics* (Cambridge University, Cambridge, 1985).
[322]I. M. Ward and J. Sweeney, *The Mechanical Properties of Solid Polymers*, 2nd ed. (John Wiley & Sons, Chichester, 2005).
[323]Z. Song and K. Komvopoulos, Mech. Mater. **61**, 91 (2013).

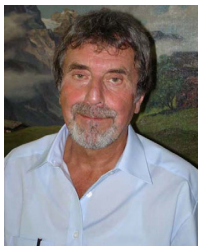

Stan Veprek is professor emeritus of the chemistry of inorganic materials at the Technical University Munich. He studied physics at the Charles University in Prague and received Dr. Phil. in chemistry at the University of Zurich. He conducted research in a variety of fields, such as diagnostics of glow discharge plasmas, plasma-induced CVD and PVD, nanocrystalline silicon and germanium, organometalic CVD, low-temperature epitaxy of silicon and heteroepitaxy of 4C-SiC, restoration of archeological metallic artifacts, development and industrialization of hard and superhard nanocomposites, and more recently first-principles theoretical studies and nonlinear FEM of superhard materials, particularly of the nanocomposites. He was visiting scientist and professor at a variety of institutions and universities in the United States, United Kingdom, Japan, Singapore, China, and Brazil. He received various awards such as the Silver Medal of the Societe d'Encouragement Pour la Recherche et l'Invention, Paris (1979), Silver Medal (1991) and Honorary Doctorate (Dr. h.c.) from the Masaryk University Brno, Czech Republic (1999), the Blaise Pascal Medal of the European Academy of Sciences (2004), the AVS John Thornton Memorial Award of the American Vacuum Society (2005), Honorary Professor of the Qingdao University of Science and Technology (2009), the Award for Career Achievements by the organizers of the Int. Conf. for Diffusion in Solids and Liquids (July 2010), and the R.F. Bunshah Award and ICMCTF 2011 Lecture of the American Vacuum Society—Advanced Surface Engineering Division (May 2011). Since his formal retirement in October 2004, Stan published about 70 papers and presented more than 80 invited, keynote, and plenary lectures at international conferences.